INVESTIGATING THE REFRACTIVE INDEX CHANGE OF DONOR – pi – LINKER – ACCEPTOR PHOTORESPONSIVE MATERIALS

by

Michael Wayne Adams
B.Sc., University of British Columbia, 1992

THESIS SUBMITTED IN PARTIAL FULFILLMENT OF
THE REQUIREMENTS FOR THE DEGREE OF

MASTER OF SCIENCE

In the
Department
of
Chemistry

© Michael Wayne Adams 2008

SIMON FRASER UNIVERSITY

Spring 2008

APPROVAL

Name: Michael Wayne Adams

Degree: Master of Science

Title of Thesis: Investigating the Refractive Index Change of Donor - pi
                                             - Linker - Acceptor Photoresponsive Materials

Examining Committee:

      Chair   Dr. Paul C.H. Li
                                             Associate Professor, Department of Chemistry

Dr. Neil R. Branda
Senior Supervisor
Professor, Department of Chemistry

Dr. Melanie A. O'Neill
Supervisor
Assistant Professor, Department of Chemistry

Dr. Steven Holdcroft
Supervisor
Professor, Department of Chemistry

Dr. Robert A. Britton
Internal Examiner
Assistant Professor, Department of Chemistry

Date Defended/Approved: April 3, 2008

Abstract

The arrival of new photonic devices will revolutionize the nature of communication and information technologies that employ light to code, process and transfer information. The fact that photoresponsive materials can be reversibly modulated between one of two distinct forms by irradiation has attracted growing interest in photonic and optoelectronic applications. Materials that are capable of controlled modulation between discrete isomers are good candidates for the elaboration of devices exhibiting photoswitched properties such as light absorption, fluorescence, electronic conduction, and light refraction. Specifically, the refractive index changes in organic photochromic materials has led to proposals for their use in a number of optical waveguide components. While dithienylethenes have been the focus of recent research efforts, their application into these technologies inherently suffers from design limitations. A modified dithienylethene architecture exhibiting strong charge-transfer excitations within a non-centosymmetric scaffold is proposed to overcome traditional boundaries. These nonlinear materials may therefore provide a new class of highly integrated optoelectronic and photonic systems for communication, signal processing and interconnection.

Keywords: photochromism, refractive Index, dithienylethene, ellipsometry

To PJ,

who knows nothing of chemistry,

and to Sam, who knows everything of me.

Acknowledgements

Mr. Simon Trudel for Ellipsometry Assistance.

Mr. Hideh Asanuma for Ellipsometry Assistance.

Mr. Tony Wigglesworth for Atomic Force Microscopy Assistance.

Mr. Usama Al-Atar for X-ray Diffraction measurements.

Mr. Simon Wong for Mass Spectrometry measurements.

Table of Contents

List of Equations

List of Figures

List of Schemes

List of Tables

List of Abbreviations

Å   angstroms

AcOH   acetic acid

AFM   atomic force microscopy

AM1   Austin Model 1

ATR-IR   attenuated total reflection infrared

BTE   bis(thiophene-3-yl)ethane

$C_2H_4Cl_2$ dichloroethane

CD_2Cl_2 deuterated dichloromethane

$CDCl_3$ deuterated chloroform

$CH_2(CN)_2$ malanonitrile

CH_2Cl_2 dichloromethane

CH_3CH_2OH ethanol

$CHCl_3$ chloroform

CI   chemical ionization

cm   centimetres

CT   charge transfer

d   doublet

DCTE   dicyanoethylene-thienylene

DCTFP   dithienylperfluorocyclopentene

DIBAL   diisobutylaluminium hydride

DMAC   dimethylacetamide

DMF	dimethylformamide
DTE	Dithienylethene
D-π-A	donor-π-linker-acceptor
E	photon energy
Et_2O	diethyl ether
eV	electron volts
HOMO	highest occupied molecular orbital
in vacuo	under vacuum
J	coupling constant
LRMS	low resolution mass spectroscopy
LUMO	lowest unoccupied molecular orbital
M	molarity
m	multiplet
m/z	mass to charge ratio
mg	milligrams
MHz	megahertz
mL	millilitres
mm	millimetres
mmol	millimoles
mp	melting point
M_w	molecular weight
n	refractive index

Ñ	complex index of refraction
n-BuLi	*n*-butyllithium
NCS	*n*-chlorosuccinimide
NLO	nonlinear optical
nm	nanometres
NMR	nuclear magnetic resonance
°C	degrees Celsius
PC	photochromic
Pd(PPh$_3$)$_4$	palladium tetrakis(triphenylphosphine)
Ph-B(OH)$_2$	phenylboronic acid
PMMA	polymethylmethacrylate
PSS	photostationary state
PTFE	polytetrafluoroethylene
r_e	extinction ratio
R$_{ms}$	root mean square roughness
rpm	revolutions per minute
s	singlet
SHG	second harmonic generation
silica	silica gel
t	triplet
UV	ultraviolet
UV-VIS	Ultraviolet-visible

$V^{1/2}$	standard deviation
W	watts
wt.%	weight percent
α	polarizability
B	first hyperpolarizability
Δ	heat
δ	chemical shift
Δn	change in refractive index
$\Delta\alpha$	change in polarizability
ε	molar absorptivity
λ	wavelength
λ_{max}	absorption maximum
μ_{ind}	induced dipole
μL	microlitres

1 Introduction

1.1 Molecular Devices

A device is tool or an invention designed to perform a particular purpose or function.[1] A molecular device is a collection of molecules assembled to achieve a specific task. Interest in molecular electronics has accelerated with the increasing demand for the miniaturization of electronic devices.[2] Driving forces such as cost, performance, reliability and speed dictate the likelihood of a device going to production.[3] As devices become smaller and more sophisticated, the current "scaling down" approach to manufacturing will reach intrinsic limitations. Contemporary attitudes towards fabricating nanoscale devices involve starting at the atomic or molecular level and "building up". Improvements in cost, size, and efficiency may be achieved through incorporation of these "building block" molecules into functioning devices.[4] While assembly of the molecular framework of a device is significant, the ability to *control* the function that the device performs is key. Central to design is the capability to reversibly change the properties and functions of the molecules, in turn allowing manipulation of the bulk material. Ideally a chemist will incorporate elements into the scaffold which will provide modulation between "on" and "off" states. The ability to efficiently and reversibly "switch" a material between functions is of prime interest in modern optoelectronic and photonic devices.[5]

1.2 Modulating Refractive Index

The next revolution in the multibillion dollar information technology industry will rely on the development of photonic materials that guide, direct and process light.[6] Photonic devices will contain fewer constituent parts than their electronic counterparts making them a cleaner, faster, more compact and versatile form of information processing.[5] High performance electro-optic switching elements for telecommunications are based on materials with high nonlinear optical (NLO) properties and polarizabilities.[7] Materials possessing second-order NLO optical behaviour must have specific structural and/or electronic properties. Typically, a polarisable π-conjugated framework incorporating a strong electron-donor and –acceptor group at opposite ends of the linear π-pathway will result in an asymmetric charge distribution. To date, research in developing new NLO materials has focused on tailoring the electronic nature of the donor, acceptor and linker toward their applications in modulating the phase, frequency and polarizability of light.[8-11] This thesis addresses the idea of integrating nonlinear elements within a photoresponsive architecture, such that the second-order NLO polarizabilities of molecules may be reversibly modulated. Structural modification of the bridging group, brought on by external irradiation of the active chromophore, provides a mechanism to regulate electronic communication between the donor and acceptor components. A molecule that can interconvert between two isomers, toggling high and low polarizabilities, offers the potential to reversibly modulate properties associated with NLO susceptibilities, specifically refractive index. Such materials can be usefully applied in optical communications and information processing.[12] The possibility of obtaining local

2

changes of the refractive index by material irradiation opens the way for the fabrication of devices such as waveguides and fully integrated photonic circuits.

1.3   Optical Devices

1.3.1 Waveguides

In order for optical logic devices to communicate with each other on a chip, the light signals between them need to be guided. For directing the flow of light on a chip, it is contained within a waveguide (Figure 1.3.1).[13] Waveguides consist of a material (core) with a refractive index higher than that of the surrounding medium (cladding). This difference in refractive index allows for total internal reflection at the walls of the waveguide, confining the light within.
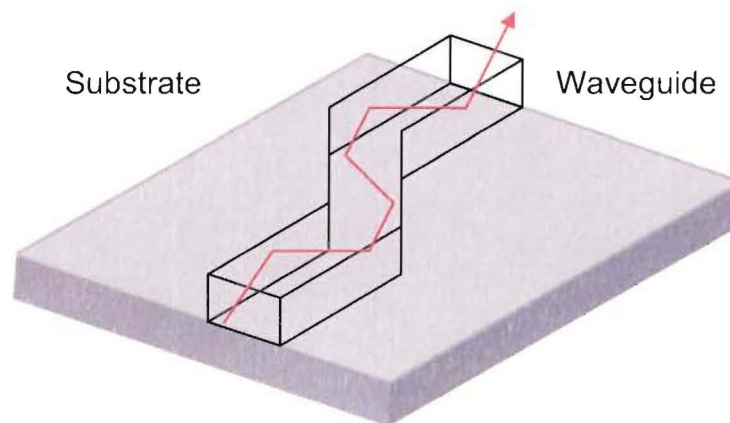
Figure 1.3.1 A waveguide is a transparent channel on a substrate whose refractive index is different than that of the materials on all sides. They confine light (red arrow) by means of total internal reflection.

Current waveguides are manufactured by depositing an entire flat layer of waveguide material onto the substrate and then using photolithography to etch away part of the layer, leaving only the strips in the desired pattern.[13] Typical waveguide materials include silica and silicate glasses, gallium and indium derivatives, and lithium niobate doped with titanium or hydrogen ions. These crystalline inorganic materials are difficult to grow and consequently expensive. There is now an increasing interest in developing organic NLO materials for optical waveguides, as these can be less costly and may be laid down using much simpler technologies such as injection molding, embossing, or even ink jet printing.[14]

1.3.2 Optoelectronic Devices

Electronic switching involves electrons that are rerouted along a conducting pathway by an applied voltage – one electronic signal is used to control another. An electro-optic switch is a device in which an electric field directs the path of a light beam by changing the refractive index of a waveguide material (Figure 1.3.2). These devices take advantage of the effect of an electric field on the refractive index of an NLO material. By applying voltage across the bottleneck, the electric field polarizes the NLO material and alters the refractive index of the two waveguides.

Waveguide

Light

(a)　　　　　　　　　　(b)
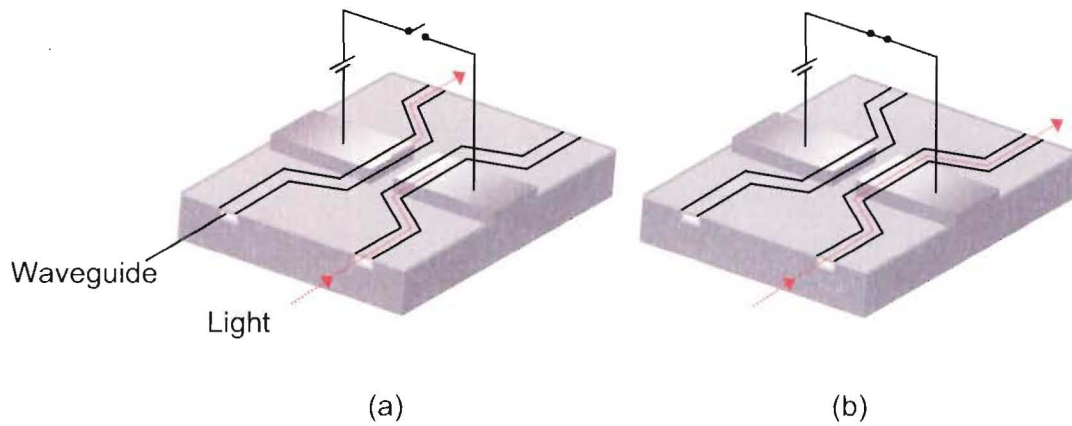
Figure 1.3.2 An electro-optic switch controls the path of a light signal through a waveguide. (a) Light in the lower waveguide interacts nonlinearly with the upper waveguide and switches channels, a phenomenon know as *crosstalk*. (b) If an electric field is applied across the bottleneck, the nonlinear interaction between waveguides is modified, and the light remains in a single channel.

A Mach-Zehnder interferometer is an electro-optic device that modulates light signals by breaking them up into discrete "digital" pulses or for altering the frequency of a pulsed signal (Figure 1.3.3). In telecommunications the *extinction ratio* (r_e) is the ratio of two optical power levels of a digital signal generated by an optical source.
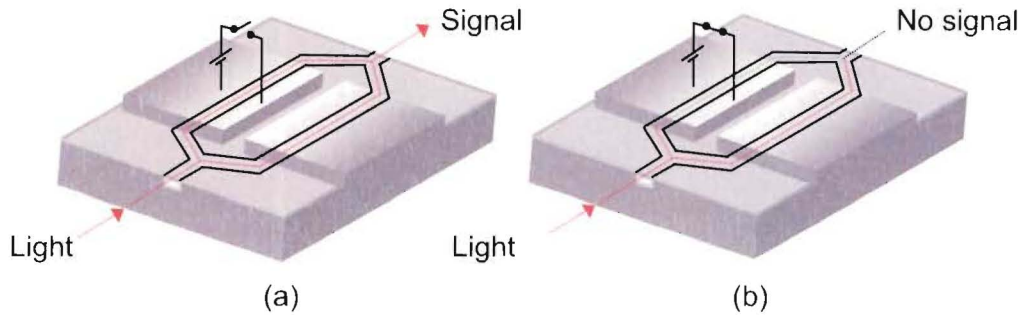
Figure 1.3.3 A Mach-Zehnder interferometer controls the phase and frequency of a light signal through a waveguide. If an electric field is applied across a single channel, the refractive index changes, causing wave interference at the output.

Mach-Zehnder modulators also take advantage of the effect of an electric field on the refractive index of an NLO material. Figure 1.3.3 (a) shows that the incident light is split into two beams, each of which is directed along a separate waveguide in the NLO material before being merged again. The transmittance of the interferometer is then 1, and the output may be classified as the "on" signal. When a voltage is applied across one of the branches (b), the refractive index of the waveguide material changes and the light beam along that branch is slowed down. When the two beams merge again they are out of phase and interfere destructively. If the optical path in that channel is changed enough to place it exactly $\lambda/2$ out of phase with the unperturbed beam there will be complete destructive interference when the two beams are reunited. The transmittance of the interferometer is then 0, and the output of the switch may be classified as

"off". Thus, by modulating the applied voltage, the extinction ratio (on/off) can be modulated with the same frequency. In fact, the transmittance can be set to any value between 0 and 1 by adjusting the voltage, The Mach-Zehnder interferometer can therefore be used as either a switch or a modulator. Current commercial optoelectronic devices achieve extremely high modulation frequencies up to rates of twenty billion times per second.[5]

1.3.3 Photonic Integrated Circuits

Optoelectronic devices use an electric field to control a light beam. In a truly photonic switch, one light beam will control another. Fully optical integrated circuits are called photonic integrated circuits (Figure 1.3.4).

(a)   (b)
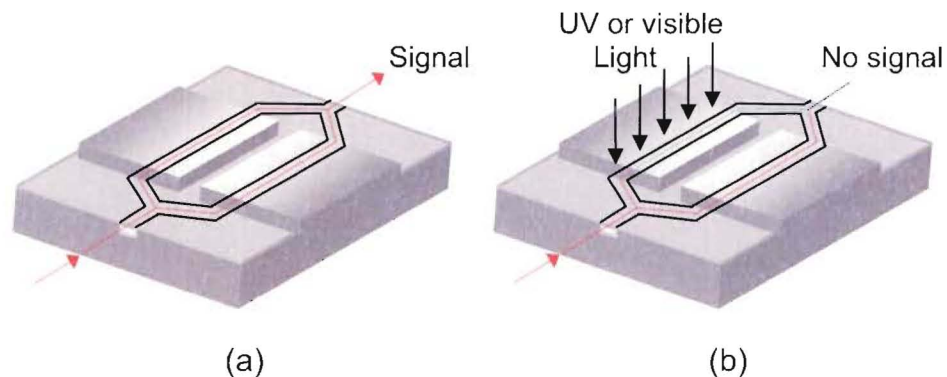
Figure 1.3.4 A fully optical Mach-Zehnder Interferometer. (a) Incident light is split and directed along separate waveguides in a photosensitive NLO material before being merged. (b) When ultraviolet (> 450 nm) or visible (450 – 600 nm) light is applied across one of the branches, the refractive index of the waveguide material changes, and recombination results in destructive interference.

Photonic circuits have several advantages over their "hybrid" counterparts. An all photonic transistor would have a faster switching speeds than traditional varieties. Optical circuit components will in principle contain fewer constituent parts making them easier and cheaper to package into chips. As a result, photonic devices will permit engineers to contemplate entirely new types of circuit design and architecture. However, none of these developments can happen without materials whose response to light is highly useful.

1.4   Nonlinear Optics

Molecules with diffuse electron clouds exhibit larger polarization changes in response to an oscillating electric field than molecules with localized electrons.[15] Rearrangement of the delocalized electrons in a material creates an additional charge density. As an incident light wave interacts with the electron cloud of a material it slows down. Molecules with larger dipole moments and polarizabilities will have a higher refractive index.

Nonlinear optics deals with the interaction of applied electromagnetic fields in various materials to generate new electromagnetic fields, altered in frequency, phase, or other physical properties.[7] A nonlinear optical response means that the amount of light transmitted through a substance is not proportional to the amount of incident light. Optical nonlinearity may additionally create a difference between the frequency of the incident light and the light that exits the material. In this way, nonlinear optical (NLO) materials may act as

switches where electromagnetic fields can be used to control and direct the path of light.[5]

When a molecule is subjected to an oscillating external electric field (light), the induced change in molecular dipole moment (polarization) results in an induced dipole moment μ_{ind}. At low electric field strengths μ_{ind} is linearly proportional to the electric field, the proportionality factor being the first-order polarizability α. At high electric field strengths, higher order terms become relevant, and the induced dipole moment is expressed by (Equation 1.4.1), where summation over repeated indices is implied.[16]

$$\mu_{ind} = \alpha E + \beta E^2 + \gamma E^3 + ...,$$

Equation 1.4.1 The induced change in polarization expressed by a power series in the field strength E. The coefficients α, β and γ are components of the linear polarizability, the first hyperpolarizability, and the second hyperpolarizability tensor, respectively. The terms beyond the first describe a nonlinear response to the incident electric field.

Second-order nonlinear effects of molecular materials are ultimately related to the first hyperpolarizability, β, which relates the polarization to the square of the field strength.[7] The β tensor is responsible for NLO effects such as second-harmonic generation (frequency doubling), frequency mixing, and the electro-optic effect (change of refractive index). Thus a nonlinear response is one that does not vary in direct proportion to the stimulus, rather nonlinear responses embrace just about any other alternative to this kind of simple behaviour. For

molecular materials to exhibit second-order nonlinear optical behaviour, the molecules which constitute them must have specific structural and/or electronic properties.

1.4.1 Nonlinear Materials

The search for new efficient organic materials to be used in nonlinear optics has considerably extended over the past two decades. Materials possessing second-order NLO properties originate from molecules that have strong intermolecular charge-transfer (CT) excitations in a non-centrosymmetric molecular environment.[17] The symmetry limitations are due to β, the first hyperpolarizability parameter in Equation 1.4.1, which as a second-order tensor vanishes in a centrosymmetric environment.[18] Typical organic architectures that satisfy the requirements necessary for second-order NLO behaviour consist of a polarisable molecular system (e.g., a π-conjugated pathway) having an asymmetric charge distribution (e.g., with donor and/or acceptor substituents). The necessary structural motif can be reduced to a donor-(π-linker)-acceptor (D-π-A) architecture (Scheme 1.4.1). Such systems can be described as one dominant hyperpolarizability component lying in the direction of the charge transfer.[7]
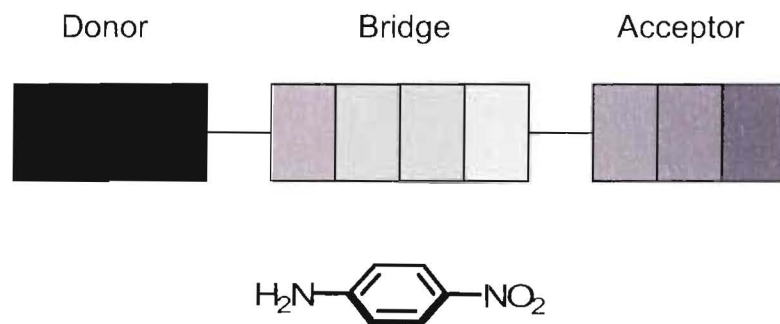
Scheme 1.4.1 The prototypical dipolar D-π-A *p*-nitroaniline molecule.

A variety of strategies for obtaining second-order NLO organic molecules have been developed within the molecular scheme formed by a D-π-A structure. The design of new second-order chromophores has focused primarily on engineering the electronic nature of the donor and the acceptor,[19] and the conjugation length of the bridge.[20]

1.4.2 Switching the Optical Response

To alter the second order NLO properties of a material, modifications need to be made at the molecular level. First hyperpolarizabilities of molecules may be manipulated by reversibly modifying the properties of specific parts of an active molecule, usually by on/off switching.[16] Switching mechanisms that generate an alteration of the π-bridge involve the loss or gain of conjugation, and can regulate the electronic communication between donor and acceptor components (Scheme 1.4.2). A molecule that can be interconverted between two isomers, where each has a unique π-conjugation pathway between donor and acceptor, offers the

potential to reversibly modulate NLO susceptibilities and the properties associated with them.
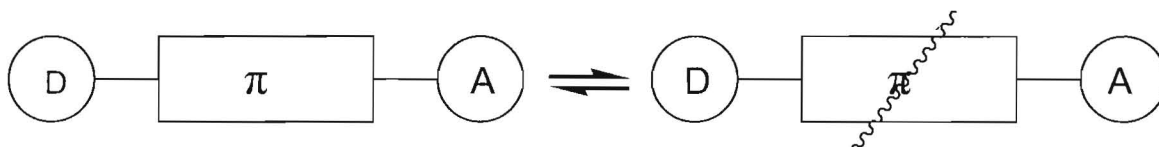
Scheme 1.4.2 Alteration of the π-bridge involving reversible loss or gain of conjugation regulates electronic communication between the donor and the acceptor.

.

1.5   Molecular Switching

A molecular switch is a molecule that can be reversibly shifted between two or more stable states by responding to the application of external stimuli.[21] These molecules typically undergo dramatic changes in their physico-chemical properties and can act as dynamic switching components in optoelectronic devices and functional materials.[22] The alterations in the electronic structure of the molecules typically result in variations of physical properties such as electrical conductance,[23-25] luminescence,[26-28] optical rotation,[29-31] and refractive index.[32-37] Photons are a particularly practical stimuli as modern lasers are monochromatic, can be tuned, and offer fast response times along with highly localized areas of exposure.

1.6   Photochromism

Photochromism is the light-induced interconversion between different isomers having different absorption spectra. Molecules that are capable of

12

interconverting between two isomers that differ are termed photochromic compounds (Equation 1.6.1). [22,38]

$$A \underset{h\nu_2}{\overset{h\nu_1}{\rightleftharpoons}} B$$
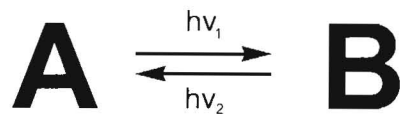
Equation 1.6.1 Irradiation of isomer **A** with one wavelength of light ($h\nu_1$) results in a photoisomerization reaction producing isomer **B**. The reverse reaction is performed by irradiation of isomer **B** with a different wavelength of light ($h\nu_2$).

As it is desirable to independently address each state of the molecule, the isomers should have well separated absorption bands in the UV-Vis absorption spectrum. Figure 1.6.1 outlines a representative example for the absorption spectrum of a photoinduced isomerization between isomers **A** and **B**.
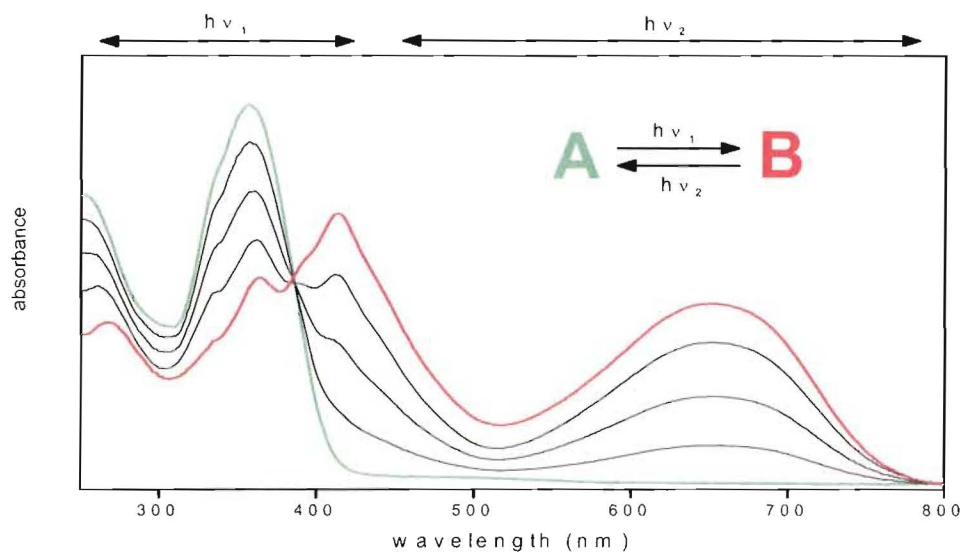
Figure 1.6.1. Irradiation of **A** at a wavelength in the UV region ($h\nu_1$) results in a decrease of the absorption band in the UV region. Simultaneously there is an increase of an absorption band in the visible region due to the production of isomer **B**. Irradiation of **B** at a wavelength in the visible region ($h\nu_2$) results in a reverse isomerisation reaction back to isomer **A**.

The *isobestic point* is the wavelength where the absorption spectra in the photochemical isomerisation reaction intersect. It is at this wavelength where the sum of the absorbance of all species present in solution remains constant. An isobestic implies that the photoisomerization between the two forms is a one step process provided that there are no other species present that absorb at the wavelength of the isobestic point. For the purposes of this thesis the presence of an isobestic in the UV-VIS absorption spectra will indicate a "clean" conversion between the two isomers.

1.7 Requirements for Photochromic Compounds

In order to be practical for use in functioning materials technologies photochromic compounds must satisfy numerous physical and chemical requirements. The vast majority of photoswitchable molecular architectures are limited by: (1) the thermal reversibility of the photochromic reactions, (2) the low fatigue resistance over repetitive cycles, (3) the efficiency of both the forward and reverse photoreactions, and (4) the difficulties associated with synthetic modification of the molecular scaffold.[21,22,36] Among the many photochromic materials available, dithienylethenes (DTE) are the most promising for technological applications since they usually satisfy all the fundamental requirements for the production of a device.[25,32,39]

1.8 Dithienylethenes

The vast majority of photoswitchable systems are unable to meet the stringent requirements needed for practical use in functional material technologies. Compounds possessing the 1,2-dithienylethene backbone are the most promising candidates for the elaboration of devices exhibiting photoswitched properties, such as light absorption[40], fluorescence[41], electronic conduction[42], and light refraction [43] (Equation 1.8.1).
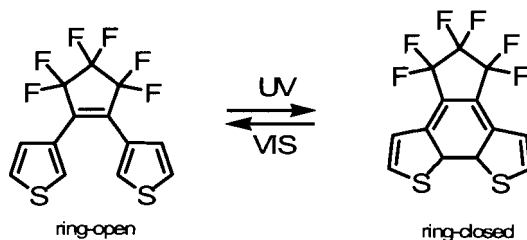
Equation 1.8.1 A photoswitchable Dithienylethene

DTE derivatives exhibit an impressive degree of thermal stability of the two isomers (remains cyclized in the dark for >3 months at 80°C), efficiency of the photochromic process – in terms of sensitivity and response time to electromagnetic stimulus, and high fatigue resistance (>10,000 cycles).[44-51] Dithienylethenes are also of interest since their isomerization requires very little change of shape. This means that their isomerization in a solid matrix can take place much more quickly than with most other photochromic molecules.[36]

The photochromic reaction of these compounds belongs to the class of electrocyclic reactions according to Woodward and Hoffman, and can be viewed as a reversible interconversion between a cross conjugated "open form" and a linearly π-conjugated "closed form" (Equation 1.8.2). [52,53]
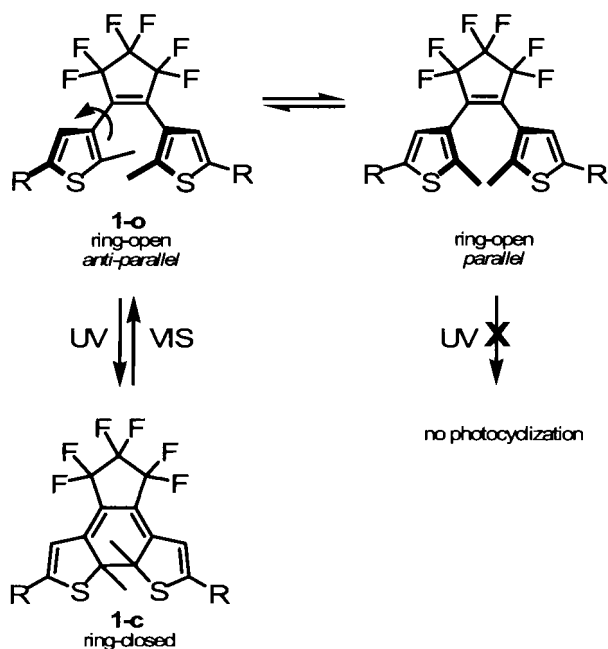
Equation 1.8.2 The photoisomerization of dithienylalkenes. While ring-open isomer can adopt both parallel and antiparallel conformations, only the antiparallel conformer photocyclizes.

DTEs contain hexatriene skeletons that undergo a reversible 6π-electrocyclization reaction. Light activation of the ring-open isomer promotes an electron from the ground state HOMO of the 1,3,5-hexatriene system into the LUMO. Ring-closure can only occur via a conrotatory process (both reacting orbitals turn in the same direction) due to preservation of the π-orbital symmetry. Consequently only the photoexcited antiparallel conformer will ring close.[36,38] Disrotatory ring-closure (both reacting orbitals turn in the opposite direction) is thermally allowed from the parallel ground state, however does not occur practically due to the large activation barrier imposed by the steric hindrance of the central methyl substituents, and an energetically unfavourable product.[51]

The photoinduced electrocyclization from **1-o** to **1-c**, responsible for the increase in the electronic delocalization of the molecule, also generates an increase of the polarizability of the electronic cloud of the photochromes (Equation 1.8.3). They are then able to change the refractive index of the medium in which they are incorporated.[54-57] The magnitude of change in refractive index is correlated to the change in the length of conjugation.[15]
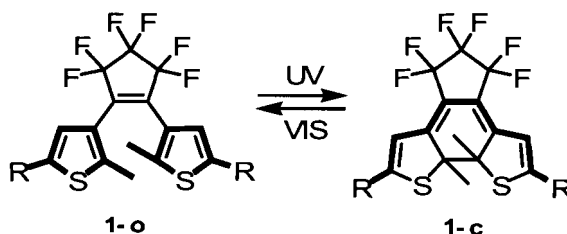
Equation 1.8.3 The isomerization of **1-o** to **1-c** is accompanied with a change of conjugation along the backbone. Delocalization of the electron cloud across the molecule increases polarizability.

While dithienylethenes demonstrate properties necessary for a practical functioning material (thermal irreversibility, high efficiency, extreme fatigue resistance), they also have drawbacks that limit the scope of their use in optical device applications. DTEs have a limited number of sites available for functionalization and they display a reduction in the efficiency of photoreactions as conjugation length is increased.[58]

1.9 Photostationary State

It is ideal if the two isomers of a photochromic system absorb in well-separated regions of the UV-VIS spectrum whereby each isomer can be irradiated independently. Nevertheless organic photochromic compounds commonly have individual isomers with absorption bands located in the same region of the spectrum. The area defined as $h\nu_1$ in Figure 1.6.1 affords absorption by both isomers **A** and **B**. Consequently, irradiating at a wavelength of light within this "crossover" region results in two competing photoisomerization reactions (**A** $\rightarrow$ **B**, and **B** $\rightarrow$ **A**). The *photostationary state* (PSS) or photoconversion is the point at which equilibrium at a given wavelength is reached and is defined by Equation 1.9.1.[59]

$$PSS = \frac{\text{\# of molecules that isomerized}}{\text{total \# of molecules}} \cdot 100\%$$

Equation 1.9.1 Photostationary state.

^{1}H NMR spectroscopy is useful for monitoring the progress and photostationary state of photochemical interconversion. The extent of ring-cyclization can be obtained by measuring the relative integrals of the areas under the peaks for corresponding pairs of signals for the ring-open and the ring-closed isomers. Typically, any set of protons giving distinct, well resolved resonances for both photoisomers can be used to measure the extent of photocyclization. The

photostationary state is reached at the point where additional irradiation no longer results in any change to the corresponding ring-open and ring-closed integrals. Photochromic systems capable of being fully converted between isomers are of great importance since they provide a handle for complete "on-off" type of switching.[60]

1.10 Photochemical Cycling

In order to be a functional switching element that will allow the properties and functions of a device to be turned "on" and "off" on demand, dithienylethene based materials must be capable of interconverting between their ring-open and ring-closed form without degrading or forming photochemical side-products, a property termed as *photofatigue resistance*. Compounds that can undergo numerous cycles without significant photodegradation are termed photofatigue resistant. Dithienylethenes have high photofatigue resistance and can be cycled up to 10,000 times with little observable degredation.[36] Photofatigue resistance results over hundreds of cycles are typically obtained using an automated cycling system. As this apparatus was not available in our research group, manual cycling experiments were performed by alternate irradiation with UV and visible light, while the UV-VIS absorption spectrum was concurrently monitored over ten cycles.

1.11 Photochromic Compounds Based on a Mono-Thienylcyclopentene Backbone

Dithienylethenes have a limited number of sites where functional groups may be attached, primarily the 2- and 5-positions of the heterocycles (A and B, respectively in Equation 1.11.1).
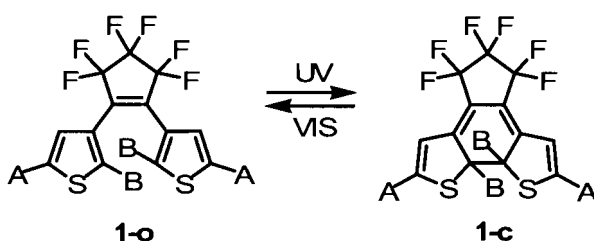
Equation 1.11.1 A DTE derivative

It is often the case that introduction of particular functional groups at these sites results in thermal reversibility[61] or poor efficiency of the photoreactions.[62]

Increasing the length of the conjugated substituents on the heterocycles shows a decrease of efficiency for both the ring-opening and the ring-closing reactions. Irie et al.[63] reported that the photochromic reactivity of oligothiophene substituted 1,2-dithienylcyclopentenes decreases with increasing chain length of the oligothiophene unit. In the extreme case,[58] a DTE derivative incorporating carotenoids reached an upper limit of π-conjugation length where the ring-opening reaction no longer occurred (Figure 1.11.1). It was suggested that the

inhibition of the ring-opening photoreaction is due to a reduced excitation density at the central 1,2-dithienylperfluorocyclopentene unit (DCTFP), with the majority of excitation density residing mainly on the carotenoid substituents. Derivatives beyond the limit of conjugation act as unidirectional photoswitches only, generating photostable closed isomers. Due to this threshold of π-conjugation across the backbone of the molecule, electron delocalization and polarizability are also restricted.
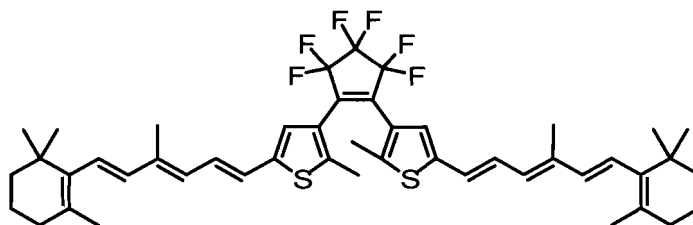
Figure 1.11.1 A carotenoid DTE derivative.

Recently Branda and Peters,[64] and Yokoyama[65] investigated the photochromic properties of a modified hexatriene system that is similar in structure to 1,2-dithienylethenes except that one of the thiophenes rings has been replaced with a substituted olefin (Equation 1.11.2).

R=CH₃ or Ph
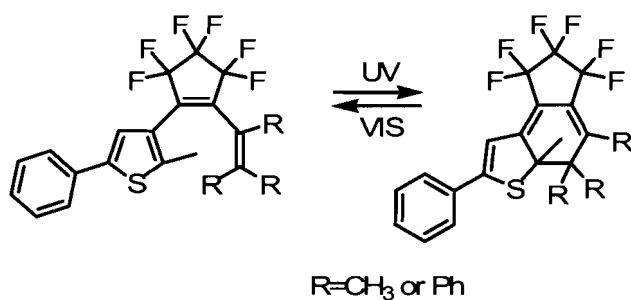
Equation 1.11.2 A modified hexatriene scaffold based on 1,2-dithienylethenes.

This novel molecular scaffold presents an opportunity to design uniquely tailored systems unavailable to traditional DTE architecture without sacrificing photochromic behaviour. The use of this backbone has led to the development of an alternative polarisable π-conjugated framework, where the presence of strong electron donor and acceptor groups at opposite ends of the linear π-pathway creates an asymmetric charge distribution (Equation 1.11.3).
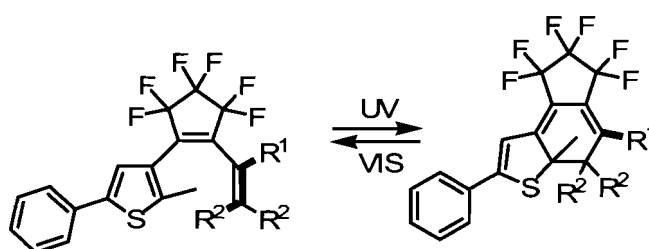
Equation 1.11.3 An alternative π-conjugated pathway. Isomerization is accompanied with a change in conjugation.

1.12 A Donor-π-Linker-Acceptor System

The restrictions with the DTE architecture include a limited number of available sites for functionalization and an upper limit of π-conjugation along the backbone where the ring-opening reaction no longer occurs. A new molecular scaffold that replaces one of the thiophene heterocycles with a trisubstituted alkene produces a hexatriene that overcomes these limitations. Recently, Branda and Wüstenberg[17] demonstrated a novel design having strong charge transfer excitations within a non-centrosymmetric structure. By incorporating strong electron donor and acceptor groups at opposite ends of this new linear π-pathway it is possible to create an asymmetric charge distribution. The structural motif can be simplified to a donor-(π-linker)-acceptor (D-π-A) architecture (Equation 1.12.1).

DCTE-o   **DCTE-c**
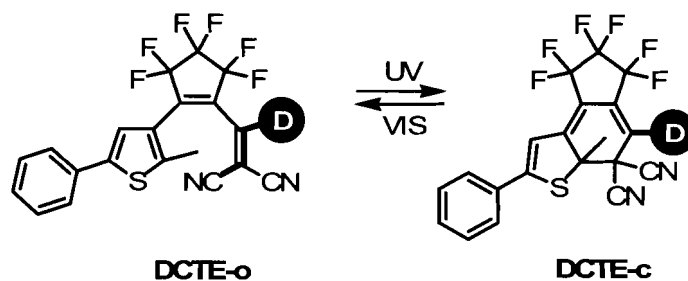
Equation 1.12.1 Photoswitching of the linear π-conjugation in the D-π-A system between the ring-open form (DCTE-o) and the ring-closed form (DCTE-c).

The D-π-A component in the illustrated dicyanoethylene-thienylethene (DCTE) architecture exists only when the compound is in its ring-open form

24

(DCTE-o), in which the linear π-pathway can be traced between the dicyanoethylene acceptor group and the appropriately place donor (highlighted in Equation 1.12.1). The change in hybridization of the carbon involved in forming the new C-C single bond from sp^2 to sp^3 introduces a break in the linear π-conjugated pathway and insulates the donor from the acceptor. Photoregulation of the D-π-A pathway allows reversible modulation of both the π-conjugated framework and any strong charge-transfer excitations between the donor and acceptor. A molecule with such design will provide the capacity to control nonlinear optic susceptibilities and the properties associated with them. This thesis will investigate the changes in refractive index of a series of novel molecules that integrate the D-π-A pathway within the DCTE architecture.

1.13 Preview

The work presented in this thesis has focused on investigating the refractive index change of novel photochromic dicyanoethylene-thienylethene architectures.

Chapter 2 discusses the synthesis and properties of a DCTE series and a reference DTE hydrazone derivative. The potential polarizability changes of this sequence of molecules is examined through computer modelling, and photochromic reactions of the designs are reported, including UV-VIS characterization, photostationary state, and photofatigue analysis.

Chapter 3 focuses on the application of spectroscopic ellipsometry for measuring light induced refractive index changes in the DCTE series generated in chapter 2. Photoinduced refractive index, the relationship between refractive index and polarizability, and previous models presented for applications in photonic integrated circuits are discussed. Fabricated films comprising of the active chromophores doped in PMMA are characterized by spectroscopic ellipsometry, atomic force microscopy and x-ray diffraction. The index of refraction of these films are modelled through ellipsometric data, and the modulated change in refractive index between ring-open and ring-closed isomers is resolved. Film properties such as thickness, surface roughness, volume change, and crystallographic structure are determined. The chapter concludes with a discussion of the results of this research and identifies potential areas for further research within this project.

2 Design of DCTE Systems

2.1 D-π-A Architectures for Modulating Refractive Index

In order to integrate photoresponsive elements into the D-π-A framework,

a "hybrid" architecture was developed which has the appealing properties of both

systems.[17] These novel molecules provide mechanisms to regulate the electronic

communication between donor and acceptor components. The concept is

illustrated in Equation 2.1.1.

DCTE-o   **DCTE-c**
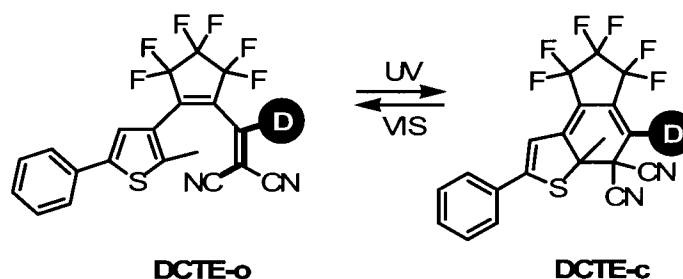
Equation 2.1.1 Photoswitching of the linear π-conjugation between donor and acceptor groups in a D-π-A system.

The depicted dicyanoethylene-thienylene (DCTE) architecture permits the

D-π-A element in its ring-open (DCTE-o) form only. This linear π-pathway can be

traced between the dicyanoethylene acceptor group and the represented donor.

Irradiation with UV light produces the ring-closed isomer and introduces a break

in the π-bridge. Electronic communication between the donor and acceptor group

becomes insulated. The process is reversible with exposure to visible light, which

provides for the controlled modulation of NLO properties associated with the first hyperpolarizability β, such as the index of refraction.

2.2 Synthetic Methods

A series of photoresponsive DCTE systems **3-9** were synthesized for photoswitchable refractive index studies (Scheme 2.2.1). The molecules were selected to exhibit a progression in the respective donor strength, beginning with a non-donating hydrogen **3** through to a trimethoxy benzene **7**. A withdrawing nitro group **8** was also considered in order to observe the effect, if any, of a dual acceptor assembly. In an attempt to create a benzyl acid chloride group for further functionalization, the bis switch **9** was formed. Preparation of **3o-8o** begins with 2-methyl-3-(perfluorocyclopent-1-enyl)-5-phenylthiophene (**1**), which has previously been shown to be a useful starting material for the preparation of dissymmetric photoswitches.[64] While treatment of **1** with sodium iodide in DMF at 150 °C produces 3-(3,3,4,4,5,5-hexafluoro-2-iodocyclopent-1-enyl)-2-methyl-5-phenylthiophene (**2**) at 12-15 % yields, changing the solvent to dimethylacetamide (DMAc) and increasing the temperature to 165 °C increases the reaction efficiency to 25%. In both cases the starting material (**1**) was recovered for further reactions. Addition of 12-crown-4 and 15-crown-5 in an attempt to coordinate free sodium ions did not show any improvement on reaction yields.

The anion generated from **2** and *n*-butyllithium treated with dimethylformamide (DMF) or the corresponding organozinc derivative of **2** and the appropriate acid chloride,[17] which is catalyzed by a solution prepared from

[Pd(PPh$_3$)$_2$]Cl$_2$ and i-Bu$_2$AlH dissolved in anhydrous benzene. Zinc and catalyst are not required for addition of the nitrobenzene acid chloride, although their use did not reduce or improve reaction yields. The aldehyde **3'** and corresponding ketones **4'- 8'** were then reacted with malanonitrile to afford the DCTE derivatives **4-8**.[17] While addition of 4-(dimethylamino)benzoyl chloride to the **2** did yield the corresponding ketone, treatment of the resultant dimethylamino ketone with malanonitrile resulted in no product. Substitution of titanium chloride with titanium isopropoxide did not improve these results.
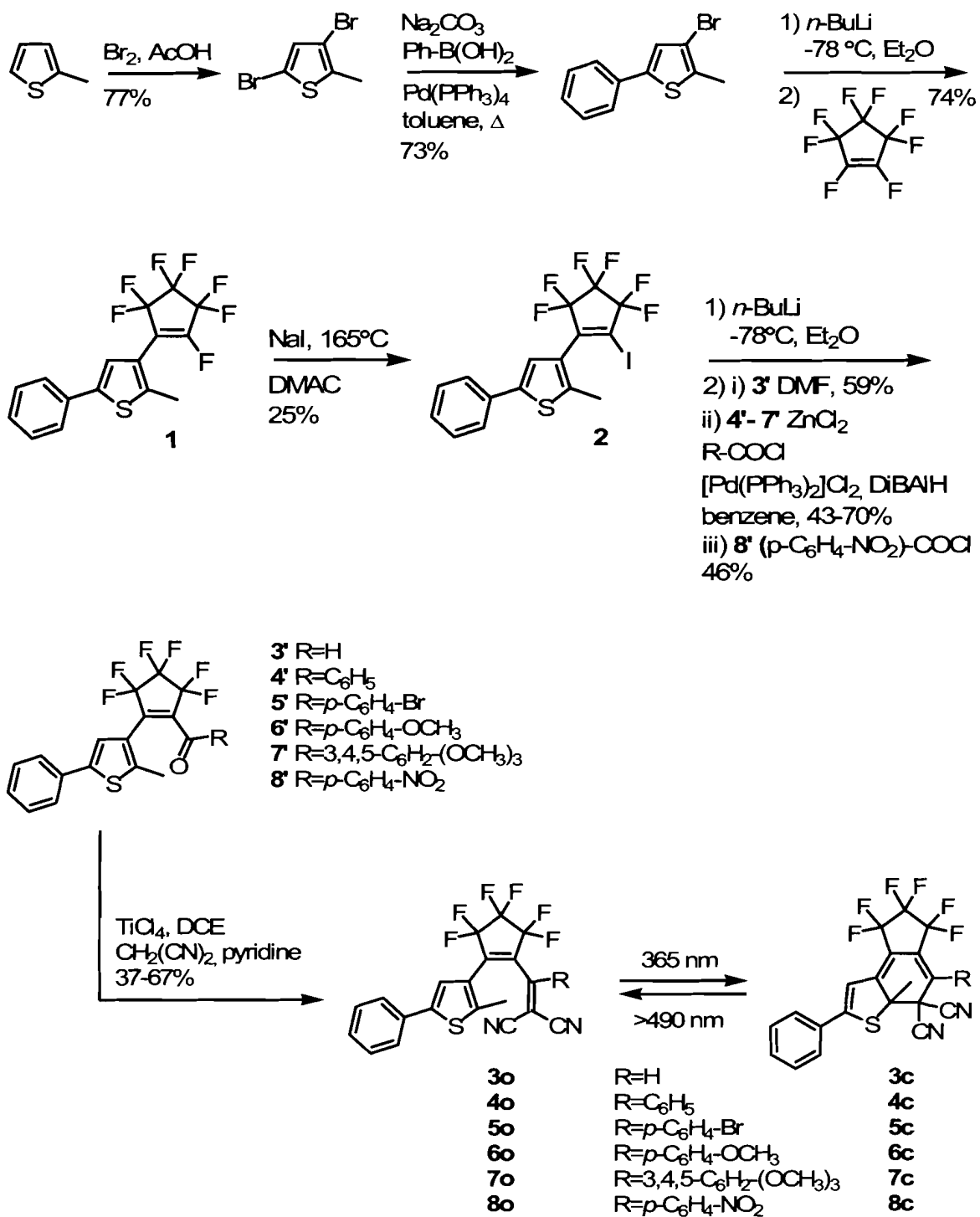
Scheme 2.2.1 Synthesis and photochromic reactions of DCTE derivatives.

Compound **9** was an unexpected product in the attempt to affix terephthaloyl chloride (Scheme 2.2.2).

Structure **2**

1) n-BuLi
   -78°C, Et₂O
2) ZnCl₂
3) terephthaloyl chloride
   [Pd(PPh₃)₂]Cl₂, DiBAlH
   benzene, 38%

Structure **9'**

TiCl₄, DCE
CH₂(CN)₂, pyridine
48%

Structure **9oo**

365 nm ⇅ >490 nm
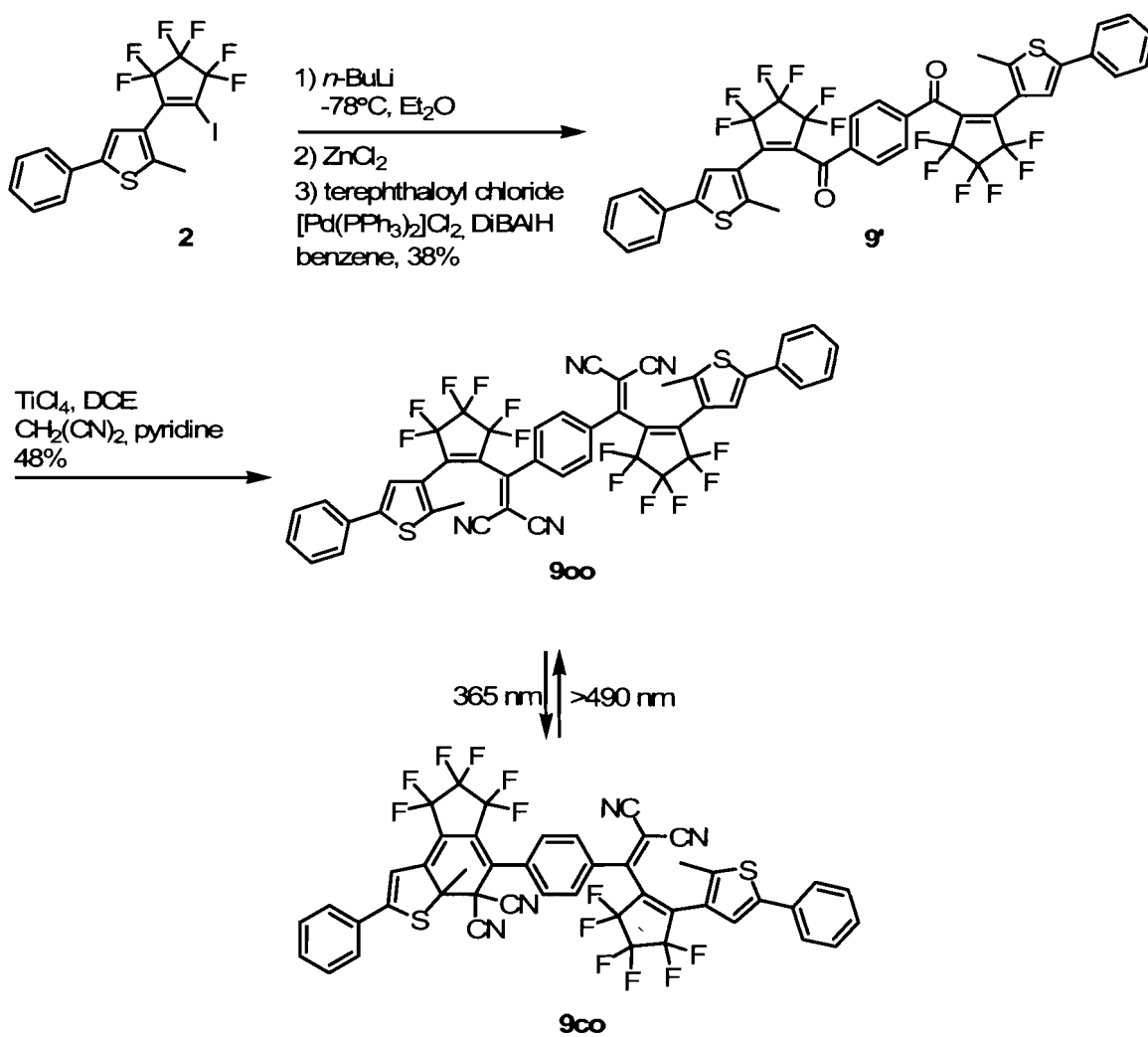
Structure **9co**

Scheme 2.2.2 Synthesis and photochromic reaction of a Bis-DCTE derivative.

31

Although the bis-(dicyanoethylene-thienylene)- benzene structure in **9oo** does not provide the necessary D-π-A architecture required for NLO molecules, the ring closed isomer(s) suggest a more extensive π-conjugated backbone than **3-8** due to a second electrocyclic ring-closing reaction within the molecule. However, earlier reports[66] have shown that two dithienylcyclopentenes which are covalently linked together at the 5-positions through a conjugated spacer display inhibition of the second ring-closing reaction. *Ab initio* calculations show that the electron density predominantly resides on the conjugated framework that is produced during the first cyclization reaction, and not at the carbon of the terminal thiophene ring where the new bond in the second ring-closing reaction would be formed. It is believed that the lack of electron density at this reactive carbon centre may be the reason why the second cyclization is inhibited. ^{1}H NMR of **9c** irradiated with 365 nm light for 30 minutes suggests only a single side ring-closing reaction occurs within the molecule, characteristic of bis dithienylcyclopentenes. For the purposes of this thesis, **9c** will refer to the single ring-closed isomer of compound **9**.

In order to suitably assess the refractive index change of **3-9** it is important to associate them with a reference model. Zerbi and coworkers[67] measured an increase in refractive index for a DTE hydrazone **10** of Δn = 0.005 at 1500 nm. Due to equipment limitations within our research facilities, the method of thin film fabrication reported by Zerbi cannot be reproduced. In order to compare **3-9** with **10**, the DTE hydrazone was synthesized, fabricated and examined in an identical manner as the test materials (Scheme 2.2.3).
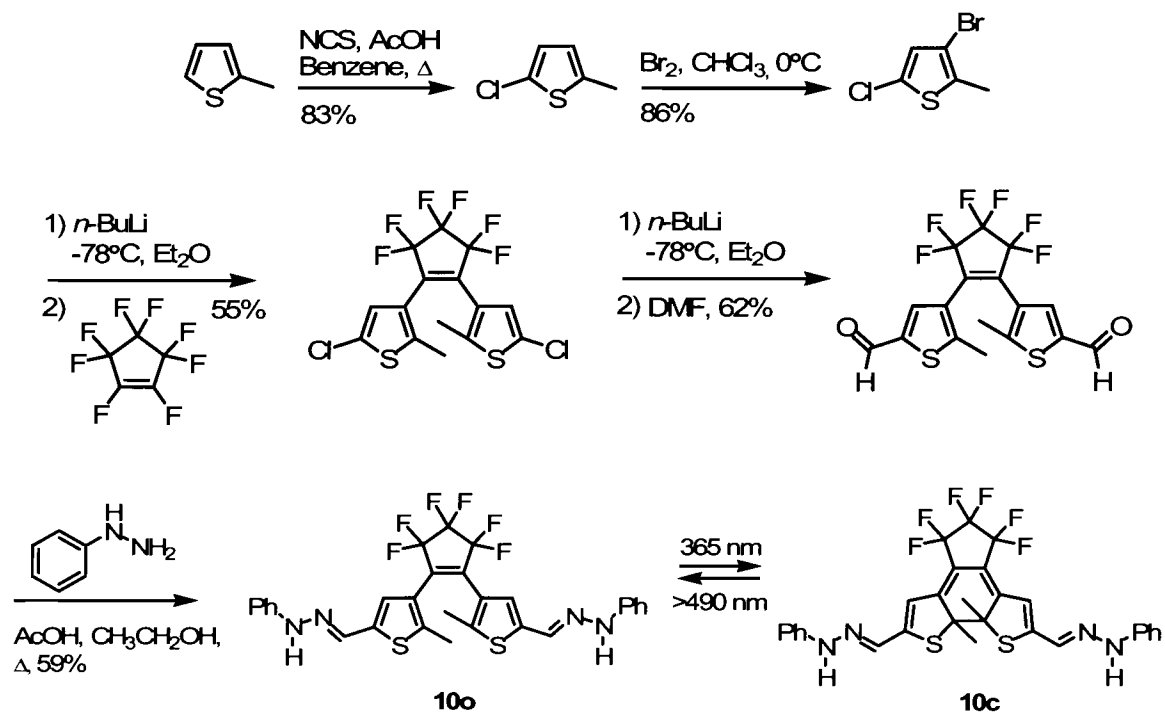
Scheme 2.2.3 Synthesis of a DTE Hydrazone derivative.[67]

2.3 Photochromic reactions of DCTE Designs

The results of the photoinduced isomerisation experiments, carried out by irradiating the CHCl$_3$ solutions (2x10^{-5} M in DCTE component) with 365 nm light using a hand-held UV lamp are summarized in Table 2.3.1.

Table 2.3.1 Photostationary state at 365 nm by ^{1}H NMR and UV-VIS characterization of DCTE ring-open and ring-closed isomers.

Sample	PSS (%)	λ_{max}(nm)/ϵ (10^4 Lmol^{-1}cm^{-1}) ring-open	λ_{max}(nm) /ϵ (10^4 Lmol^{-1}cm^{-1}) ring-closed (at PSS)
3	18%	281/1.39	444/0.40
4	38%	293/1.23	464/0.78
5	35%	261/0.92	470/0.72
6	56%	280/1.55	473/1.22
7	41%	281/1.06	481/0.59
8	40%	288/1.37	475/0.70
9	15%	287/1.35	486/0.61
10	60%	357/1.50	661/0.72

The photostationary states of **3-9** were determined by monitoring the photochromic interconversion between the ring-open and ring-closed isomers using ^{1}H NMR spectroscopy. Irradiation of CD_2Cl_2 solutions of **3o-9o** (2.3 x 10^{-3} M) with a handheld 365 nm light resulted in the appearance of a new peak, as a singlet, corresponding to the thiophene-C5 methyl group .The samples were irradiated with 365 nm light until no further change in the relative integration between the ring-open singlets and the ring-closed singlets was observed. The

photostatinary states were not optimized as the most favourable wavelength for each compound was not available. The photostationary state was determined by calculating the ratio of ring-closed isomer to total isomers.

UV-Vis spectra for **3-10** are shown in Figure 2.3.1a. Within the first 10 seconds of irradiation with 365 nm light, new absorption bands appear in the visible region of the UV spectra as the compounds are converted to their coloured ring-closed isomers. At the concentrations used (2×10^{-5} M), increases in the visible bands level off after 180 seconds of irradiation, with the exception of **7** which did not level off until after 240 seconds. The resulting coloured solutions can be decolourized by irradiation with a 150-W tungsten light source fitted with a 490 nm cut off filter to eliminate higher energy levels, which resulted in the complete disappearance of the absorption bands in the visible region of the UV spectrum. The ring-closing and ring-opening isomerisation reactions were repeated over ten cycles in order to determine the photochromic performance. No significant degradation to side products from the photoreactions occurred after 10 cycles as indicated by the lack of decrease of the modulated absorbance values in Figure 2.3.1b.

(a) **3**

(b)

(a) **4**

(b)

(a) **5**

(b)

36

(a) **6**

(b)

(a) **7**

(b)

(a) **8**

(b)

37

(a) **9**

(b)

(a) **10**
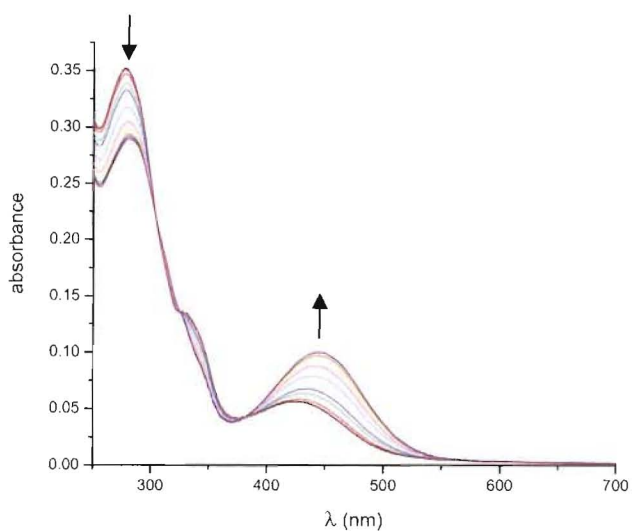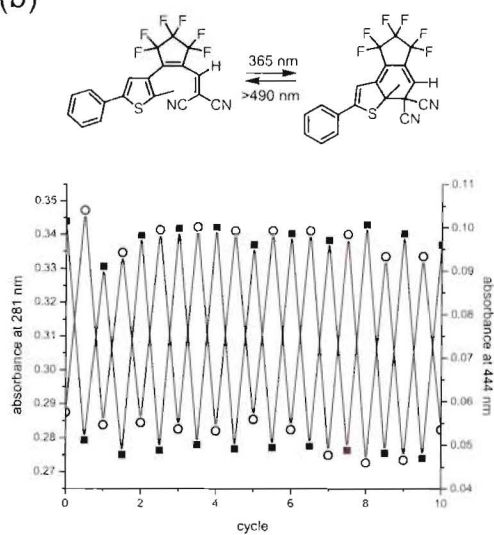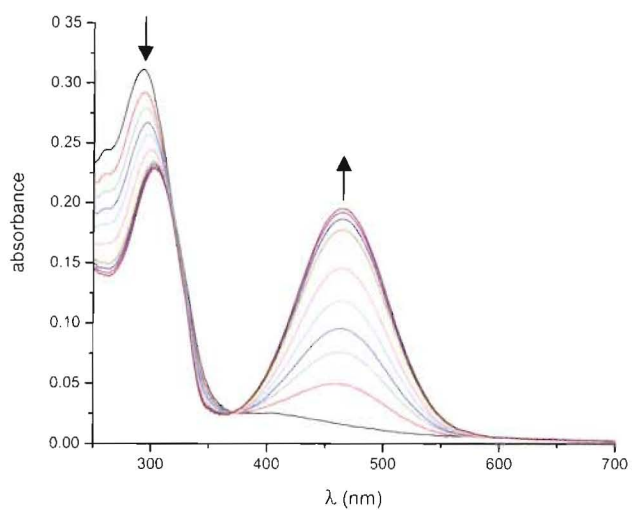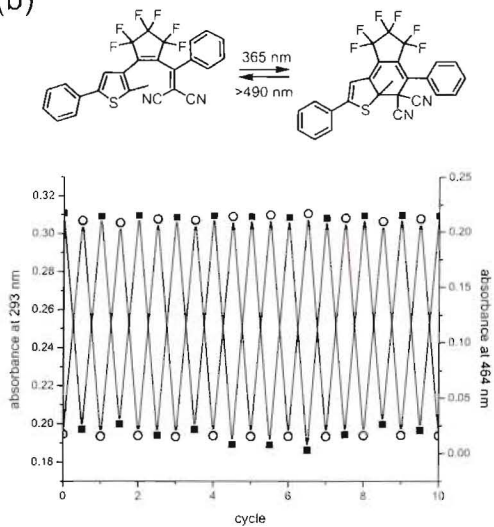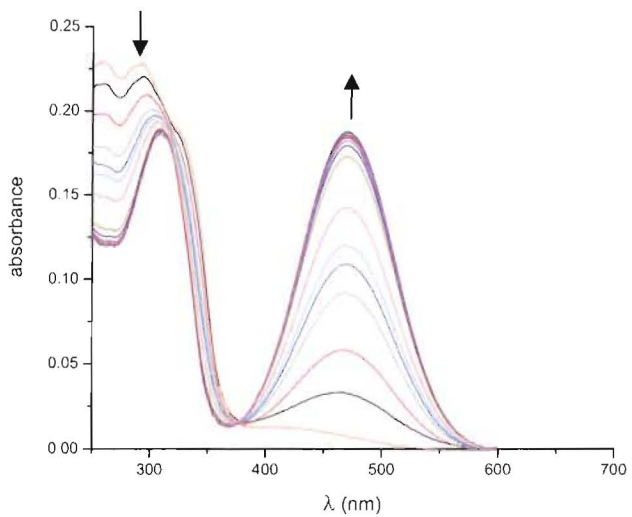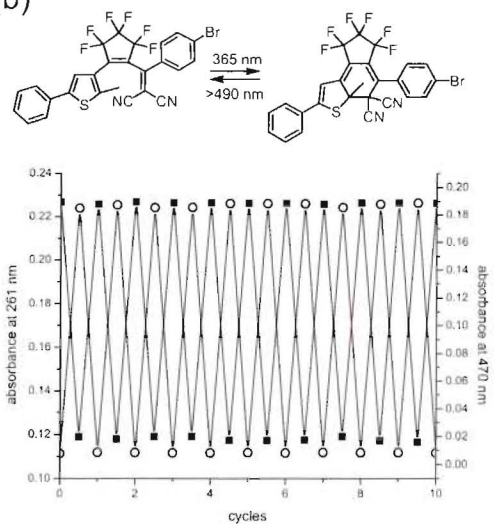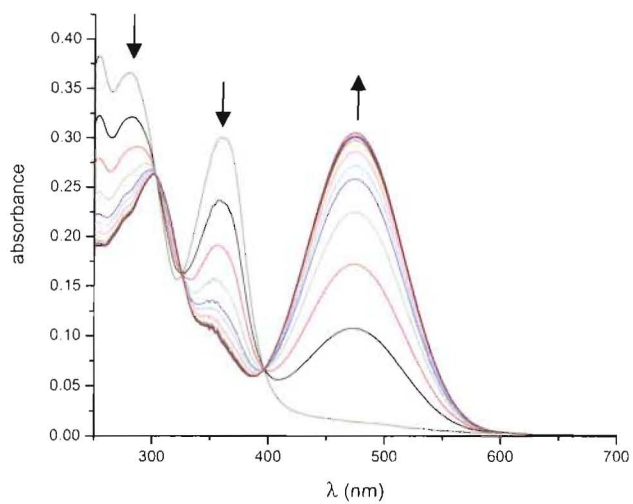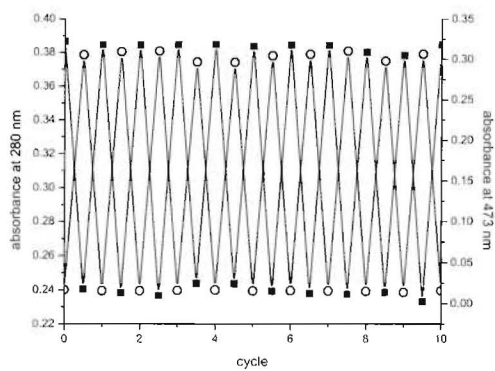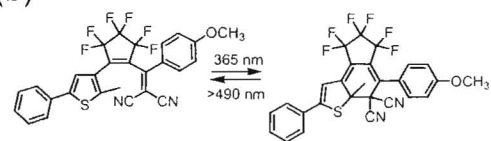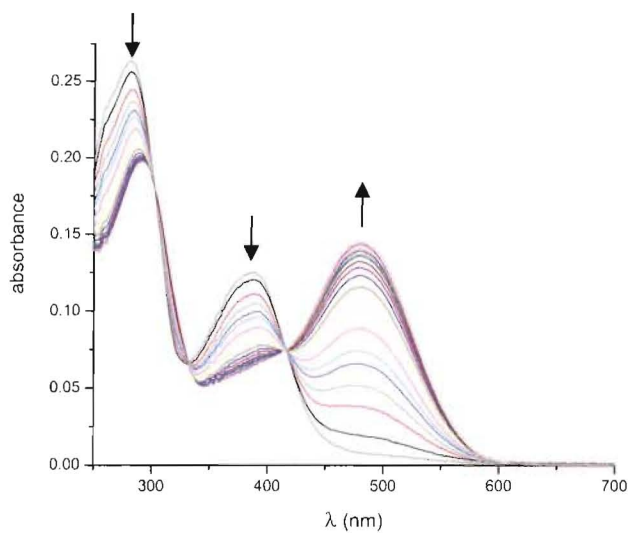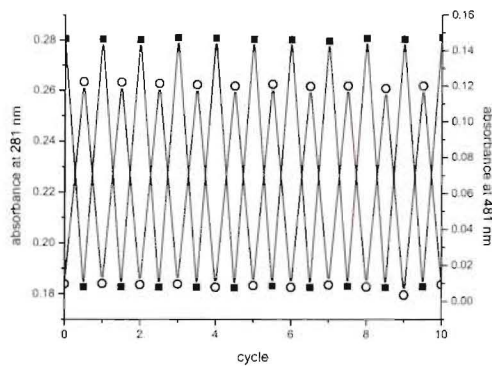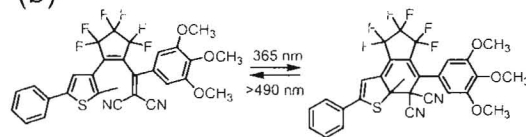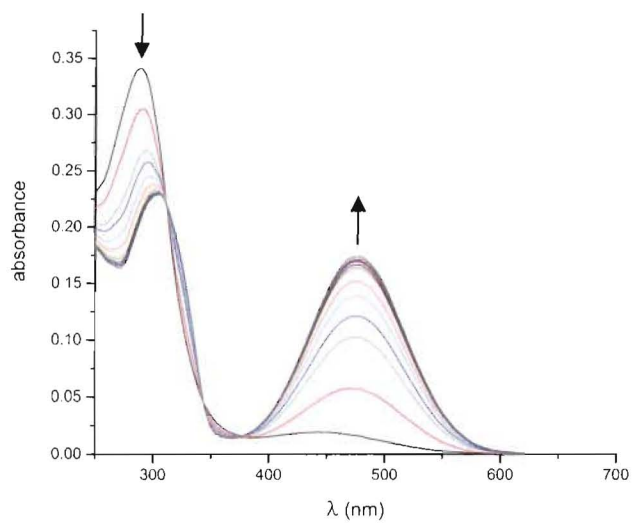
(b)
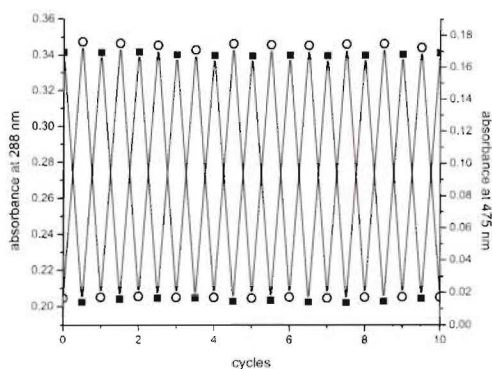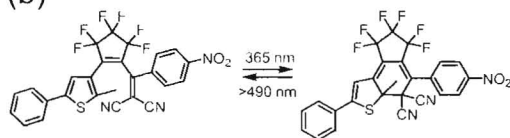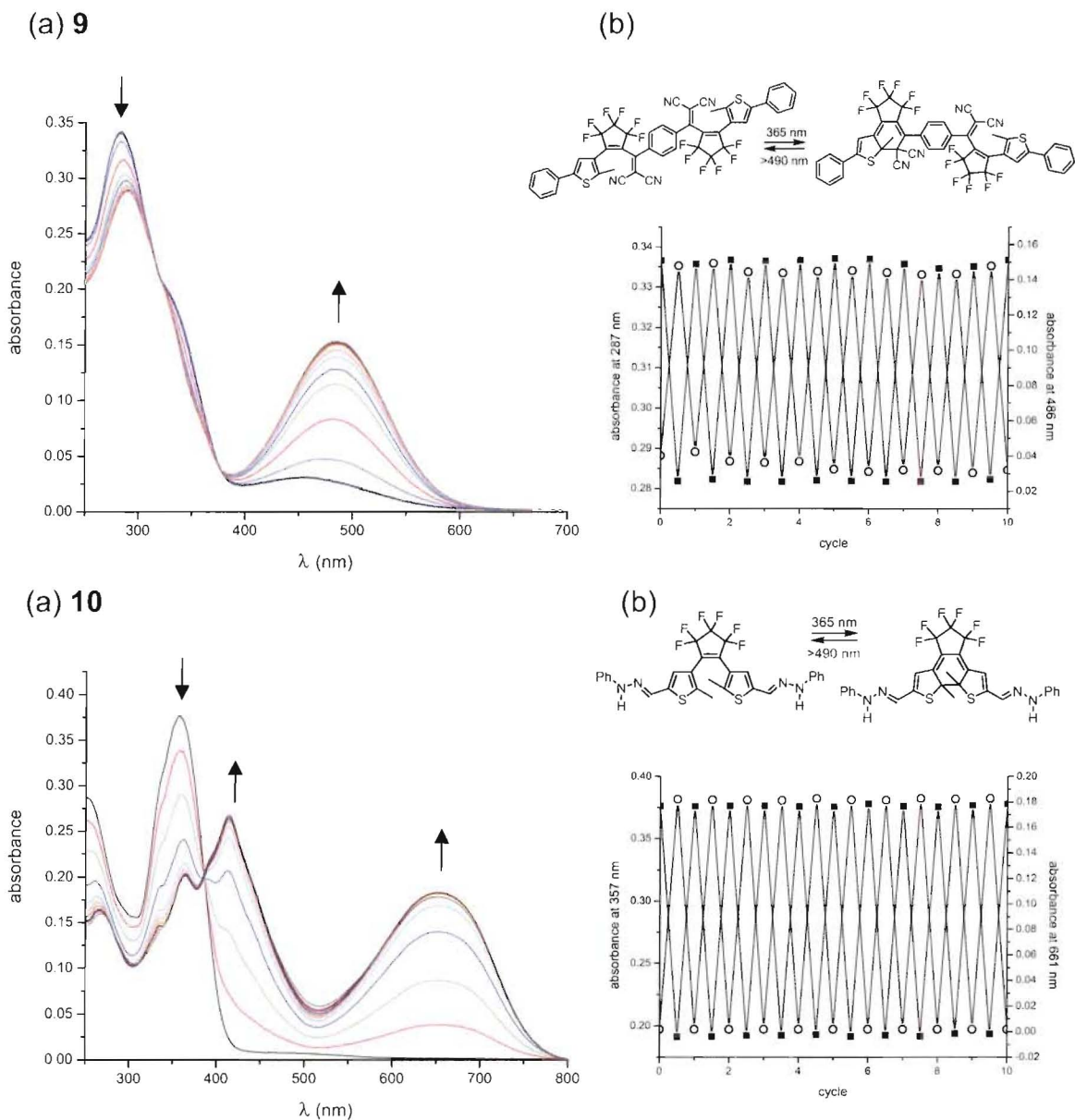
Figure 2.3.1 (a) Representative changes in the UV-Vis absorption spectra of DCTE derivatives and DTE hydrazone upon irradiation with 365 nm light. Total irradiation periods are 0, 10, 20, 30, 40, 50, 60, 70, 80, 90, 120, 180, 240 seconds. All concentrations are 2×10^{-5} M in CH_2Cl_2 with respect to the photochromic unit. (b) Modulated absorbance at 365 nm for ring-open (■) and ring-closed (o) λ_{max} during alternate irradiation with 365 nm light for 240 sec, then >490 for 180 sec.

38

2.4 Ring-open and Ring-closed Polarizability

The series of compounds **3-9** were developed in order to investigate any trends in refractive index change which may be associated with molecular structure. The predicted differences in refractive index between the ring-open and ring-closed isomers are due to differences in the polarizability of the two isomers. Both isomers are comprised of two different intramolecular π-conjugated pathways that exhibit dissimilar polarization changes in response to an external field (Scheme 2.4.1).

1o   **1c**

— D-π-A pathway 1
— backbone pathway 2
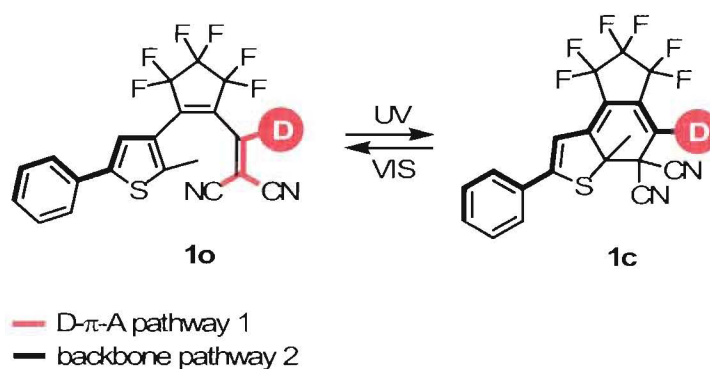
Scheme 2.4.1 Alternating π-conjugated pathways within ring-open and ring-closed isomers. Photocylization reduces the polarizability along pathway 1, while simultaneously increases the polarizability along pathway 2.

The ring-open isomers are characterized by a D-π-A architecture (pathway 1) resulting in high first and second order polarizabilities, while the backbone (pathway 2) maintains π-electron density localized on the aromatic rings. The ring-closed isomer introduces a break in the D-π-A system (pathway

1), insulating electronic communication between the donor and acceptor, resulting in reduced second order polarizability. The π-electron density of the ring-closed isomer is distributed along the linear π-conjugated backbone (pathway 2), resulting in a higher polarizablity than in the ring-open form.

The polarizability of pathway 1 and pathway 2 within each isomer will have dissimilar responses to an external field. It isexpected that the highly polarisable D-π-A pathway of the ring-open isomer will increase the refractive index of the molecular material, while the localized π-electron density on the backbone is less polarisable. The interrupted D-π-A pathway of the ring-open isomer will see a reduction of polarizability and a subsequent decrease in refractive index, while the delocalized π-electron density of the extended π-conjugated backbone will increase refractive index due to higher polarizability. Predicting the net static polarizability within each isomer can be achieved using commercially available software.

2.4.1 Predicting Static Polarizability

In order to determine the static polarizability (α) of both isomers, molecular modelling calculations (semi-empirical AM1) were performed. In order to determine the validity of AM1 calculations for estimating static polarizability, the known α values[68] for a series of substituted benzene derivatives was compared to the calculated values (Table 2.4.1). [69]

Table 2.4.1 Calculated static polarizabilites compared to reference values for a series of substituted benzene derivatives.

Compound	α_{calc} $(\times 10^{-30}\,\mathrm{m}^3)^a$	α_{ref} $(\times 10^{-30}\,\mathrm{m}^3)^b$
benzene	48.4	10.2
phenol	52.5	10.5
toluene	58.4	12.1
aniline	57.8	12.1
anisole	62.0	13.1
nitrobenzene	63.2	13.8

[a] Semi-empirical AM1 calculations of static polarizability using the POLAR function in Spartan™ '02 for Macintosh. [b] Reference values were determined experimentally.

While the trends of α_{calc} and α_{ref} are the same, Table 2.4.1 shows that AM1 calculations over estimate-values of static polarizability. In order to accurately predict α values for the DCTE isomers in this study, the calculated values must be corrected for any ambiguity. This correction can be achieved by using a linear least squares regression analysis of the data. Plotting the α_{ref} against the α_{calc} generates a linear relationship and provides a correction factor that can be used for other compounds (Figure 2.4.1). While the regression analysis does not offer an optimal fit to the data (R=0.96), the trend suggests overall that polarizability

will increase with photocyclization to the extended conjugation of the ring-closed isomer.
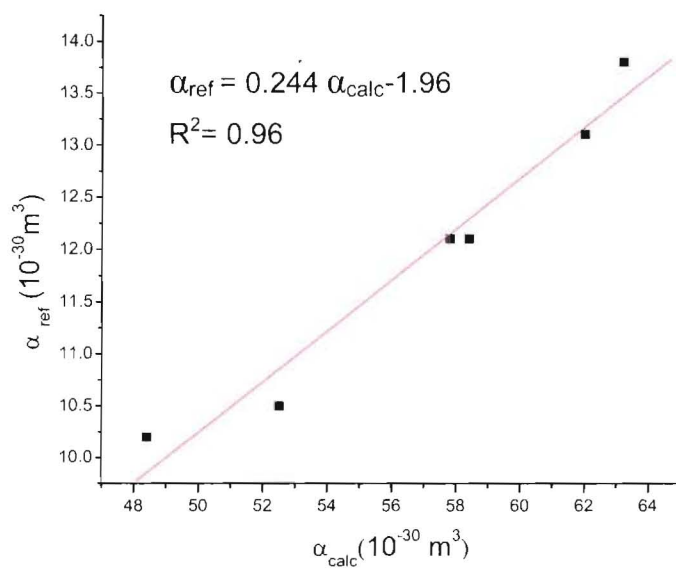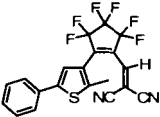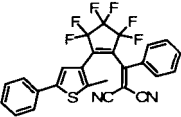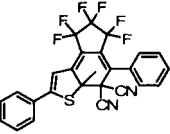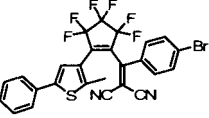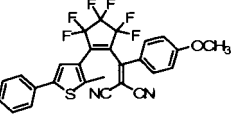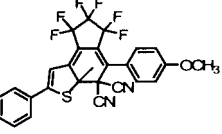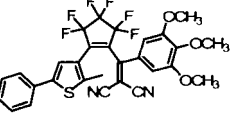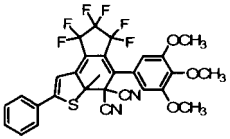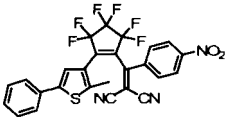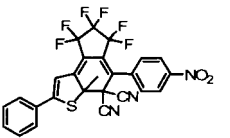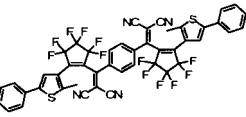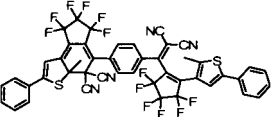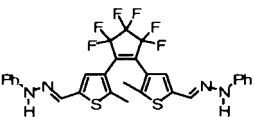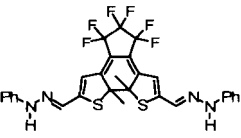
Figure 2.4.1 Correlelation between AM1 calculated and reference polarizabilities.

Calculated and subsequently corrected polarizability values for **3-10** are summarized in (Table 2.4.2).

Table 2.4.2 Calculated static polarizabilites compared to corrected values for a series of DCTE derivatives.

Structure	α_{calc} [a] $(x10^{-30} m^3)$	corrected α [b] $(x10^{-30} m^{3)}$	Volume [b] $(\text{Å})^3$
3o	218.9	51.2	326.9
3c	224.0	52.7	321.5
4o	267.2	63.2	398.5
4c	286.2	67.9	392.9
5o	279.9	66.3	417.7
5c	301.2	71.5	412.1
6o	285.1	67.6	424.2
6c	306.8	72.8	418.3
7o	314.3	74.7	474.8

7c		335.8	80.0	469.3
8o		285.7	67.8	421.5
8c		308.0	73.1	415.8
9o		488.5	117.2	711.9
9c		514.1	123.4	707.0
10o		362.7	86.5	452.0
10c		384.0	91.7	447.7

[a] Semi-empirical AM1 calculations of static polarizability and volume using the POLAR function in Spartan™ '02 for Macintosh. [b] The calculated polarizability values were corrected using the linear least squares fit provided in Figure 2.4.1.

The corrected polarizabilities in Table 2.4.2 show an increase in α when the compound is isomerized to the ring closed form in all cases. These values suggest that the observed refractive index should increase upon photocyclization from the ring-open to the ring-closed isomer, however these values do not

consider any second order effects associated with the highly polarisable D-π-A pathway. Therefore, any effects due to the D-π-A pathway must be determined experimentally.

2.4.2 Determining Second-order Polarizability

The AM1 software utilized is only able to predict the static polarizability (α) of a molecule. The calculations do not consider any NLO properties of the structure and cannot resolve any second-order polarizability (β) which may affect the index of refraction of the material. In fact, determining second-order nonlinear effects experimentally proves to be a considerable challenge. Second-harmonic effects require non-centrosymmetry at the molecular level and macroscopic level. A solution containing nonlinear optical active molecules is isotropic, and no second-harmonic generation (SHG) can occur in attempted polarization. Nonlinear chromophores can be incorporated into thin solid films, however the non-centrosymmetry rule remains. This requires the sample to be ordered in one way. Typically, dipolar chromophores are dissolved into a polymer host or attached to a polymer backbone, and then spin coated to generate a thin film. To achieve the necessary non-centrosymmetry the chromophores in the polymer matrix need to be poled (Figure 2.4.2). [16]
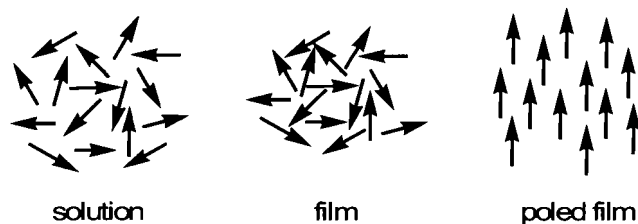
Figure 2.4.2 Representation of chromophore ordering in macroscopic materials.

Poling is done by aligning the dipolar chromophores with a strong orientating electric field (electric field poling), while heating the polymer to its glass transition temperature where it becomes rubbery. Cooling the system in the presence of the field freezes the orientation of the chromophores. Unfortunately, organic materials synthesized for incorporation into nonlinear optical polymers exhibit tradeoffs between nonlinearity and physical properties, such as thermal and chemical stability, and low optical loss (high transparency). Organic molecules for NLO applications need to endure extremely high temperatures during fabrication processes, which has proven to be extremely difficult without compromising the molecules nonlinearity.[7] In this thesis, poling was not performed due to equipment limitations and the need to research isotropic films first. Therefore, the photoinduced refractive index change of **3-10** in amorphous doped polymer films will be determined through spectroscopic ellipsometry.

3 Refractive Index Changes by Spectroscopic Ellipsometry

3.1 Introduction to optical switching and refractive index

The need for materials with a refractive index that can be modulated by using electromagnetic radiation is widely recognized.[70-72] Photoinduced refractive index changes in dye-doped polymer films have considerable potential for use in optoelectronic devices such as modulators, diffraction gratings, and optical waveguides.[73] The advent of such photonic devices, which allow local changes of refractive index by irradiation with light, have the capacity to transform the global optical communications industry.[74] In order to be useful, the photoresponsive material must undergo a reversible, large and stable refractive index change (Δn) of 10^{-2} at wavelengths ranging from 1000–1550 nm. These wavelengths represent the most important range of transmission within the telecommunications field as they allow very high speed digital communication.[12]

Suitable materials for integration within these technological applications must satisfy all the fundamental requirements for the fabrication of a device, including thermal stability, sensitivity to electromagnetic stimulus, and high fatigue resistance.[67] Photoresponsive dithienylethenes satisfy these criteria and have been shown to undergo photoinduced refractive index changes in sol-gel materials,[75] amorphous films,[76] and doped polymer films.[77] For dye/polymer systems, a high content of the active component is advantageous as it results in an amplification of the desired effect, however there is a limit of concentration above which segregation of the chromophore takes place. Concentrations lower

than 10% have to be considered to guarantee the homogeneity of the polymer solution.[67]

3.2 The Interaction of Light with Matter

3.2.1 The Complex Index of Refraction

When electromagnetic radiation arrives at the interface between air and a material some of the light may be reflected back into the first medium (air), while some may enter the second medium (the material of interest) where it slows down, changes direction, and in certain cases is absorbed (Figure 3.2.1). From an optics point of view the second medium is characterized by its complex index of refraction $\tilde{N}$ (Equation 3.2.1), which is a combination of a real number n, the refractive index of the material, the extinction coefficient k, and the imaginary number, j .[78]
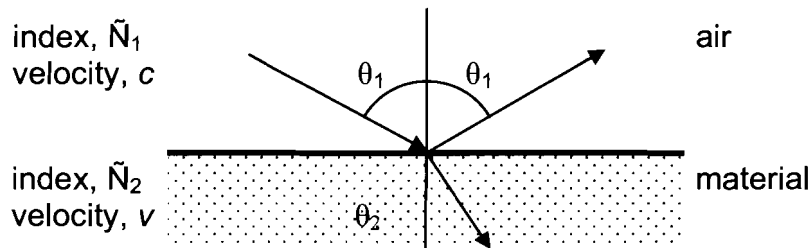
Figure 3.2.1 Light interacting with a plane parallel interface between air and a material with complex index of refraction $\tilde{N}_2$.

48

$$\tilde{N} = n - jk$$

Equation 3.2.1 The complex index of refraction.

In a dielectric material, the incident light wave, which may be viewed as an oscillating electric field, interacts with the electron cloud of the material and is slowed down. The extinction coefficient k is a measure of how rapidly the intensity decreases as the light passes through the material. The refractive index of a material n, is an inverse measure of the speed of the phase velocity of light in the material υ, related to the speed of light in free space, c (Equation 3.2.2).

$$n = \frac{c}{\upsilon}$$

Equation 3.2.2 Refractive index.

3.2.2 Refractive index and Polarizability

The relationship between refractive index and polarizability (α) as a function of wavelength must be considered when developing photoresponsive materials for large and stable refractive index changes. The correlation between refractive index and polarizability is described by (Equation 3.2.3).[68]

$$\alpha(\upsilon) + \frac{d^2}{3kT} = \frac{3}{4\pi n}\left[\frac{n^2(\upsilon)-1}{n^2(\upsilon)+2}\right]$$

Equation 3.2.3 The relationship between polarizability α, and index of refraction n, where both are frequency dependant functions, n is the gas number density and d is the dipole moment.

Electrons, being charged particles, respond to an external electric field. The bonding electrons in a molecule have a degree of mobility, and their charge distribution will be affected by an external electric field, which creates an induced dipole in addition to any permanent dipole which may be present. Polarizability is the relative tendency of a charge distribution, such as an electron cloud, to be distorted from its normal shape by an external field. Molecules with delocalized electron clouds should have higher polarizbilities than molecules without since their diffuse electron clouds exhibit larger polarization changes in response to external field.[15]

50

The refraction of light is dependant upon polarization within a molecule. A light wave is accompanied by an oscillating electric field at right angles to the direction of propagation. The electric field produces a corresponding oscillating dipole in the molecule. This interaction reduces the velocity of propagation of the incident wave, and the more easily polarized the molecule the higher the refractive index (Equation 3.2.3).[79] As a result, properties of a molecule such as dipole moment and polarizability, can affect the properties of a bulk material, such as refractive index.

3.3 Measuring Changes in Refractive Index

Early papers reported the change of the refractive index of bis(thiophene-3-yl)ethane (BTE) derivatives embedded in an amorphous polymer matrix (films doped with 10 wt.-% of photochromic compound) at 633 nm, showing results in the order of 10^{-3} (Figure 3.3.1).[54,80] Numerous reports[36,56,81,82] have described dye doped polymer films with refractive index changes ranging between 10^{-4} and 10^{-3} at wavelengths below 1300 nm. Very few papers have dealt with the change of the refractive index at 1550 nm, which represents the most important wavelength of transmission in the telecommunications field.
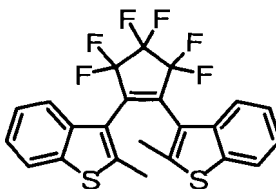
Figure 3.3.1 A BTE derivative, 1,2-bis(2methylbenzo[b]thiophen-3-yl)hexafluorocyclopentene (BTF6).

Ebisawa et al.[37] first reported a self-holding optical switch that employed a photochromic (PC) guest/host polymer cladding consisting of 12 wt.% BTF6 and poly(trifluoroethyl methacrylate methyl methacrylate). Cross-bar switching was achieved by using ultraviolet (313 nm) and visible (>500 nm) light. The Δn of the PC cladding was 0.0003 at 1550 nm.

Kim and co-workers went on to fabricate an all optical Mach-Zehnder modulator using dye doped polymer waveguides containing BTF6 and polycarbonate.[83,84] The photoinduced refractive index change was 0.0006 at 1550 nm for a BTF6 concentration of 37 wt.%. The device exhibited an extinction ratio of -12 dB at the wavelength of 1550 nm using UV (365 nm) and visible (514 nm) light.

One drawback with the previous reports, is that the refractive index values were measured using the prism coupling method, which is performed at fixed wavelengths. Spectroscopic ellipsometry is a superior technique for materials characterization as it permits the simultaneous determination of refractive index and film thickness over a user defined wavelength range. This technique was

recently used by Zerbi et al.[67], who reported the largest refractive index change

to date for a dye doped polymer assembly at 1500 nm. A series of DTE

derivatives was measured by ellipsometry over a broad wavelength range (260-

1700 nm). A film containing 5.8 wt.% of a DTE hydrazone **2.2** in

polymethylmethacrylate (PMMA) underwent a Δn of 0.005 at 1500 nm when

irradiated with UV (365 nm) light. The ring-closed form in Equation 3.3.1 has a

higher refractive index because it is more polarisable than the ring-open form.
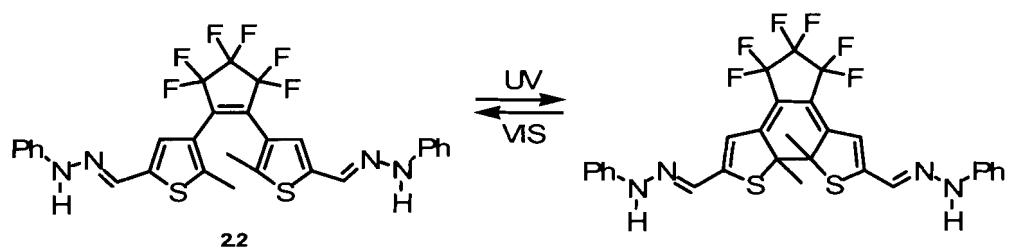
Equation 3.3.1 A DTE Hydrazone derivative.

3.4 Spectroscopic Ellipsometry

3.4.1 Elliptically Polarized Light

Spectroscopic ellipsometry involves the reflection of elliptically polarized light from the surface of the material of interest. When photons are emitted from an incandescent source their electric fields are orientated in all different directions. This is called unpolarized light. If the photons in the light beam are orientated in a given direction the light is referred to as polarized light. Elliptically polarized light can be viewed as the sum of two plane polarized waves of the same frequency that are out of phase. [13] The exception being waves that are 90° out of phase and of the same amplitude, which constitutes circularly polarized light. Circularly and elliptically polarized light are termed for the shape of their electric component when viewed end on (Figure 3.4.1).

plane   circular   elliptical
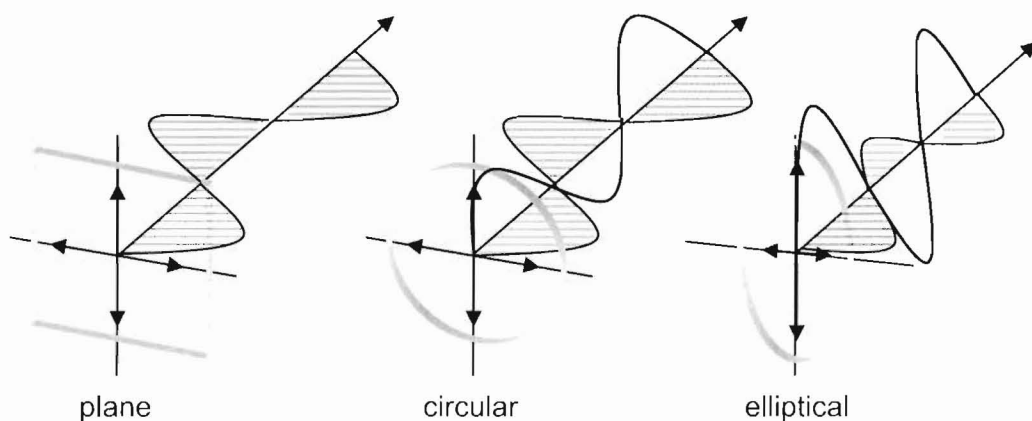
Figure 3.4.1 The shape of circularly and elliptically polarized light viewed end on.

3.4.2 The Reflection of Light

Ellipsometry involves light making a reflection from the surface of interest. In order to write the equations which describe the effect of the reflection on the incident light, it is necessary to define a reference plane. The plane of incidence is defined as the plane which contains both the incoming beam and the normal to the surface (Figure 3.4.2). The amplitude of the electric field wave in the plane of incidence is called E_p, while that of the wave perpendicular to the plane is E_s. These light waves are referred to as the p-wave and the s-wave, respectively. [78]
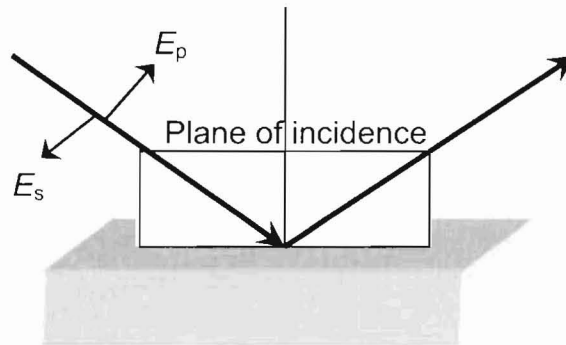
Figure 3.4.2 Reflection on elliptically polarized light from the surface of interest

3.4.3 The fundamental equation of ellipsometry

Ellipsometers measure the quantities Δ and Ψ. The value Δ represents the change in the phase difference between the p-wave and the s-wave before and after reflection of elliptically polarized light from the sample surface. The value Δ is the phase shift. The value Ψ represents the amplitude reduction of both the s-

wave and the p-wave after reflection of elliptically polarized light from the sample surface. The value Ψ is the amplitude change, and is contained in Equation 3.4.1.

$$\rho = \frac{|R_p|}{|R_s|} = \tan\Psi e^{j\Delta}$$

Equation 3.4.1 The fundamental equation of ellipsometry.

The values Δ and Ψ are the real and imaginary part of the complex ratio R_p/R_s where R_p and R_s represent the total reflection coefficients for the p-wave and the s-wave.[78]

3.4.4 Modelling

Spectroscopic ellipsometry measures both Δ and Ψ directly as a function of wavelength. It is necessary to fit these quantities to an assumed model in order to extract information about the thickness and optical properties of the material. Fitting is achieved with the aid of computer modelling using commercially available ellipsometry software. Experimental data is compared to calculated values using an iterative fitting algorithm. The closeness of the calculated data to the experimental data set is allocated as "the goodness of fit parameter χ^2". The software is designed to minimize the value of χ^2. A fit where χ^2 < 1 is considered to be a good fit. In this experiment, the ring-open and ring-closed forms of the films are treated as amorphous dielectric materials. The

optical properties of a dielectric material as a function of photon energy (E) are described in **Error! Reference source not found.** and **Error! Reference source not found.**[85] Fitting the experimental data to these equations allows for both the refractive index and the extinction coefficient of the material to be determined simultaneously.

$$n(E) = \sqrt{\varepsilon_\infty} + \frac{B_0 \cdot E + C_0}{E^2 - B \cdot E + C}$$

Error! Reference source not found.

$$k(E) = \left\{ \frac{A \cdot (E - E_g)^2}{E^2 - B \cdot E + C} \quad \text{when } E > E_g \right.$$

Error! Reference source not found.3

$$k(E) = 0 \ \textit{when} \ E \leq E_g$$

where

$$B_0 = \frac{A}{Q} \cdot \left(-\frac{B^2}{2} + E_g \cdot B - E_g^2 + C \right)$$

$$C_0 = \frac{A}{Q} \cdot \left(\left(E_g^2 + C \right) \cdot \frac{B}{2} - 2 \cdot E_g \cdot C \right)$$

$$Q = \frac{1}{2} \cdot \sqrt{4 \cdot C - B^2}$$

Equation 3.4.2, Equation 3.4.3 The amorphous model for dielectric materials describes the optical properties of a dielectric material as a function of photon energy (E). The values n and k are the real and imaginary parts of the complex index of refraction, E_g is the optical band gap, ε_∞ is a constant greater than unity, and A, B, and C are non-zero constants.

3.5 Thin Film Characterization

3.5.1 Ellipsometry Measurements

Amorphous films (350-600 Å) of compounds **3-10** doped in PMMA (M_w=120 000) were spin-coated onto 1 cm^2 silicon (100) substrates with a 14.1 Å thick native SiO_2 layer. Films were irradiated (bleached) for 30 minutes using the light of a 150 W tungsten source that was passed through a 490 cut off filter to eliminate higher energy light. Immediately following bleaching, the films were analyzed by spectroscopic ellipsometry over a broad wavelength range (450-1700 nm). After recording the ellipsometric spectrum for the ring-open form, samples were bleached again for 30 minutes, and a second analysis was performed. The samples were kept in the same location on the sample stage to ensure the measurements were taken on the same spot on the film. After recording the ellipsometric spectrum for the ring-open form, samples were isomerized to the ring-closed form by irradiating with 365 nm light for 10 minutes. The ellipsometric spectrum for the ring-closed isomer was then recorded over a broad wavelength range (600–1700 nm). The ring-closed isomers were analyzed over a smaller wavelength range so as to minimalize the absorption of light, as the closed isomers absorb in both the UV and visible regions of the spectrum. After recording the ellipsometric spectrum for the ring-closed form, samples were irradiated again with 365 nm light for 10 minutes, and a second analysis was performed. As no further change was observed upon an additional 10 minutes of irradiation, it was concluded that these exposure times were sufficient to reach the PSS of the films. The samples were kept in the same location on the sample

stage to ensure the measurements were taken on the same spot on the film. Multiple locations on a film of **6** were analyzed in order to assure reproducibility across the same film surface. Single spots were analyzed on all other films.

3.5.2 Fitting the Data

The ring-open and ring-closed isomers of films **3-10** were treated as amorphous dielectric materials and fit to the amorphous model. Film thickness and optical properties of the material were simultaneously determined by this model. In all cases, the χ^2 values were less than 1 indicating a good fit to the model for an amorphous material. The data for the ring-open isomers was fit over a large range (450 – 1700 nm) in order to minimize χ^2 and to maximize the data points describing the optical properties of the material. The data for the ring-closed isomers was adjusted and fit over a smaller range (600 – 1700) in order to match the range of the measured data. Ellipsometric plots for **6o** and **6c** are shown in Figure 3.5.1, which display an excellent fit of the experimental data to the amorphous model used for fitting.

(a)   **3o**   **3c**

60

5o

5c

(a) **6o[1]**

6c[1]

(b) **6o[1]**

6c[1]

(a) **7o**

7c
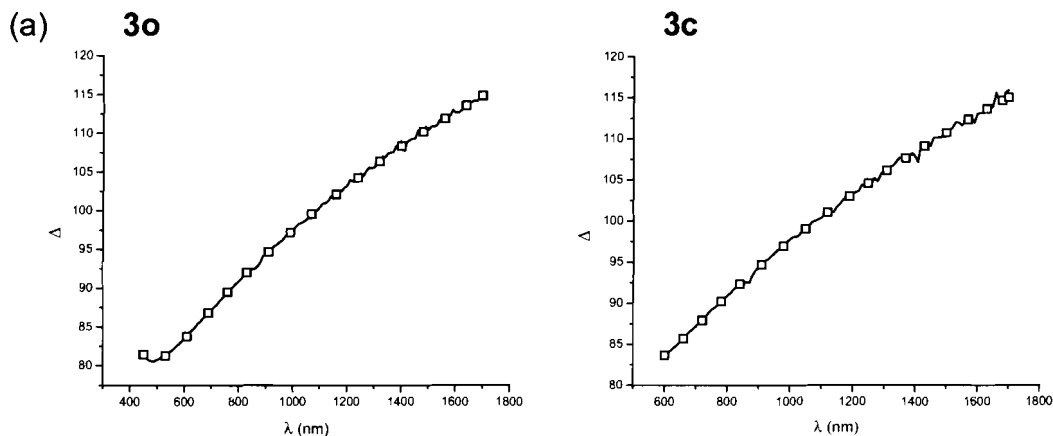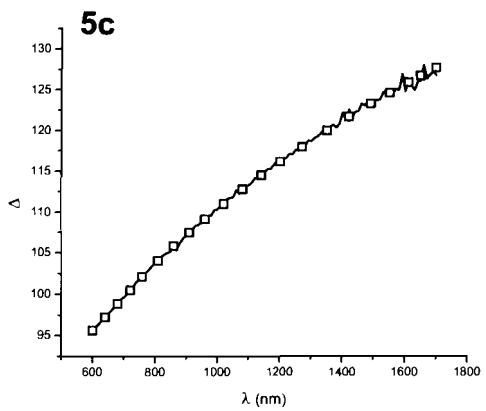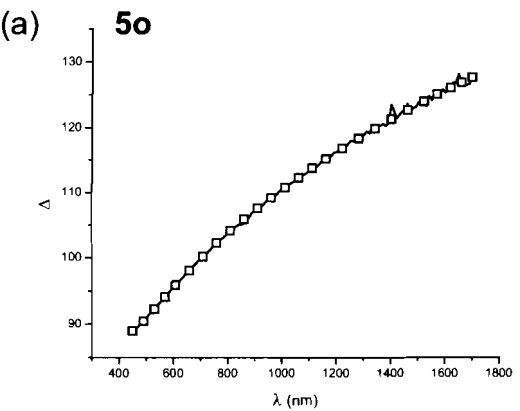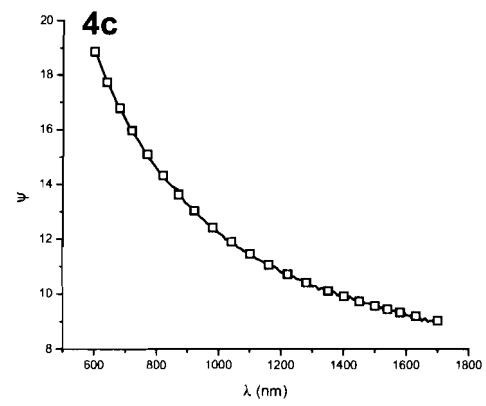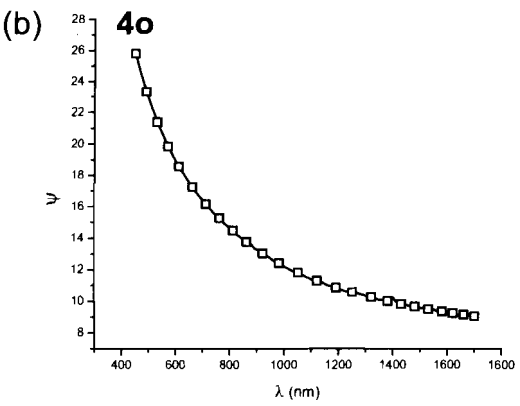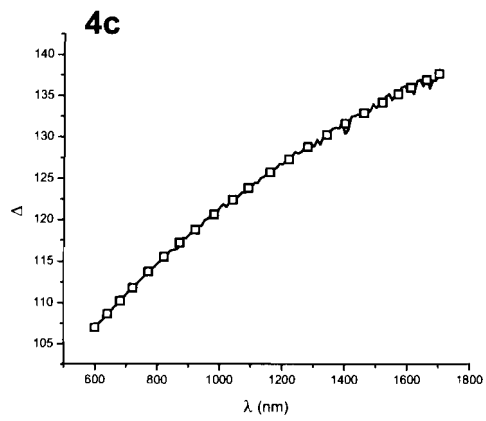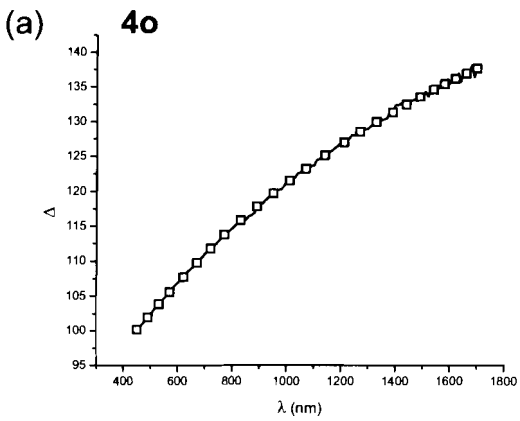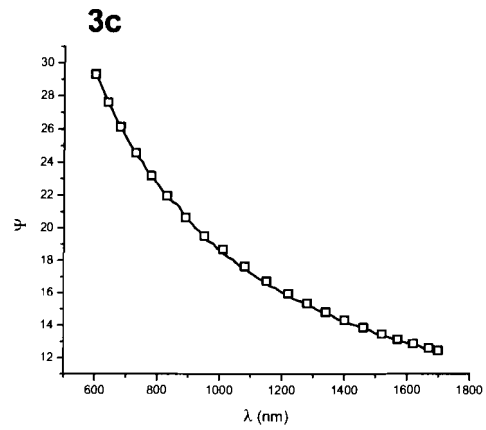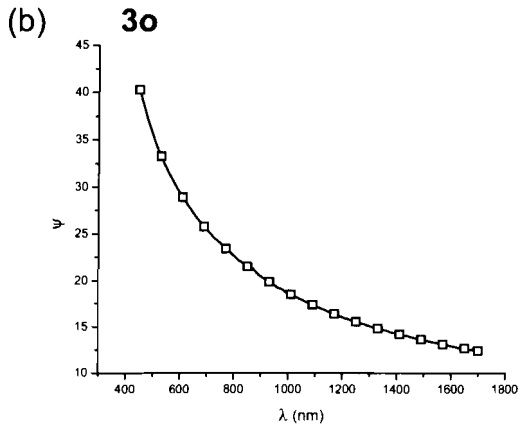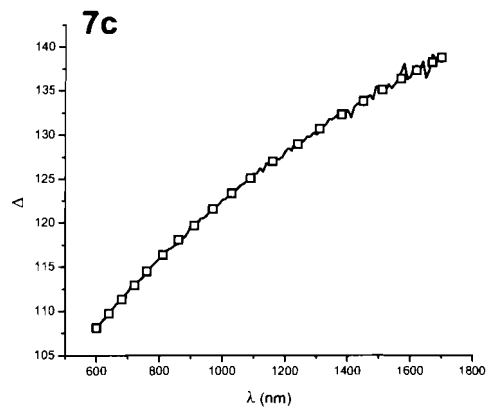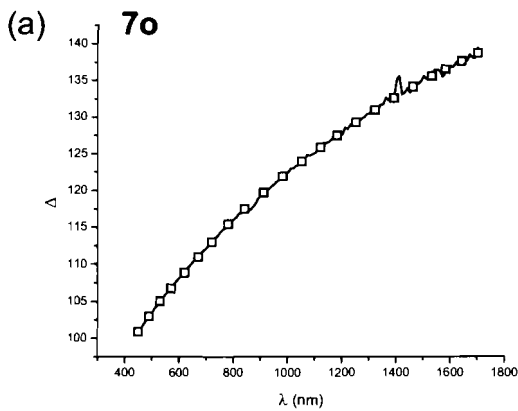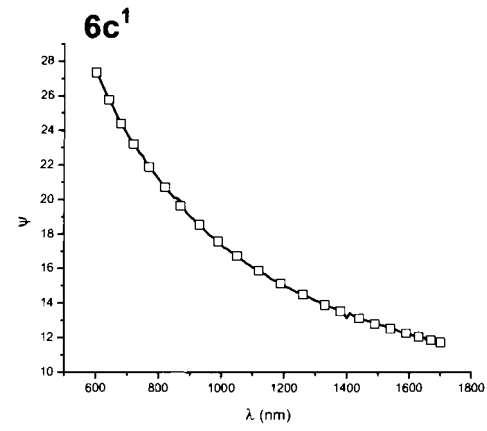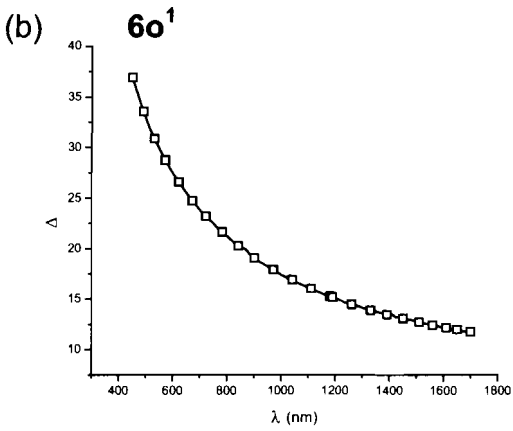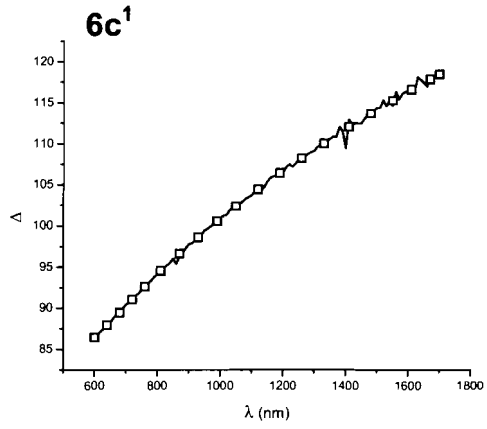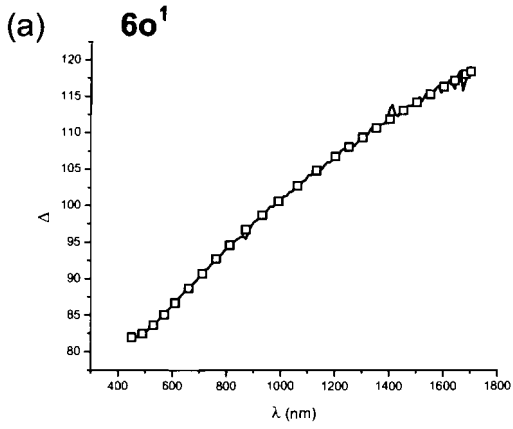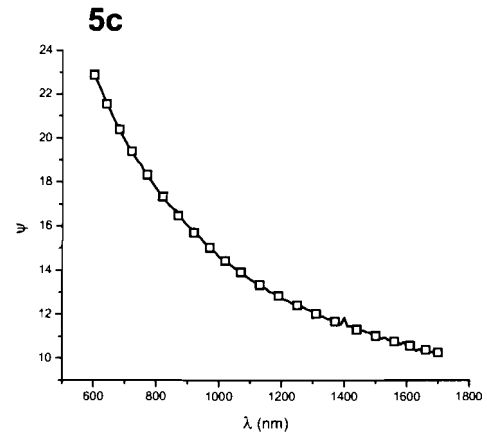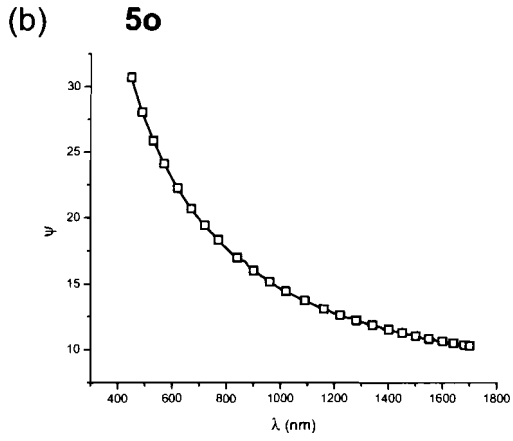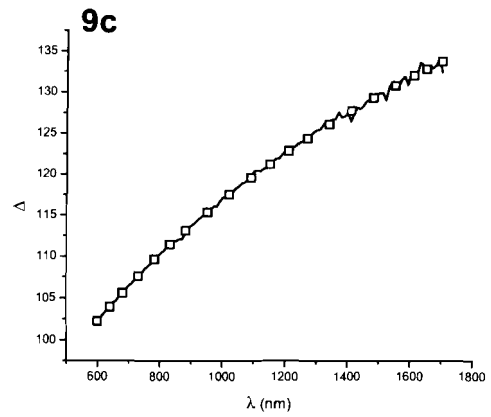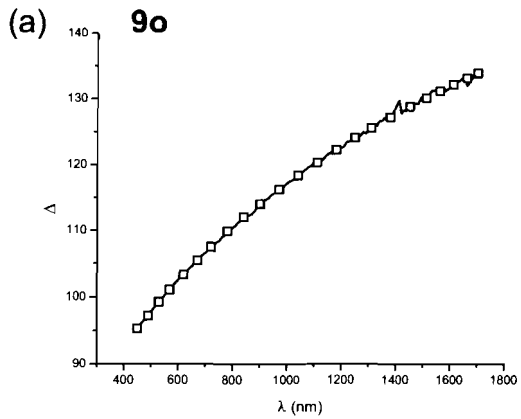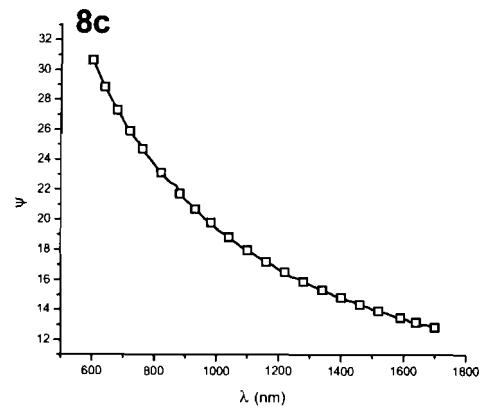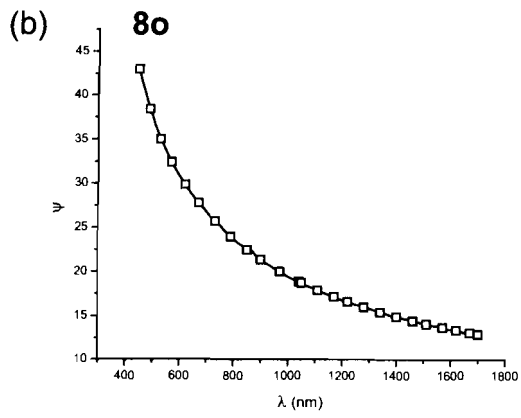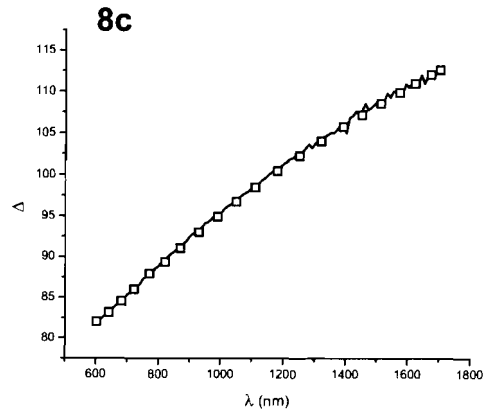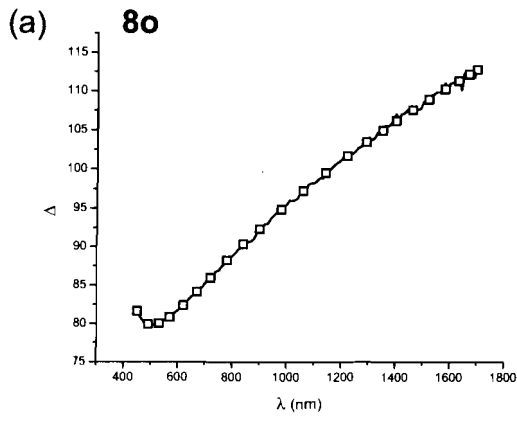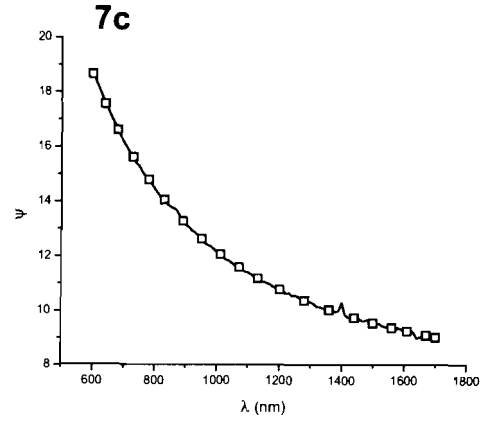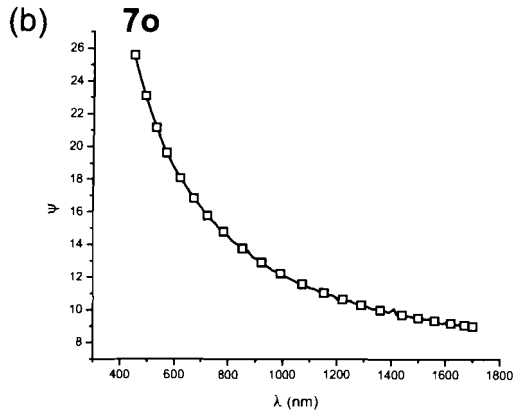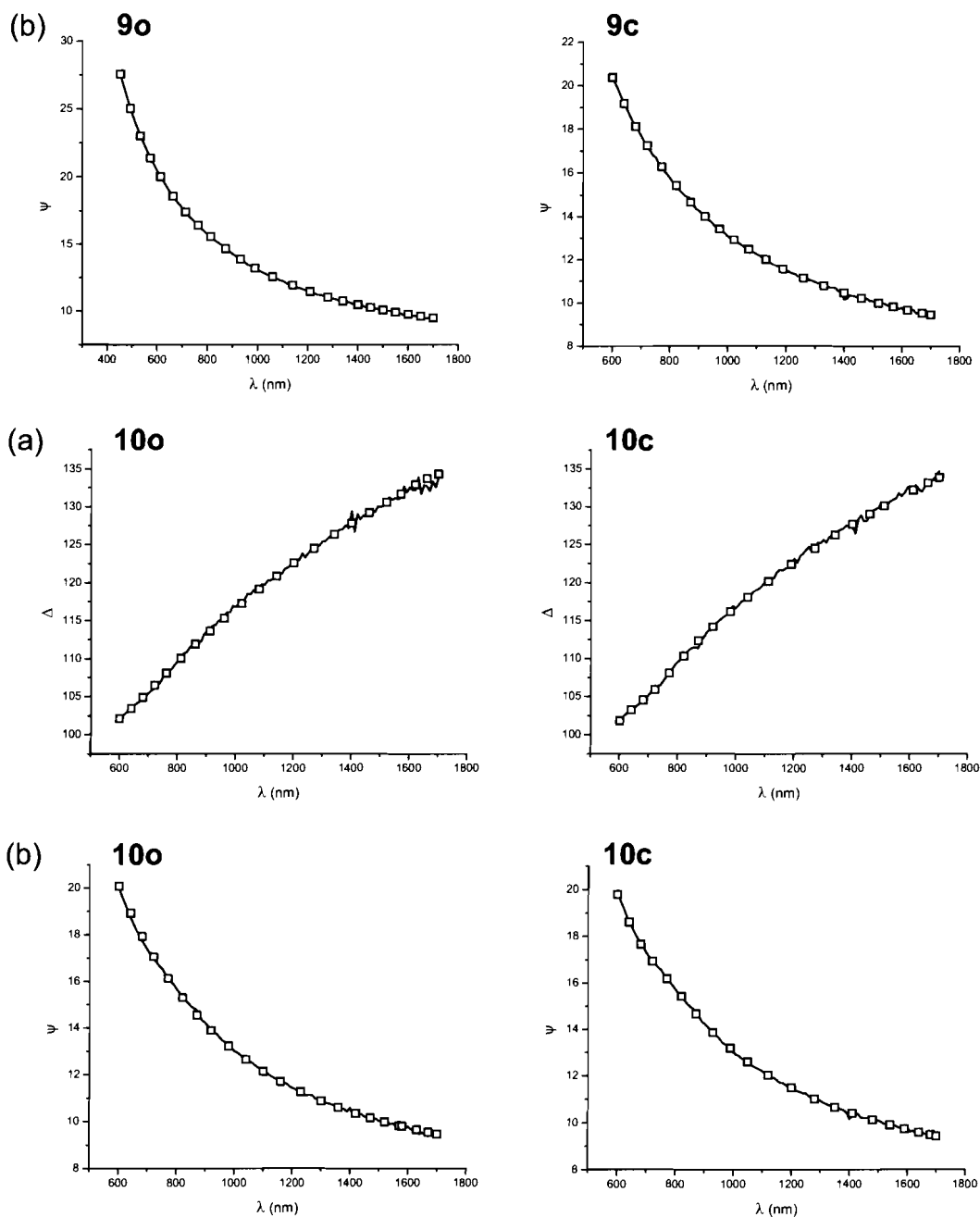
Figure 3.5.1 Experimental and simulated ellipsometric plots of Δ and Ψ for films of **3o-10o** and **3c-10c** after irradiation with 365 nm light for 10 minutes. (a) Simulated Δ plots (open squares) overlay the experimental data (black line). (b) Simulated Ψ plots (open squares) overlay the experimental data (black line). For clarity some (50%) of the data points were removed from the simulated Δ and Ψ data sets. 6o[1] and 6c[1] indicates one location (of three) on the same film which were examined.

Films of **3-10** were prepared under identical conditions and analyzed by spectroscopic ellipsometry before and after irradiation with 365 nm light. In the case of film **6** three different locations on the same film surface were analyzed. Individual spots on each film were analyzed twice for both the ring-open and ring closed forms. The average fit parameters for the model of an amorphous material were determined for each film in both ring-open and ring-closed form and are reported in table Table 3.5.1.

Table 3.5.1 Fit parameters for the amorphous models.

Sample[a]	$\varepsilon_\infty{}^{b}$	A	B	C	ε_g (eV)
3o	2.28531	0.08423	7.69478	23.18688	3.05511
	±0.033	±0.016	±0.44	±108	±0.24
3c	2.26962	0.03878	3.52378	10.28034	1.74125
	±0.033	±0.016	±0.44	±1.8	±0.24
4o	2.43702	0.03844	7.61601	17.70738	3.34174
	±0.041	±0.037	±0.28	±1.1	±0.15
4c	2.36613	-0.03169	4.57426	7.12499	2.46253
	±0.060	±0.027	±0.031	±0.58	±0.20
5o	2.21875	0.05335	8.26910	17.41950	5.35866

	±0.042	±0.037	±0.045	±0.55	±0.35
5c	2.17051	-0.05787	4.60030	7.08084	2.803288
	±0.056	±0.022	±0.28	±0.36	±0.17
6o[1]	2.19189	0.04277	8.97888	17.21508	2.87186
	±0.035	±0.010	±0.30	±.023	±0.18
6c[1]	2.21471	0.01690	5.01797	6.38216	3.40201
	±0.036	±0.019	±0.15	±0.37	±0.32
6o[2]	2.16679	0.04684	9.281706	17.67619	2.70048
	±0.042	±0.013	±0.49	±0.80	±0.19
6c[2]	2.15446	-0.04176	4.37010	6.67411	2.92291
	±0.52	±0.015	±0.29	±0.41	±0.21
6o[3]	2.18478	0.04345	9.10260	19.45173	3.53565
	±0.058	±0.024	±0.82	±1.9	±0.46
6c[3]	2.18994	0.01416	5.01751	6.39933	3.51276
	±0.031	±0.012	±0.14	±0.34	±0.30
7o	2.35401	0.01621	8.21422	16.16054	4.27286
	±0.062	±0.024	±0.32	±0.96	±0.36

7c	2.26272	-0.06195	4.57667	6.42229	2.59562
	±0.092	±0.032	±0.39	±0.46	±0.25
8o	2.17870	0.03970	8.83276	18.02352	3.21688
	±0.031	±0.038	±0.20	±0.77	±0.19
8c	2.20251	002594	4.99665	6.29681	3.04954
	±0.026	±0.031	±0.11	±0.26	±0.23
9o	2.357398	0.01485	7.86322	19.05964	3.125415
	±0.030	±0.013	±0.64	±2.3	±0.25
9c	2.261087	-0.03720	4.55387	6.78350	2.75926
	±0.078	±0.027	±0.26	±0.50	±0.26
10o	1.14138	-1.19894	7.74804	16.0169	4.69991
	±0.27	±0.44	±0.30	±1.3	±0.38
10c	2.299529	0.00934	3.56645	3.23732	1.06471
	±0.069	±0.0037	±0.068	±0.13	±0.12

[a]$6o^{1-3}$ indicates different locations on the same film which were examined, 1, 2 or 3 respectively. [b]Amorphous fit parameters reported are the average of two experiments at the same location on the same film (3 locations for **6**) ± the standard deviation, where A, B, and C are constants, ε_g is the optical energy gap and ε_∞ is a constant greater than unity. The model describes n and k as a function of photon energy.

The statistical dispersion for the reported values was determined using the standard deviation ($V^{1/2}$) of a random variable method (Equation 3.5.1). [86]

$$V^{1/2} = \left(\frac{\Sigma d^2}{n} \right)^{1/2} = \left[\frac{\Sigma(x - \bar{x})^2}{(n-1)} \right]^{1/2}$$

Equation 3.5.1 Standard deviation of random variables. d is the deviation of the results from the mean value, x is the result, $\bar{x}$ is the mean, and n is the number of samples examined.

3.5.3 Surface Roughness

The roughness of a surface can have two effects on ellipsometry measurements. Rough surfaces can cause the incident light beam to scatter during the course of the measurement. If the surface is too rough it can cause depolarization of the reflected light beam.[78] A second effect relates to the interfacial layer between the bulk film and air. The roughness of this layer is a measurement of the void space in the surface of the film. Under ambient conditions this void space contains air and may have optical constants that are intermediate between the bulk material and air.[78] One way to overcome this problem is to include a characteristic roughness layer within the ellipsometric model. The models used for this study did not include a void layer as no improvement in the quality of fit was observed. In order to further disregard a void layer from the ellipsometric models, measurements of surface roughness were performed by atomic force microscopy.

3.5.4 Atomic Force Microscopy

Atomic force microscopy (AFM) is a technique used in materials science that images the surface topology of a material.[87] AFM makes use of a highly sharpened microscopic tip attached to an oscillating cantilever which rasters across the surface and responds to height differences in surface topology. A piezoelectric traducer, which translates current into mechanical motion, is used to raster the tip along the sample. The X, Y, and Z position of the tip along the surface is tracked by a laser that is reflected off the tip to a photodiode detector. As the tip encounters a change in surface topology it responds accordingly as the force between the tip and the surface changes. At any given time during a scan, the tip position is recorded and translated into a topological image of the surface. It is best to use tapping mode AFM for soft materials as the oscillating cantilever simply taps the surface during imaging rather than being in constant contact with the material. Tapping mode AFM minimizes the lateral force between the tip and the surface in order to prevent damage to the film during the imaging process. AFM is extremely sensitive to height deviations in the sample surface and is an excellent technique for evaluating surface roughness of a material.[88] Surface roughness of a sample is reported as the root mean square roughness R_{ms}. Root mean square roughness is defined as the square root of the mean value of the squares of the distance of the points from the image mean value.

$$R_{ms} = \sqrt{\sum_{i=1}^{N} \langle Z_i - |Z| \rangle}$$

Equation 3.5.2 Root mean square roughness where Z_i is the height of point N_i, $|Z|$ is the average sample height and N is the number of points on the image.

The minimal changes in the film thickness by ellipsometry indicate that the ring-open isomer and ring-closed isomer of the material are occupying similar volumes. The minimal change of volume was previously predicted by AM1 calculations (Table 2.4.2). This inference is supported further by AFM measurements. AFM images of the studied films appeared similar before and after irradiation with UV light and had no discernable features (Figure 3.5.2). Atomic force microscopy of the surface of the films indicated that the surface roughness did not change appreciably when the samples were irradiated with UV light (Figure 3.5.3). In all cases, the root mean square roughness was less than 1 nm over an area of 0.01 mm^2. A low R_{ms} value indicates that the average film thickness at point N_i does not change significantly when the samples are irradiated with UV light. AFM analysis of the films indicates that in all cases the amount of void space at the interfacial layer between the bulk film and air is constant, and any changes observed in refractive index are due to a change in molecular structure of the material rather than a change in surface topography.
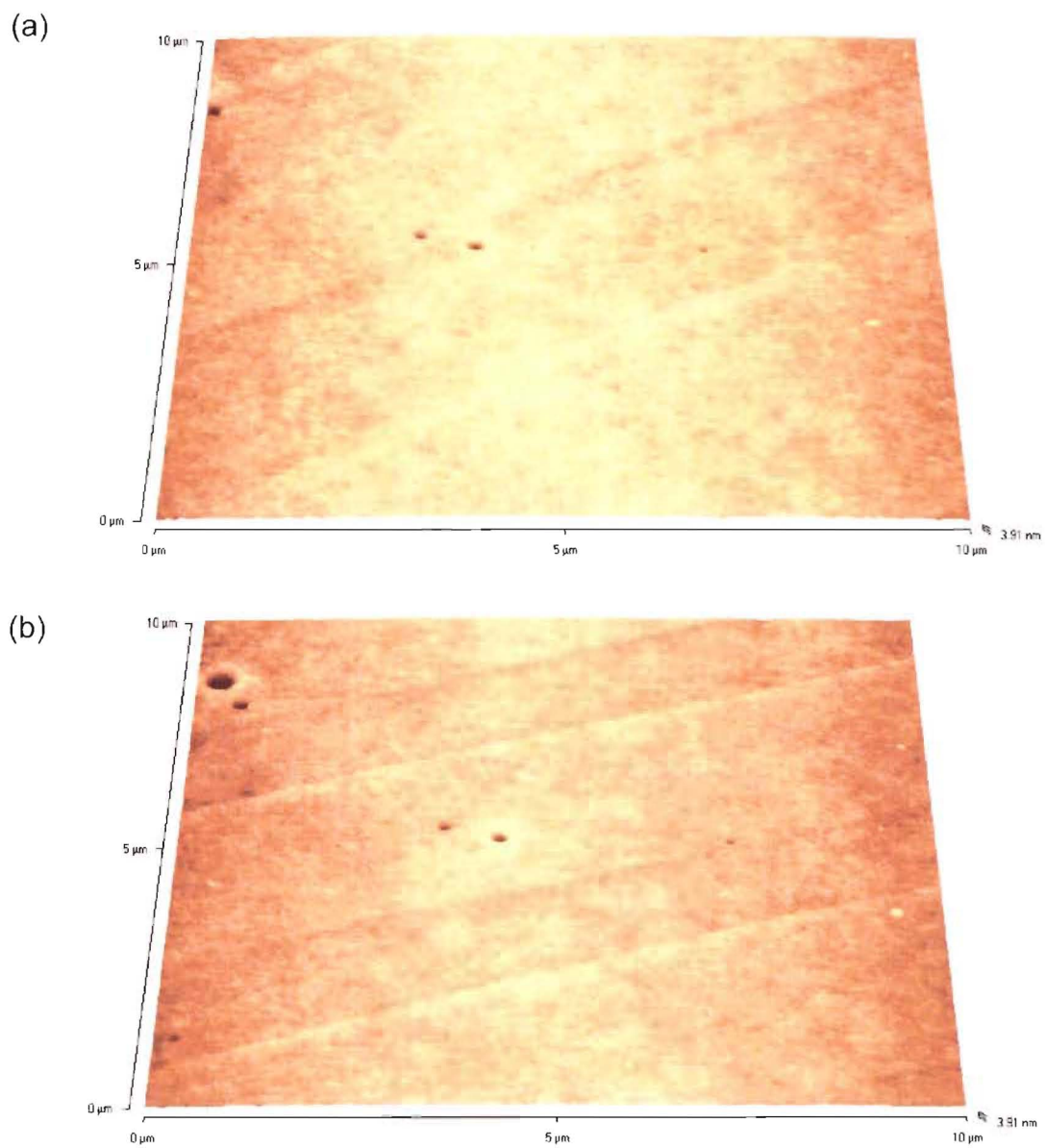
Figure 3.5.2 AFM images of a thin film of **7**/PMMA. (a) **7o** spin coated on a silicon substrate, (b) **7c** after irradiating the film with 365 nm light for 10 minutes.

(a)
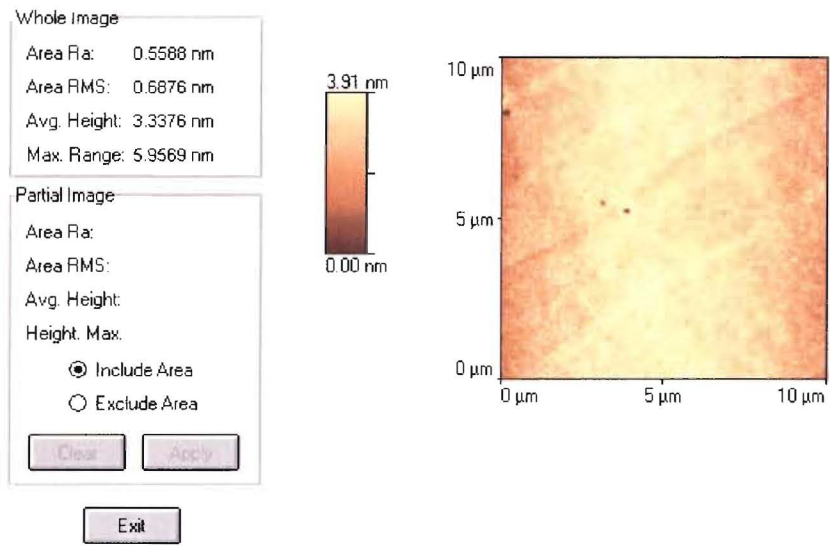
(b)
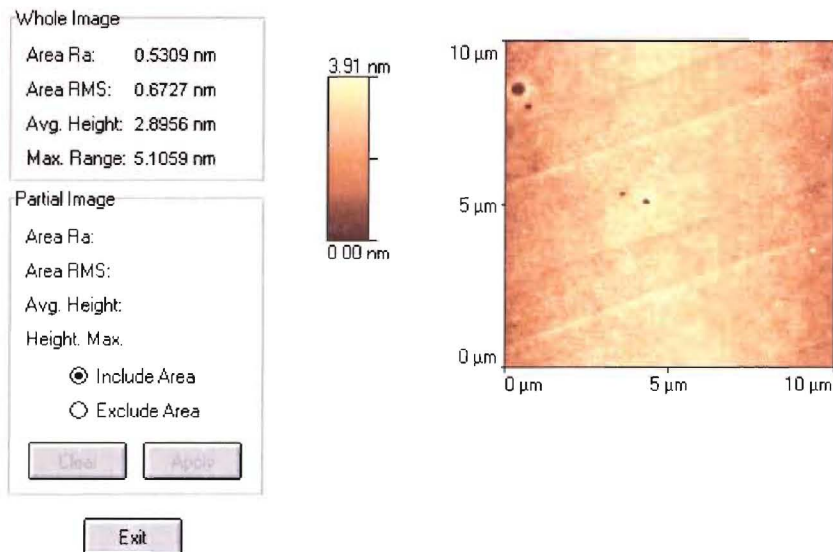
Figure 3.5.3 AFM surface roughness measurements of a thin film of **7**/PMMA. (a) **7o** spin coated on a silicon substrate, (b) **7c** after irradiating the film with 365 nm light for 10 minutes. A comparison of area RMS shows that the surface roughness of the films did not change appreciably when the sample was irradiated with UV light.

Atomic force microscopy is also capable of measuring film thickness directly. Ellipsometers measure Δ and Ψ as a function of wavelength and then fits these quantities to an assumed model to extract information about thickness. AFM was used in order to corroborate the calculated film thickness provided by the fitting algorithm of the ellipsometry software. A thin film of **7** was prepared and measured via ellipsometry to determine the thickness (Table 3.5.2). A portion of the sample was scored to the substrate and then the AFM was used to measure the depth of the groove (Figure 3.5.4). AFM measurements support the film thickness calculated by the assumed amorphous model of ellipsometry.

Table 3.5.2. Fit parameters and film thickness by ellipsometry of 2 locations on sample **7**.
[a] **7**[1-2] indicates different locations on the same film which were examined, 1 or 2 respectively.

Sample[a]	AOI ($°$)	χ^2	Thickness (nm)
7[1]	70.6	0.433	207.7
7[2]	70.6	0.455	206.9
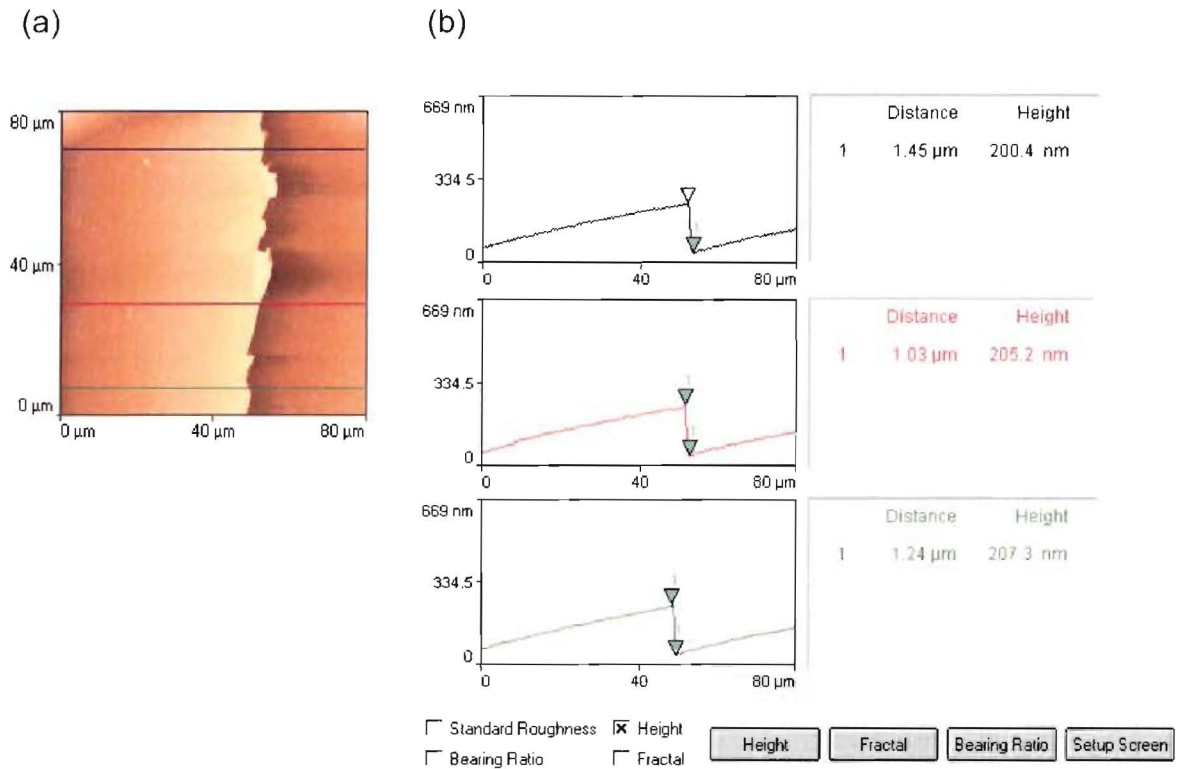
Figure 3.5.4 Measurement of film thickness by AFM. (a) Topological image of sample **7** after scoring showing the film surface (left) and substrate surface (right) along with three reference points used over an 80 μm^2 area. (b) Relief diagrams of the height difference at each reference point.

The results of AFM thickness measurements indicate that the calculated film thickness determined by spectroscopic ellipsometry using the amorphous model are an excellent fit.

3.5.5 Powder X-Ray Diffraction

The ellipsometry data was fit to an amorphous material model. This fit assumes that the films are themselves amorphous. Powder diffraction

experiments of the material spin-coated as a film on quartz and silicon substrates were conducted to validate this assumption. Figure 3.5.5 shows the appropriate substrate peaks for crystal silicon (Si) and quartz (SiO_2) with no evidence of x-ray diffraction from the film. This implies that the material is amorphous when spin coated as a thin film and that the use of an amorphous material model is fitting.
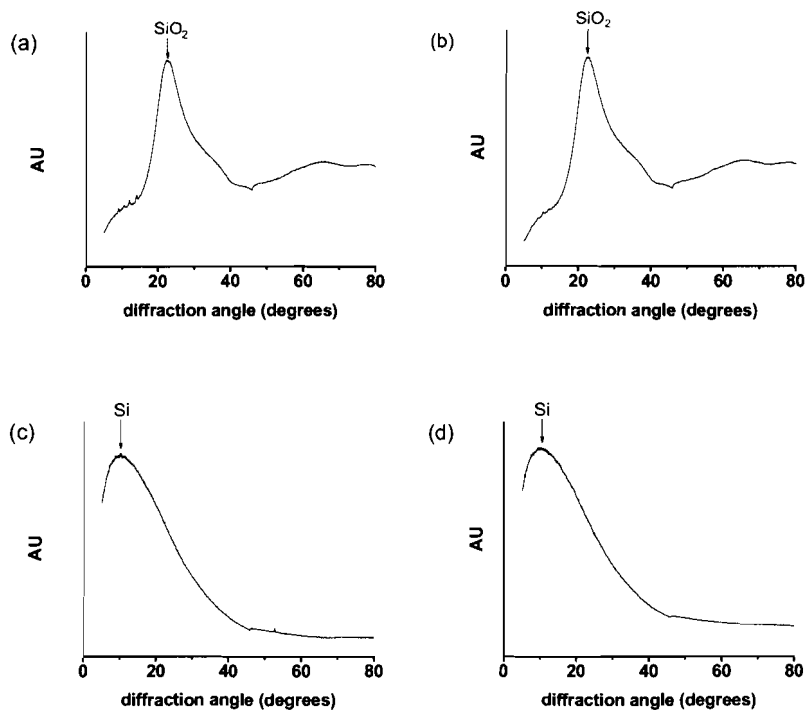
Figure 3.5.5 Powder diffraction patterns for samples of **6** spin coated on quartz and silicon substrates. (a) quartz substrate, (b) a 50 nm thick film of **6** on quartz, (c) silicon substrate, (d) a 50 nm thick film of **6** on silicon.

3.6 Ellipsometry Results

The photoinduced refractive index changes in **3-10** over a broad wavelength range (600-1700 nm) are summarized in Figure 3.6.1. The model for

74

amorphous materials was used to fit the experimental ellipsometry data and simultaneously determine the index of refraction at the appropriate wavelengths.

(a) 3

(b) 3

(a) 4

(b) 4

(a) 5

(b) 5
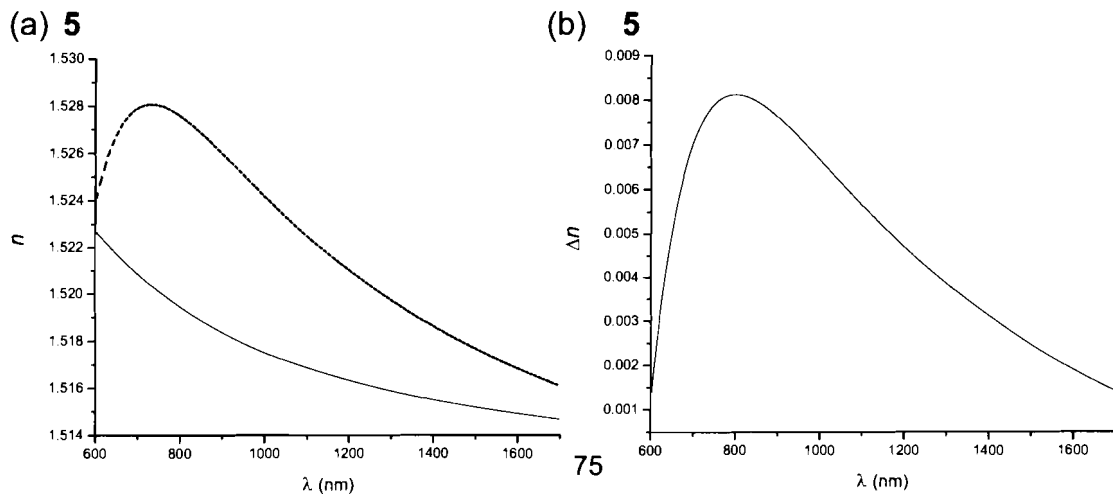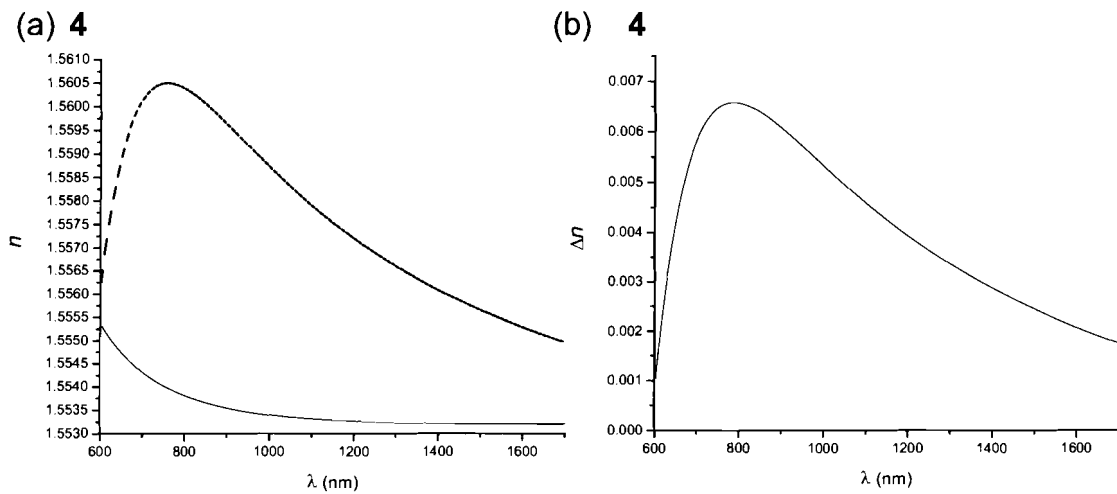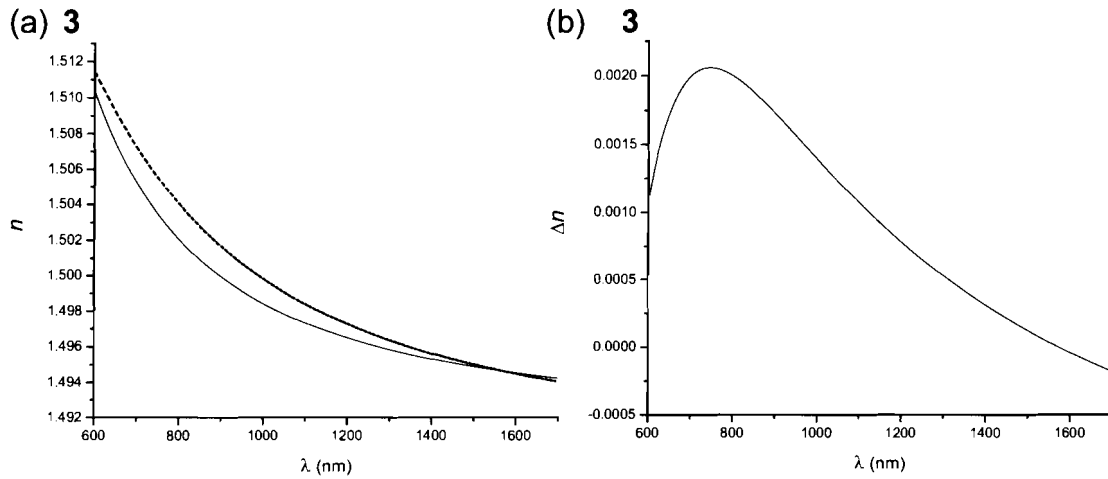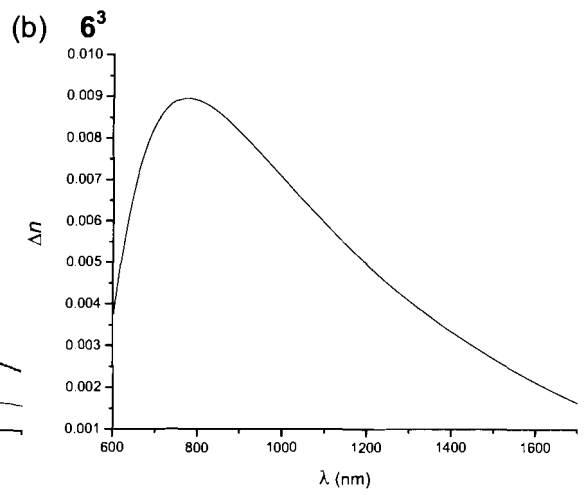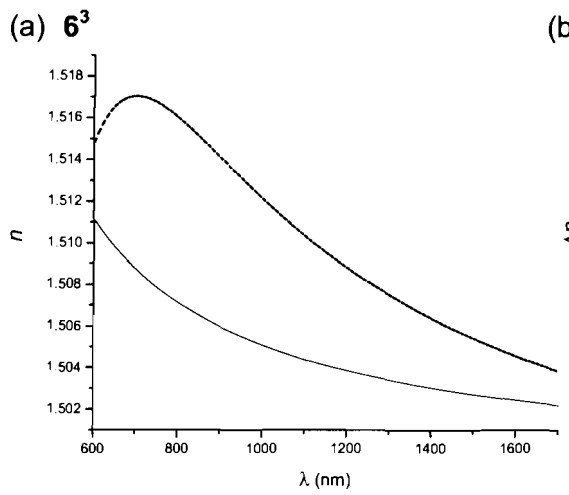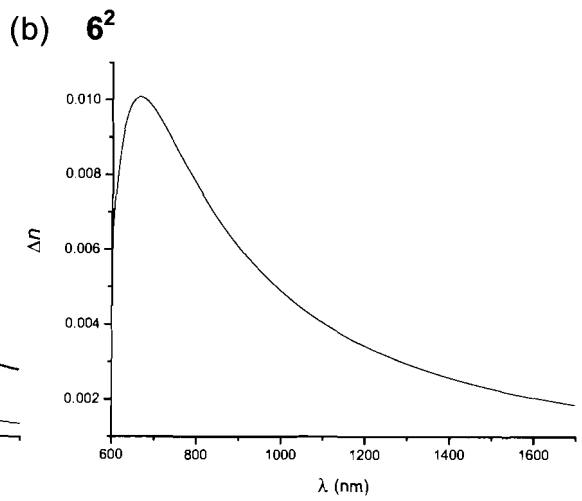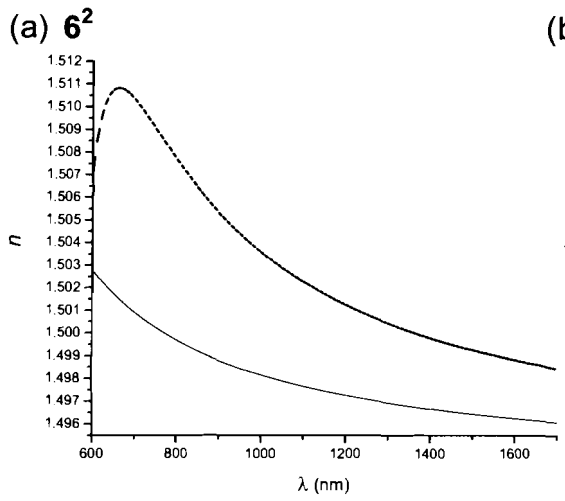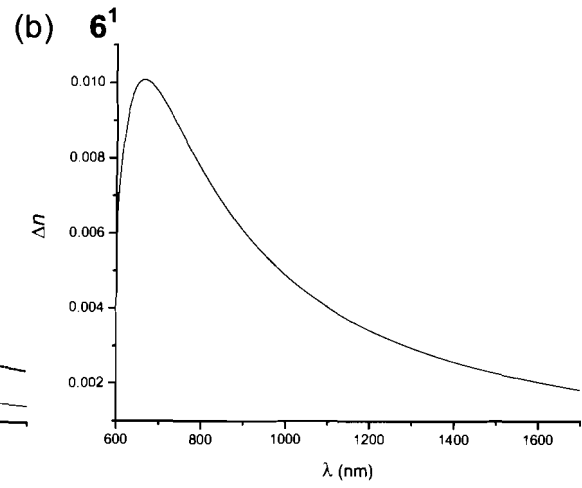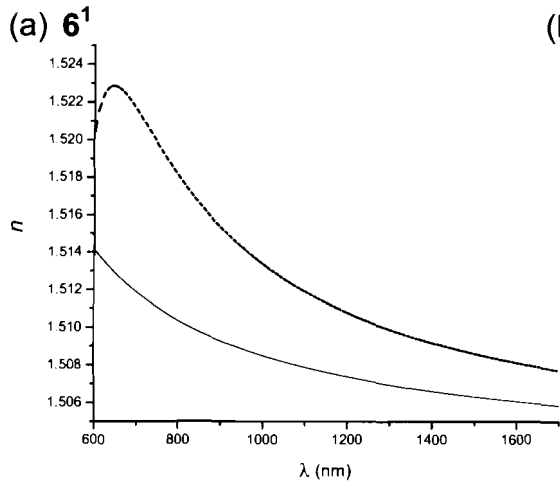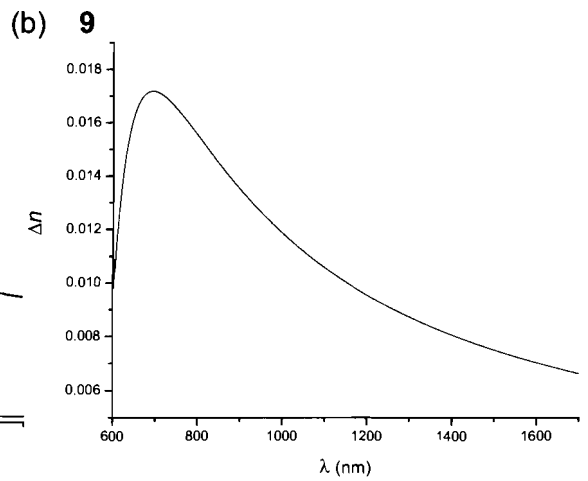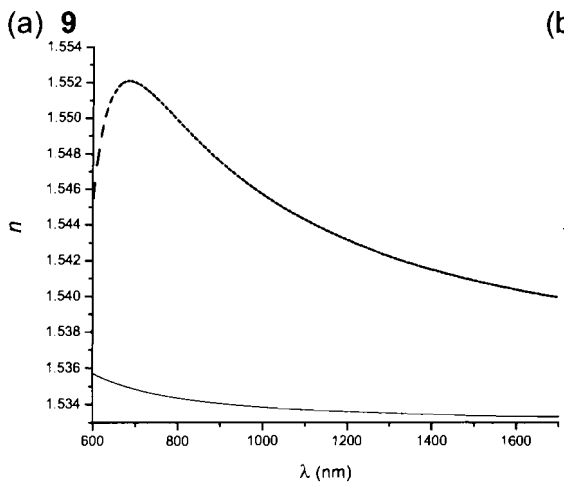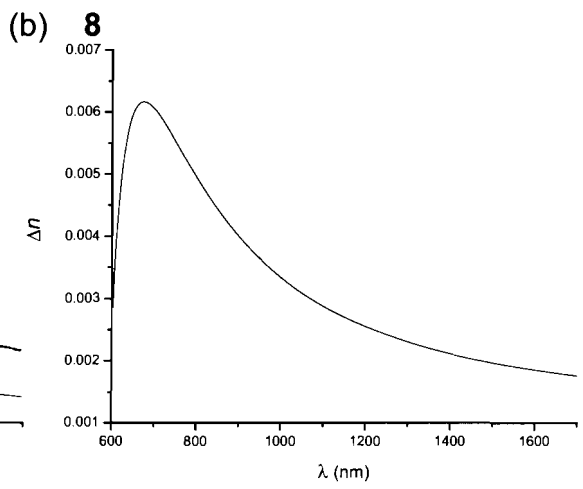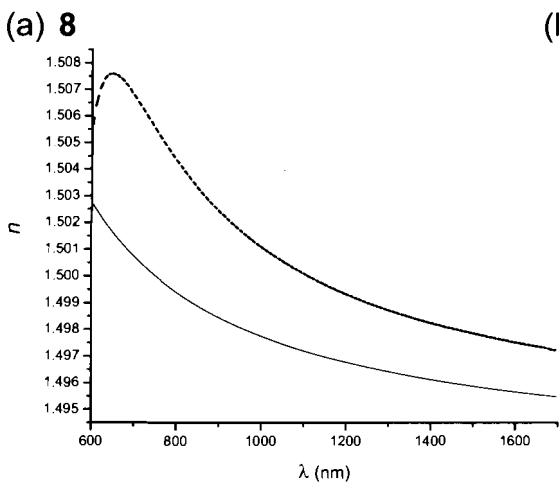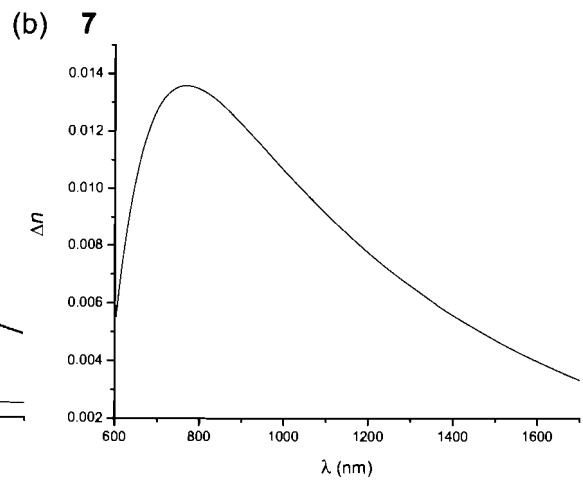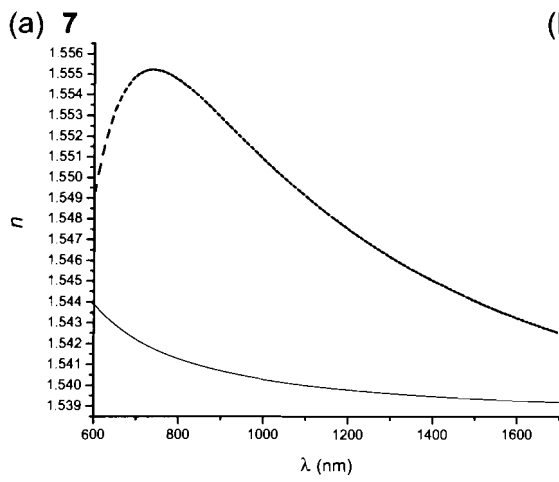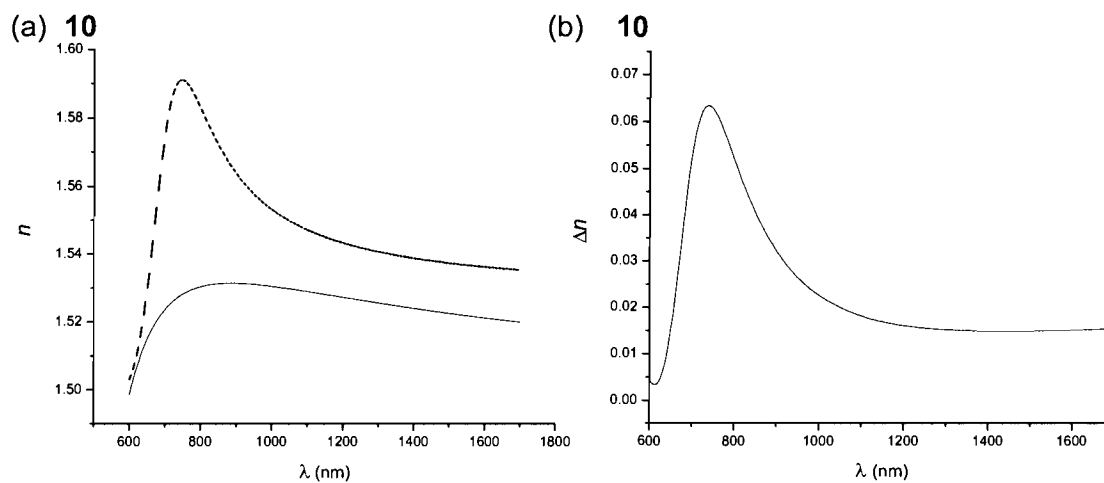
Figure 3.6.1 Index of refraction changes induced by photoswitching. (a) Refractive index profile for ring-open isomer (solid line) and ring closed isomer (dashed line) of **3-10** from 600-1700 nm, the area of primary interest for commercial applications. (b) Photoinduced variation in refractive index (Δn) between **3o-10o** and **3c-10c** in the near IR region of the spectrum. The ring closed isomer was generated by irradiating with 365 nm light for 10 minutes.

The index of refraction for the ring-open and the ring-closed isomers of **3-10** at the functional wavelengths of 1500 nm and 1550 nm are summarized in Table 3.6.1.
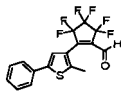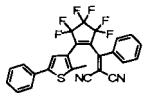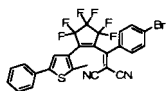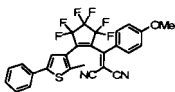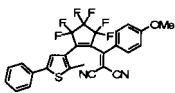
Table 3.6.1 Index of refraction for the ring-open and ring-closed isomers of **3-10**

at practical wavelengths.
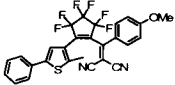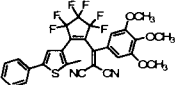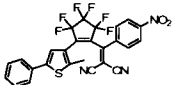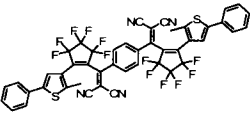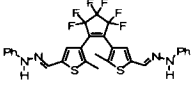
Sample	Thickness (Å)	χ^2	n (1500 nm)[a]	n (1550 nm)[a]
3o	835.8	0.0520	1.49487	1.49468
3c	836.6	0.0958	1.49499	1.49472
4o	309.3	0.0235	1.55321	1.55321
4c	309.4	0.0232	1.55546	1.55527
5o	432.5	0.0366	1.51518	1.51504
5c	429.5	0.0282	1.51766	1.51723
6o^1	564.0	0.0520	1.50632	1.50619
6c^1	563.5	0.0509	1.50859	1.50834
6o^2	576.6	0.0309	1.50270	1.50256
6c^2	570.6	0.0651	1.50539	1.50495
6o^3	577.9	0.0398	1.49644	1.49634
6c^3	577.9	0.0412	1.49926	1.49902
7o	303.8	0.0357	1.53935	1.53930
7c	304.8	0.0445	1.54406	1.54362
8o	662.0	0.0416	1.49587	1.49576
8c	660.5	0.0313	1.49784	1.49767
9o	352.2	0.0299	1.53340	1.53337
9c	355.7	0.0450	1.54090	1.54063
10o	331.7	0.1250	1.52246	1.52178
10c	348.4	0.0279	1.53732	1.53673

[a] Values shown are based on the average fit variables from data generated by two runs using the same location on each film (provided in appendix).

The results indicate that the film thickness does not change appreciably when the samples are irradiated with UV light. In all cases the fit parameter χ^2 is <1 indicating a good fit. The photoinduced variation in refractive index (Δn) can be derived by calculating the difference in n between each isomer ($n_{closed} - n_{open}$) at the appropriate wavelength. The calculated results are shown in Table 3.6.2.

Table 3.6.2 Results of the photoinduced variation (Δn) of **3-10**. For clarity, the structure of the DCTE R group has been provided.

Sample[a]	Structure[b]	Δn (1500 nm)	Δn (1550 nm)	PSS (%)
3o-3c		0.00012	0.00004	18
4o-4c		0.00225	0.00206	38
5o-5c		0.00248	0.00219	35
6o¹-6c¹		0.00228	0.00215	56
6o²-6c²		0.00269	0.00239	56

Compound	Structure	1500 nm	1550 nm	Δ
6o[3]-6c[3]		0.00282	0.00268	56
7o-7c		0.00470	0.00432	41
8o-8c		0.00197	0.00191	40
9o-9c		0.00750	0.00726	15
10o-10c		0.01460	0.01450	-

[a] The results shown for **6** represent three different sample locations on the same thin film surface, indicating reliability of the sample. [b] For clarity only the ring-open structure has been shown.
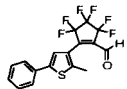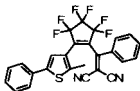
The calculated static polarizabilities (α) provided in Table 2.4.2 indicate that the refractive index of **3-9** should increase upon closing. This was observed in all compounds and suggests that the observed increase can be attributed to an increase in the polarizability of the material when it is isomerized to the ring closed material.

The measured refractive index changes at 1500 nm and 1550 nm for these materials show a variance ranging from 0.00012 to 0.00750, and 0.00004 to 0.00726 respectively. The smallest Δn values at 1500 nm were associated with R groups that do not contain a D-π-A pathway, compounds **3, 4, 5, 8.** Since these systems do not display the polarisable D-π-A pathway, any observed change of refractive are strictly due to the modification of electron delocalization

along the π-conjugated backbone. Larger changes in index of refractions were observed in architectures that include the donor-bridge-acceptor scaffold, **6, 7**. As the backbones of compounds **4-8** are very similar, the elevated Δn values for compounds **6** and **7** suggest an influence of the highly polarisable D-π-A pathway on any refractive index changes. Due the amorphous nature of the sample films, it is reasonable that any changes of refractive index associated with the polarisable D-π-A pathway are suppressed, and the observed Δn is principally due to modulation of the π-conjugated backbone within each compound. The Δn for **9** had the largest change at the of the series, which must be attributed to the change in backbone π-conjugation between the ring-open and ring-closed isomer. The π-conjugated pathway of **9c** is the most extended of the series and exhibited the largest Δn.

There is a noticeable correlation between the observed photoinduced Δn values of **3-9** and the calculated changes in static polarizability of **3-9** shown in Table 2.4.2. This relationship is summarized in Table 3.6.3.

Table 3.6.3 The correlation between observed Δn (1550 nm) and static polarizability.

Sample	Structure[a]	$\Delta \alpha$ [b] $(\times 10^{-30} m^{3)}$	Δn (1550 nm)
3o-3c		1.5	0.00004
4o-4c		4.7	0.00206

5o-5c		5.2	0.00219
6o^3-6c^3		5.2	0.00268
7o-7c		5.3	0.00432
8o-8c		5.3	0.00191
9o-9c		6.2	0.00726

[a] For clarity only the ring-open structure is been shown. [b] Differences in static polarizability were calculated using the POLAR function in Spartan™. Values shown are for the ring-open isomer subtracted from the ring-closed isomer.

The AM1 calculated $\Delta\alpha$ values of **3-9** are indicative of polarizability changes due to modulation of the backbone only, as demonstrated by the near identical terms of **4-8**. Though the observed Δn values of **3-9** follow a similar increasing trend to that of $\Delta\alpha$, a discrepancy is apparent for **6-7**, which exhibit an increase that is not predicted by computer modelling. AM1 calculations do not account for any polarizability changes associated with the reversible disconnection of the D-π-A pathway. The observed amplification of Δn in **6-7** suggests an influence of the highly polarisable D-π-A pathway on the index of refraction.

Refractive index changes for the reference DTE hydrazone (0.01450) were higher than those reported by Zerbi and coworkers (0.005).[67] The discrepancy can be attributed to differences in thin film fabrication due to lack of comparable equipment. The reference films were fabricated at a spin rate of 10,000 rpm, while the films for this study were limited to a spin rate of only 6,000 rpm. While the ellipsometer software does factor film thickness into the amorphous model, it is probable that the hydrazone films fabricated for this thesis contained a higher concentration of the photoactive molecule than those prepared by Zerbi. It is important to note that the results obtained for all compounds were smaller than the reference DTE hydrazone, yet comparable to the DTE hydrazone Δn reported in the literature (0.005).[67]

3.7 Conclusions

A series of photoresponsive hexatriene derivatives, where the linear π-conjugation between donor and acceptor groups can be reversibly disconnected, were synthesized in order to investigate the change of the refractive index (Δn) between two states. The derivatives were fully characterized and displayed excellent photochromic activity without any observable photodegradation. Films of PMMA with an active chromophore (5.8 wt.%) were fabricated by spin-coating from toluene solutions. Atomic force microscopy measurements demonstrated that the films displayed no significant changes to surface roughness or volume when irradiated with UV light. X-ray diffraction confirmed that the fabricated films were amorphous. Ellipsometry has been shown to be an effective tool for the application of studying photoinduced refractive index changes across a broad

spectral range (600-1700 nm). The results obtained revealed the influence of the electronic effect of the D-π-A system on Δn: the presence of a donor-π-linker-acceptor group produced an increase in Δn.

3.7.1 Future Work

Photoresponsive materials that include a highly polarisable D-π-A pathway show a refractive index change (Δn) that is larger than similar architectures without such components. Though the observed influence of the D-π-A framework on Δn is small, the potential towards a more pronounced change remains to be explored. Fabrication of films in which the samples are ordered (poling) warrants investigation. Poled films may display an enhanced Δn since the dipoles of the active photochromes are arranged to face a similar orientation. A direct comparison of the films in this study and films fabricated using poling techniques may provide useful insight towards the influence of the integrated D-π-A pathway on Δn.

Although dispersing the active dye in a polymer matrix is the easiest strategy to prepare photochromic films, inherently the films fabricated for the work in this thesis suffer from a low concentration of photoactive die (5.8 wt.%). From a practical standpoint, dispersed monomeric films limit the content of chromophores to less than 10 wt.%.[67] Undoped photochromic polymers are advantageous over their doped counterparts as they typically display a higher concentration of the active photochromic unit. Previous pendant and main chain

DTE polymers have shown that an increased concentration of photoactive ompound within the material results in the amplification of the desired effect.[89-91] It would be interesting to incorporate **3-9** into copolymer designs and explore any trends in Δn associated with these high content systems.

The synthetic route used to construct the DCTE backbone is particularly versatile. The choice of donor and acceptor groups that may be introduced at the ends of the π-pathway remains unrestricted, while alternating the length of the π-linker is similarly unconstrained. Additionally compounds **5-7**, which are characterized by bromo and methoxy functional motifs respectively, unlock further synthetic modifications to the overall D-π-A pathway. For example, the demethylated phenol version of compound **6-7** D-π-A systems are known to behave as protein tyrosine kinase (PTK) inhibitors. PTK is a protein that plays a vital role in the proliferation of diseases such as cancer.[92] Our group is currently under way to remove the methyl group from **7** and investigate its biological activity.

4 Experimental

Materials. All solvents for synthesis were dried and degassed by passing them through steel columns containing activated alumina under nitrogen using an MBraun solvent purification system. All other solvents were used as received. Solvents for NMR analysis (Cambridge Isotope Laboratories) were used as received. Solvents for spin coating were purchased from Aldrich and used as received. Silicon (100) wafers were purchased from Wacker. PTFE syringe filters (0.2 μm) were purchased from Aldrich. Column chromatography was performed using silica gel 60 (230-400 mesh) from Silicycle Inc., or with a Teledyne Isco CombiFlash Companion sg100c and redisep normal phase silica columns, or with a CHROMATATRON. All other reagents and starting materials were purchases from Aldrich with the exception of $Pd(PPh_3)_4$ and $[Pd(PPh_3)_2]Cl_2$ which were purchased from Strem.

Techniques. ^1H NMR and ^{13}C NMR characterizations were performed on a Varian Inova 500 instrument working at 499.8 MHz for ^1H NMR and 125.7 MHz for ^{13}C NMR. Carbon peaks in the ^{13}C NMR spectra for fluorinated DTE derivatives are not observed for the central cyclopentene ring where fluorine is attached. Chemical shifts (δ) are reported in parts per million relative to tetramethylsilane using the residual solvent peak as a reference standard. Coupling constants (J) are reported in Hertz. ATR-IR measurements were performed using a Varian Scimitar 800 instrument. UV-VIS measurements were

performed using a Varian Cary 300 Bio spectrophotometer. Low resolution mass spectrometry measurements were performed using a Varian 4000 GC/MS/MS with electron impact operating at 10 mamp as the ionization source or chemical ionization (CI) with methanol. Melting point measurements were performed using a Fisher-Johns melting point apparatus.

Ellipsometry measurements were performed by using a Jovin-Yvon UVISEL Spectroscopic Ellipsometer. Curve fitting was completed using commercially available Delta-Psi software from Jovin-Yvon. Atomic Force Microscopy (AFM) images were acquired using a ThermoMicroscopes Explorer AFM equipped with an 8 μm Z-linearized (100 μm X and Y) scanner operating in non-contact mode. Commercially available (n) doped silicon non-contact AFM tips were purchased from Veeco (model 1650-00). Surface roughness measurements were calculated using ThermoMicroscopes SPM lab image analysis software. Powder diffraction measurements were measured at room temperature using Reflection mode on a Rigaku RAXIS rapid curved image plate detector with graphite monochromator, a Cu Ka radiation source (Ω = 190°, χ = 45°, Φ = 270°), a 0.5 mm collimator and 30-minute exposure. The reflected X-ray beam was measured from 5 to 80 degrees at 0.02 steps and 2 seconds per step.

Photochemistry. Standard lamps used for visualizing TLC plates (Spectroline E-series, 470 mW/cm^2) were used to carry out all the ring closed reactions. A 365 nm light source was used. Ring-opening reactions were carried out using the light of a 150 W tungsten source that was passed through a 490 cut off filter to

eliminate higher energy light. The UV-VIS spectra of this cut off filter is shown in the appendix. The UV-VIS spectra of this cut off filter is shown in the appendix. All solutions were prepared in THF at 2×10^{-5} M in the active photochromic component. Solid state UV-VIS spectra were obtained from films spin-coated onto quartz substrates.

Spin-coating. All films were spin-coated on 1 cm^2 silicon (100) substrates from toluene solution using a Laurell WS-400A-6NPP/Lite spin-coater. Substrates were cleaned by sequentially rinsing with acetone (5 mL), ethanol (5 mL), and methanol (5 mL) and dried with air filtered through glass wool before spin coating. Solutions for spin coating were prepared by dissolving the active compound (3 mg), and polymethyl methacrylate (PMMA, Aldrich, M_w=120 000) (52 mg) in toluene   (2 mL). 30 – 60 nm films for ellipsometry were prepared by saturating the substrate with 0.2 mL of solution and spinning at 4500 rpm for 80 sec. Thicker films (~200 nm) for AFM were prepared by saturating the substrate with a solution of active compound (3 mg), (PMMA, Aldrich, M_w=120 000) (52 mg), and toluene (1 mL) and spinning at 3000 rpm for 80 sec. All solutions were passed through 0.2 µm PTFE filters and added drop wise to the substrate using a syringe. Films for solid state UV-VIS spectra were fabricated in an identical procedure substituting 1 cm^2 silicon (100) with quartz. Films were allowed to air dry in the dark for 24 hours at 22 °C before testing.

Calculations. The polarizability and volume of each isomer at the ground state were determined from single point energy calculations (semi-empirical AM1) using the POLAR function in Spartan™ '02 for Macintosh from Wavefunction Inc.

Surface roughness measurements. The surface roughness of spin-coated films was evaluated using tapping mode AFM and calculated using ThermoMicroscopes SPM lab image analysis software. An area of 0.01 mm^2 was sampled for each measurement. An area of 0.08 mm^2 was sampled for film thickness measurement.

Synthetic Methods
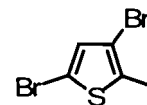
Synthesis of 3,5-dibromo-2-methylthiophene. A solution of 2-methylthiophene (10 mL, 100 mmol) and acetic acid (40 mL) was cooled in an ice bath to 0 °C with stirring. A mixture of bromine (10.3 ml, 200 mmol) dissolved in acetic acid (20 mL) was added via a dropping funnel over 1 hr. The dropping funnel was exchanged by a reflux condenser and the reaction was allowed to stir at 22 °C for an additional 12 hrs. The mixture was poured over ice (200 mL) and allowed to cool until all of the ice had dissolved. The reaction mixture was separated and extracted with Et_2O (2x100 mL) and the combined organic layers were washed with 1M NaOH (2x100 mL), then brine, dried over Na_2SO_4, filtered and evaporated *in vacuo* to a crude black oil. The crude product was distilled under reduced pressure (20 mmHG) using a fractional column. Collection at 60 °C yielded 39.2 g of 3,5-dibromo-2-methylthiphene (73%) as a colourless liquid. ^{1}H NMR (CDCl$_3$, 500 MHz): δ (ppm) = 2.34 (s, 3H), 6.86 (s, 1H).
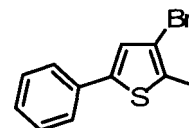
Synthesis of 3-bromo-2-methyl-5-phenylthiophene. A mixture of toluene (75 mL) and aqueous Na_2CO_3 solution (35 mL, 2 M) was deoxygenated by bubbling N_2 through the solution for 60 minutes, then treated with 3-5-dibromo-2-methylthiophene (5.00 g, 20 mmol), and N_2 was bubbled through the mixture for an additional 20 minutes. Phenylboronic acid (2.50 g, 21 mmol) in ethanol (5 mL) and $Pd(PPh_3)_4$ (0.07 g, 0.06 mmol) were added and the reaction mixture was heated at reflux for 24 hrs under an N_2 atmosphere. With the heat source removed, the reaction was allowed to cool to room temperature (22 °C). The aqueous layer was separated and extracted with Et_2O (3x50 mL) and the combined organic layers were washed with water, then brine, dried over Na_2SO_4, filtered and evaporated to dryness *in vacuo*. Purification by column chromatography (SiO_2, hexanes) yielded 3.6 g of 3-bromo-2-methyl-5-phenylthiohene (73%) as a white solid. Mp: 71-72 °C. ^{1}H NMR (CDCl$_3$, 500 MHz): δ (ppm) = 2.42 (s, 3H), 7.11 (s, 1H), 7.29 (m, 1H), 7.37 (t, 2H, J = 7 Hz), 7.51 (D, 2H, J = 7 Hz); ^{13}C NMR (CDCl$_3$ 125 MHz): δ = 14.8, 109.8, 125.3, 125.5, 127.7, 128.9, 133.5, 133.7, 141.1.
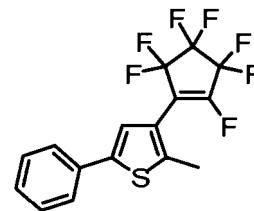
Synthesis of 1-(2-methyl-5-phenyl-3-thienyl)perfluorocyclopent-1-ene. To a 150 mL three-neck flask fitted with a magnetic stir bar, a solution of 3-bromo-2-methyl-5-phenylthiophene (2.0 g, 7.9 mmol) in anhydrous Et_2O (80 mL) was treated drop wise with *n*-butyllithium (4.0 mL, 2.5 M in hexanes, 10 mmol) over 10 minutes at -78°C under an N_2 atmosphere. The resulting suspension was stirred at this temperature for 15 minutes upon which octafluorocyclopentene (1.2 mL, 9 mmol) was added in one portion using a syringe previously cooled on dry ice. The solution continued to stir at -78°C for another hour. The cooling bath was removed and the reaction was allowed to warm to room temperature (22 °C). After quenching with saturated aqueous NH_4Cl (50 mL) the aqueous layer was separated and extracted with Et_2O (3x75 mL). The combined organic layers were washed with water, then brine, dried over Na_2SO_4, filtered and evaporated to dryness *in vacuo*. Purification by column chromatography (SiO_2, hexanes) yielded 2.10 g of 1-(2-methyl-5-phenyl-3-thienyl)perfluorocyclopent-1-ene (73%) as a pale yellow solid Mp = 35-37 °C. ^1H NMR ($CDCl_3$, 500 MHz): δ (ppm) = 2.49 (d, 3H, J = 3 Hz), 7.24 (s, 1H), 7.31 (m, 1H), 7.39 (t, 2H, J = 7 Hz), 7.55 (d, 2H, J = 7 Hz); ^{13}C NMR ($CDCl_2$, 125 MHz): δ = 14.9 (d, J = 5 Hz), 120.9, 122.7, 126.1, 128.6, 129.5, 133.6, 143.1, 143.9 (9 of 13 carbons found).
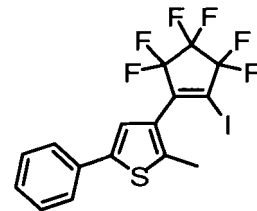
Synthesis of 3-(3,3,4,4,5,5-hexafluoro-2-iodocyclopent-1-enyl)-2-methyl-5-phenylthiophene. 1-(2-methyl-5-phenyl-3-thienyl)perfluorocyclopent-1-ene (1.75 g, 4.77 mmol) and anhydrous sodium iodide (1.40 g, 9.35 mmol), followed by anhydrous N,N-dimethylacetamide (20 mL) were added to a nitrogen flushed 100 mL schlenk tube equipped with a magnetic stir bar. The tube was sealed and the solution was heated to 165 °C in an oil bath for 6 hrs. The oil bath was turned off and the reaction was allowed to stir for an additional 16 hrs. The reaction mixture was washed with water and the aqueous layer was separated and extracted with Et_2O (3x75 mL). The combined organic layers were washed with water, then brine, dried over Na_2SO_4, filtered and evaporated to dryness *in vacuo* . Purification by column chromatography (SiO_2, hexanes) yielded 1.13 g of 3-(3,3,4,4,5,5-hexafluoro-2-iodocyclopent-1-enyl)-2-methyl-5-phenylthiophene (25%) as a white solid Mp = 74°C. ^{1}H NMR ($CDCl_3$, 500MHz): δ (ppm) = 2.46 (s, 3H), 7.10 (s, 1H), 7.31 (m, 1H), 7.39 (m, 2H), 7.55 (t, 2H, J = 7 Hz); ^{13}C NMR ($CDCl_3$, 125 MHz): δ = 15.3, 122.2, 125.9, 128.2, 129.2, 133.5, 140.6, 142.8 (8 of 13 carbons found).
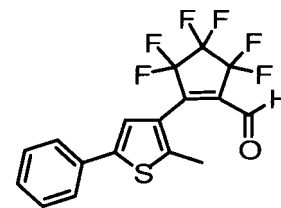
Synthesis of 3,3,4,4,5,5-hexafluoro-2-(2-methyl-5-phenylthiophen-3-yl)cyclopent-1-enecarbaldehyde. A solution of 3-(3,3,4,4,5,5-hexafluoro-2-iodocyclopent-1-enyl)-2-methyl-5-phenylthiophene (450 mg, 0.95 mmol) in anhydrous Et$_2$O (30 mL) was cooled in an acetone/dry-ice bath to -78 °C under a nitrogen atmosphere and treated with n-butyllithium (385 µL, 2.5 M in hexane, 0.96 mmol) in one portion via a syringe. The resulting pale yellow solution was stirred for an additional 15 minutes at -78 °C, upon which anhydrous DMF (220 µL, 2.8 mmol) was added in one portion using a syringe. The resulting blue-black mixture was stirred for another 15 minutes at -78 °C, and then was allowed to warm to room temperature (22 °C). After quenching with saturated aqueous NH$_4$Cl (50 mL) the aqueous layer was separated and extracted with Et$_2$O (3x50 mL). The combined organic layers were washed with water, then brine, dried over Na$_2$SO$_4$, filtered and evaporated to dryness *in vacuo*. Purification by column chromatography (SiO$_2$, hexanes/ethyl acetate 6:1), followed by recrystalization in hexanes, yielded 210 mg of 3,3,4,4,5,5-hexafluoro-2-(2-methyl-5-phenylthiophen-3-yl)cyclopent-1-enecarbaldehyde (59%) as a yellow solid Mp = 89–90 °C. ^{1}H NMR (CD$_2$Cl$_2$, 500 MHz): δ (ppm) = 2.48 (s, 3H), 7.27 (s, 1H), 7.35 (m, 1H), 7.42 (m, 2H), 7.56 (d, 2H, J = 8 Hz), 9.75 (s, 1H); ^{13}C NMR (CDCl$_3$, 125

MHz): δ (ppm) = 14.7, 122.7, 126.0, 128.7, 129.3, 132.8, 143.8, 145.6, 184.8 (9 of 15 carbons found). LRMS (CI-methanol): m/z = 377 [M+H]$^+$.
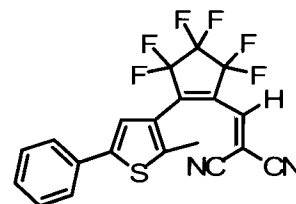
Synthesis of 2-((3,3,4,4,5,5-hexafluoro-2-(2-methyl-5-phenylthiophen-3-yl)cyclopent-1-enyl)methylene)malononitrile. A solution of 3,3,4,4,5,5-hexafluoro-2-(2-methyl-5-phenylthiophen-3-yl)cyclopent-1-enecarbaldehyde (100 mg, 0.27 mmol) and malanonitrile (35 mg, 0.53 mmol) in anhydrous dichloroethane (15 mL) was cooled in an ice bath to 0°C under a nitrogen atmosphere and treated with TiCl$_4$ (0.245 mL, 2.23 mmol) drop wise. After stirring for 5 minutes, pyridine (0.484 mL, 6 mmol) was added drop wise over 20 minutes. The ice bath was removed and the mixture was allowed to warm up to room temperature (22 °C). The purple solution was heated at reflux for 10 minutes during which time a precipitate formed and the colour changed to yellow-brown. After cooling back to room temperature (22 °C), the solvents were evaporated under reduced pressure. The solid green-brown residue was dissolved in 15% HCl (20 mL) with vigorous stirring, the aqueous layer was separated and extracted with chloroform (3 x 20 mL) and the combined organic layers were dried over Na$_2$SO$_4$, filtered and evaporated *in vacuo*. Purification by column chromatography (SiO$_2$, hexanes/ethyl acetate 6:1) yielded 43 mg of 2-

((3,3,4,4,5,5-hexafluoro-2-(2-methyl-5-phenylthiophen-3-yl)cyclopent-1-enyl)methylene)malononitrile (38%) as an orange solid Mp = 103-104 °C. ^{1}H NMR (CD$_2$Cl$_2$, 500 MHz): δ (ppm) = 2.40 (s, 3H), 7.18 (s, 1H), 7.20 (s, 1H), 7.36 (m, 1H), 7.42 (m, 2H), 7.55 (d, 2H, J = 7 Hz); ^{13}C NMR (CDCl$_3$, 125 MHz): 15.3, 92.5, 109.9, 112.6, 122.3, 124.4, 126.2, 128.9, 129.4, 132.5, 144.7, 145.3. LRMS (CI-methanol): m/z = 425 [M+H]$^+$.
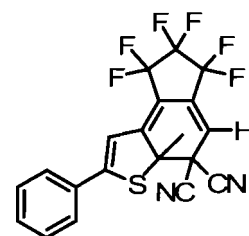
Photochemical ring-closing of 2-((3,3,4,4,5,5-hexafluoro-2-(2-methyl-5-phenylthiophen-3-yl)cyclopent-1-enyl)methylene)malononitrile. A standard glass NMR tube was charged with a 1 mL CD$_2$Cl$_2$ solution containing 1 mg of **3o**. The entire tube was irradiated with 365 nm light from a handheld TLC visualization lamp for 5 minute intervals and the photo-conversion was periodically monitored by ^{1}H NMR spectroscopy. The progress of the photocyclization was assessed by monitoring the methyl peak of the thiophene ring. At this concentration and wavelength, approximately 60 minutes was required to reach the photostationary state, which consisted of 18% of **3c**. The majority of the remaining material was assigned as the ring-open isomer. ^{1}H NMR (CD$_2$Cl$_2$, 500 MHz): δ (ppm) = 2.48 (s, 3H), 7.22 (s, 1H), 7.27 (s, 1H), 7.36 (m, 1H), 7.42 (m, 2H), 7.58 (d, 2H J = 8 H).

Synthesis of (3,3,4,4,5,5-hexafluoro-2-(2-methyl-5-phenylthiophen-3-yl)cyclopent-1-enyl)(phenyl)methanone. In a 25 mL three-necked flask, 3-(3,3,4,4,5,5-hexafluoro-2-iodocyclopent-1-enyl)-2-methyl-5-phenylthiophene (200 mg, 0.42 mmol) was dissolved in anhydrous Et$_2$O (10 mL). The solution was cooled in an acetone/dry-ice bath to -78°C under a nitrogen atmosphere and treated with n-butyllithium (200 μL, 2.5 M in hexane, 0.50 mmol) in one portion via a syringe. The resulting pale yellow solution was stirred for an additional 15 minutes at -78 °C, upon which a solution of anhydrous zinc chloride (100 mg, 0.72 mmol) in anhydrous THF (1.0 mL) was added drop wise via cannulation. The acetone/dry-ice bath was exchanged with an ice bath and after stirring for a further 30 minutes, and all solvents were removed under reduced pressure. The resulting residue was dissolved in anhydrous THF (0.5 mL), cooled in an ice bath to 0 °C, treated with benzoyl chloride (60 mg, 0.47 mmol), followed by a catalyst solution (1.0 mL) prepared from [Pd(PPh$_3$)$_2$]Cl$_2$ (21 mg) and i-Bu$_2$AlH (36 μL, 1.5 M in toluene) dissolved in anhydrous benzene (1 mL). Stirring was continued for 30 minutes at which time the ice bath was removed and the solution was stirred overnight at room temperature (22 °C). After quenching with 1 N HCl, the aqueous layer was separated and extracted with hexanes (3 x 20 mL). The

combined organic extracts were washed with saturated NaHCO$_3$, then brine, dried over Na$_2$SO$_4$, filtered and evaporated to dryness *in vacuo*. Purification by column chromatography (SiO$_2$, 5:1 hexane/ethyl acetate), followed by recrystalization in hexanes, yielded 78.8 mg of (3,3,4,4,5,5-hexafluoro-2-(2-methyl-5-phenylthiophen-3-yl)cyclopent-1-enyl)(phenyl)methanone (43%) as a yellow solid. Mp =71-72 °C; ^{1}HNMR (CDCl$_3$, 500 MHz): δ (ppm) = 2.28 (s, 3H), 7.11 (s, 1H), 7.28 (m, 1H), 7.36 (m, 4H), 7.41 (d, 2H, J = 7 Hz), 7.52 (m, 1H), 7.72 (d, 2H, J = 7 Hz); ^{13}CNMR (CDCl$_3$, 125 MHz): δ = 15.1, 88.7, 111.8, 112.1, 122.5, 123.2, 125.9, 128.5, 129.2, 129.3, 129.7, 132.1, 132.8, 134.2, 143.2, 143.4, 161.1. LRMS (CI-methanol): m/z = 453 [M+H]$^+$.
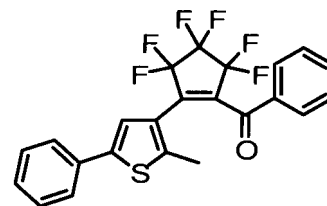

Synthesis of 2-((3,3,4,4,5,5-hexafluoro-2-(2-methyl-5-phenylthiophen-3-yl)cyclopent-1-enyl)(phenyl)methylene)malononitrile. A solution of (3,3,4,4,5,5-hexafluoro-2-(2-methyl-5-phenylthiophen-3-yl)cyclopent-1-enyl)(phenyl)methanone (73 mg, 0.16 mmol) and malanonitrile (27 mg, 0.41 mmol) in anhydrous dichloroethane (10 mL) was cooled in an ice bath to 0 °C under a nitrogen atmosphere and treated with TiCl$_4$ (0.17 mL, 1.55 mmol) drop wise. After stirring for 5 minutes, pyridine (0.33 mL, 4.1 mmol) was added drop wise over 20 minutes. The ice bath was removed and the mixture was allowed to

warm up to room temperature (22 °C). The purple solution was heated at reflux for 10 minutes during which time a precipitate formed and the colour changed to yellow-brown. After cooling back to room temperature (22 °C), the solvents were evaporated under reduced pressure. The solid green-brown residue was dissolved in 15% HCl (20 mL) with vigorous stirring, the aqueous layer was separated and extracted with chloroform (3 x 25 mL) and the combined organic layers were dried over Na$_2$SO$_4$, filtered and evaporated *in vacuo* . Purification by column chromatography (SiO$_2$, 20:1 hexane/EtOAc) on a long silica column (2.5 cm x 80cm) yielded 43.2 mg of 2-((4-bromophenyl)(3,3,4,4,5,5-hexafluoro-2-(2-methyl-5-phenylthiophen-3-yl)cyclopent-1-enyl)methylene)malononitrile (83%) as an orange oil; ^{1}H NMR (CDCl$_3$, 500 MHz): δ (ppm) = 2.43 (s, 3H), 6.87 (s, 1H), 7.31 (m, 1H), 7.37 (m, 4H), 7.52 (t, 2H, *J* = 7 Hz), 7.32 (m, 1H), 7.37 (m, 4H); ^{13}CNMR (CDCl$_3$, 125 MHz): δ =15.1, 88.8, 111.9, 112.1, 122.5, 123.3, 125.9, 128.5, 129.3, 124.2, 129.8, 132.1, 132.9, 134.2, 143.2, 143.5, 161.2. LRMS (CI-methanol): *m/z* = 501 [M+H]$^+$
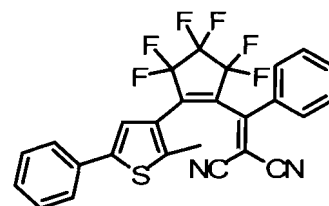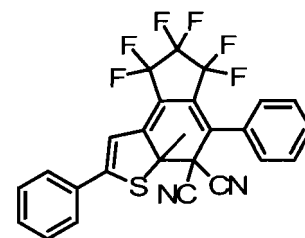

Photochemical ring-closing of 2-((3,3,4,4,5,5-hexafluoro-2-(2-methyl-5-phenylthiophen-3-yl)cyclopent-1-enyl)(phenyl)methylene)malononitrile. A standard glass NMR tube was charged with a 1 mL CD$_2$Cl$_2$ solution containing 1

mg of **4o**. The entire tube was irradiated with 365 nm light from a handheld TLC visualization lamp for 5 minute intervals and the photo-conversion was periodically monitored by ^{1}H NMR spectroscopy. The progress of the photocyclization was assessed by monitoring the methyl peak of the thiophene ring. At this concentration and wavelength, approximately 25 minutes was required to reach the photostationary state, which consisted of 38% of **4c**. The majority of the remaining material was assigned as the ring-open isomer. ^{1}H NMR (CD_2C_2, 500 MHz): δ (ppm) = 1.85 (s, 3H), 7.10 (s, 1H), 7.57 (m, 8H), 7.71 (d, 2H, J = 8 Hz).

**Synthesis of (4-bromophenyl)(3,3,4,4,5,5-hexafluoro-2-(2-methyl-5-phenylthiophen-3-yl)cyclopent-1-enyl)methanone.** In a 25 mL three-necked flask, 3-(3,3,4,4,5,5-hexafluoro-2-iodocyclopent-1-enyl)-2-methyl-5-phenylthiophene (250 mg, 0.53 mmol) was dissolved in anhydrous Et_2O (10 mL). The solution was cooled in an acetone/dry-ice bath to -78 °C under a nitrogen atmosphere and treated with n-butyllithium (250 μL, 2.5 M in hexane, 0.60 mmol) in one portion via a syringe. The resulting pale yellow solution was stirred for an additional 15 minutes at -78 °C, upon which a solution of anhydrous zinc chloride (100 mg, 0.72 mmol) in anhydrous THF (1.0 mL) was added drop wise via

cannulation. The acetone/dry-ice bath was exchanged with an ice bath and after stirring for a further 30 minutes, and all solvents were removed under reduced pressure. The resulting residue was dissolved in anhydrous THF (0.5 mL), cooled in an ice bath to 0°C, treated with 4-bromobenzoyl chloride (130 mg, 0.59 mmol), followed by a catalyst solution (1.0 mL) prepared from [Pd(PPh$_3$)$_2$]Cl$_2$ (21 mg) and i-Bu$_2$AlH (36 μL, 1.5 M in toluene) dissolved in anhydrous benzene (1 mL). Stirring was continued for 30 minutes at which time the ice bath was removed and the solution was stirred overnight at room temperature (22 °C). After quenching with 1 N HCl, the aqueous layer was separated and extracted with hexanes (3 x 20 mL). The combined organic extracts were washed with saturated NaHCO$_3$, then brine, dried over Na$_2$SO$_4$, filtered and evaporated to dryness *in vacuo*. Purification by column chromatography (SiO$_2$, 10:1 hexane/ethyl acetate), followed by recrystalization in hexanes, yielded 90 mg of (4-bromophenyl)(3,3,4,4,5,5-hexafluoro-2-(2-methyl-5-phenylthiophen-3-yl)cyclopent-1-enyl)methanone (33%) as a yellow solid. Mp = 73-74 °C; ^{1}HNMR (CDCl$_3$, 500 MHz): δ (ppm) = 2.28 (s, 3H), 7.10 (s, 1H), 7.30 (m, 1H), 7.36 (m, 2H), 7.43 (d, 2H, J = 7 Hz), 7.52 (t, 2H, J = 8 Hz), 7.59 (d, 2H, J = 8 Hz); ^{13}CNMR (CDCl$_3$, 125 MHz): δ = 14.8, 122.3, 124.2, 125.9, 128.4, 129.2, 130.6, 130.8, 132.5, 133.0, 133.7, 143.3, 143.3, 143.4, 187.9. FT-IR: 3065, 1662, 1581, 1271, 1145, 1073, 1024, 971, 816, 750, 523. LRMS (CI-methanol): Calcd for [M+H]$^+$ (C$_{23}$H$_{13}$OF$_6$BrS): m/z =531. Found: (CI-methanol): m/z = 531 ([M+H]$^+$, [^{79}Br], 83%), m/z = 533 ([M+H]$^+$, [^{81}Br], 100%).
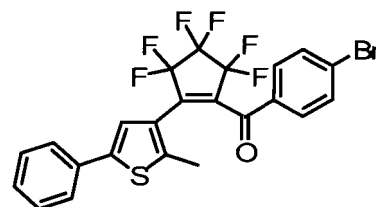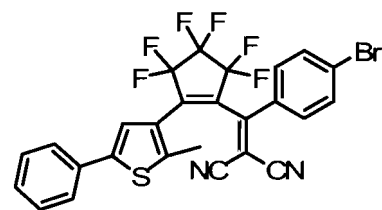
Synthesis of 2-((4-bromophenyl)(3,3,4,4,5,5-hexafluoro-2-(2-methyl-5-phenylthiophen-3-yl)cyclopent-1-enyl)methylene)malononitrile. A solution of (4-bromophenyl)(3,3,4,4,5,5-hexafluoro-2-(2-methyl-5-phenylthiophen-3-yl)cyclopent-1-enyl)methanone (43 mg, 0.081 mmol) and malanonitrile (14 mg, 0.211 mmol) in anhydrous dichloroethane (10 mL) was cooled in an ice bath to 0°C under a nitrogen atmosphere and treated with TiCl$_4$ (0.17 mL, 1.55 mmol) drop wise. After stirring for 5 minutes, pyridine (0.20 mL, 2.37 mmol) was added drop wise over 20 minutes. The ice bath was removed and the mixture was allowed to warm up to room temperature (22 °C). The purple solution was heated at reflux for 10 minutes during which time a precipitate formed and the colour changed to yellow-brown. After cooling back to room temperature (22 °C), the solvents were evaporated under reduced pressure. The solid green-brown residue was dissolved in 15% HCl (20 mL) with vigorous stirring, the aqueous layer was separated and extracted with chloroform (3 x 25 mL) and the combined organic layers were dried over Na$_2$SO$_4$, filtered and evaporated *in vacuo* . Purification by column chromatography (SiO$_2$, 20:1 hexane/EtOAc) on a long silica column (2.5 cm x 80cm) yielded 39.2 mg of 2-((4-bromophenyl)(3,3,4,4,5,5-hexafluoro-2-(2-methyl-5-phenylthiophen-3-yl)cyclopent-1-enyl)methylene)malononitrile (83%) as an orange oil. ^{1}H NMR (CDCl$_3$, 500 MHz):

δ (ppm) = 2.44 (s, 3H), 6.78 (s, 1H), 7.31 (m, 1H), 7.36 (d, 4H, J = 4 Hz), 7.43 (d, 2H, J = 9 Hz), 7.66 (d, 2H, J = 7 Hz). ^{13}CNMR (CDCl$_3$, 125 MHz): δ = 15.2, 111.6, 111.9, 122.3, 123.2, 126.0, 128.6, 129.3, 139.6, 130.6, 130.8, 132.7, 133.2, 143.4, 143.7 (15 of 22 carbons found). FT-IR: 2937, 2884, 2227, 1545,1504, 1335, 1276, 1140, 995, 968, 766, 555 cm^{-1}. LRMS (CI-methanol): Calcd for [M+H]$^{+}$ (C$_{26}$H$_{13}$N$_2$F$_6$BrS): m/z =580. Found: (CI-methanol): m/z = 580 ([M+H]$^{+}$, [^{79}Br], 100%), m/z = 582 ([M+H]$^{+}$, [^{81}Br], 15%).

Photochemical ring-closing of 2-((4-bromophenyl)(3,3,4,4,5,5-hexafluoro-2-(2-methyl-5-phenylthiophen-3-yl)cyclopent-1-enyl)methylene)malononitrile.

A standard glass NMR tube was charged with a 1 mL CD$_2$Cl$_2$ solution containing 1 mg of **5o**. The entire tube was irradiated with 365 nm light from a handheld TLC visualization lamp for 5 minute intervals and the photo-conversion was periodically monitored by ^{1}H NMR spectroscopy. The progress of the photocyclization was assessed by monitoring the methyl peak of the thiophene ring. At this concentration and wavelength, approximately 30 minutes was required to reach the photostationary state, which consisted of 35% of **5c**. The majority of the remaining material was assigned as the ring-open isomer. ^{1}H

NMR (CD$_2$C$_2$, 500 MHz): δ (ppm) = 1.75 (s, 3H), 7.02 (s, 1H), 7.32 (m, 2H), 7.43 (m, 2H), 7.49 (m, 1H), 7.63 (m, 4H).
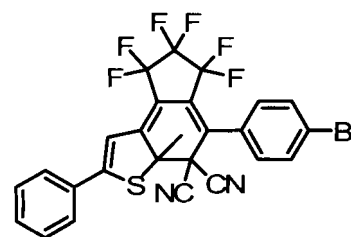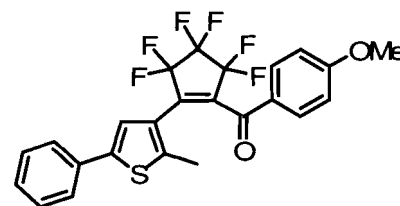

Synthesis of (3,3,4,4,5,5-hexafluoro-2-(2-methyl-5-phenylthiophen-3-yl)cyclopent-1-enyl)(4-methoxyphenyl)methanone. In a 25 mL three-necked flask, 3-(3,3,4,4,5,5-hexafluoro-2-iodocyclopent-1-enyl)-2-methyl-5-phenylthiophene (250 mg, 0.53 mmol) was dissolved in anhydrous Et$_2$O (10 mL). The solution was cooled in an acetone/dry-ice bath to -78 °C under a nitrogen atmosphere and treated with n-butyllithium (233 µL, 2.5 M in hexane, 0.58 mmol) in one portion via a syringe. The resulting pale yellow solution was stirred for an additional 15 minutes at -78 °C, upon which a solution of anhydrous zinc chloride (100 mg, 0.72 mmol) in anhydrous THF (1.0 mL) was added drop wise via cannulation. The acetone/dry-ice bath was exchanged with an ice bath and after stirring for a further 30 minutes, and all solvents were removed under reduced pressure. The resulting residue was dissolved in anhydrous THF (0.5 mL), cooled in an ice bath to 0 °C, treated with 4-methoxybenzoyl chloride (.85 µL, 0.58 mmol), followed by a catalyst solution (1.0 mL) prepared from [Pd(PPh$_3$)$_2$]Cl$_2$ (21 mg) and i-Bu$_2$AlH (36 µL, 1.5 M in toluene) dissolved in anhydrous benzene (1 mL). Stirring was continued for 30 minutes at which time

the ice bath was removed and the solution was stirred overnight at room temperature (22 °C). After quenching with 1 N HCl, the aqueous layer was separated and extracted with hexanes (3 x 20 mL). The combined organic extracts were washed with saturated NaHCO₃, then brine, dried over Na₂SO₄, filtered and evaporated to dryness *in vacuo*. Purification by column chromatography (SiO₂, 5:1 hexane/ethyl acetate), followed by recrystalization in hexanes, yielded 209 mg of Synthesis of (3,3,4,4,5,5-hexafluoro-2-(2-methyl-5-phenylthiophen-3-yl)cyclopent-1-enyl)(4-methoxyphenyl)methanone (82%) as a yellow solid. Mp = 87-89 °C. ¹HNMR (CDCl₃, 500 MHz): δ (ppm) = 2.30 (s, 3H), 3.81 (s, 3H), 6.83 (d, 2H, *J* = 9 Hz), 7.13 (s, 1H), 7.28 (m, 1H), 7.35 (t, 2H, *J* = 6 Hz), 7.43 (d, 2H, *J* = 9 Hz); ¹³CNMR (CDCl₃, 125 MHz): δ = 14.8, 55.8, 114.4, 122.6, 124.4, 125.8, 128.1, 128.2, 129.2, 132.0, 142.8, 143.0, 165.2, 186.9 (15 of 20 carbons found) LRMS (CI-methanol): *m/z* = 483 [M+H]⁺.

Synthesis of 2-((3,3,4,4,5,5-hexafluoro-2-(2-methyl-5-phenylthiophen-3-yl)cyclopent-1-enyl)(4-methoxyphenyl)methylene)malononitrile. A solution of (3,3,4,4,5,5-hexafluoro-2-(2-methyl-5-phenylthiophen-3-yl)cyclopent-1-enyl)(4-methoxyphenyl)methanone (90 mg, 0.18 mmol) and malanonitrile (30 mg, 0.45 mmol) in anhydrous dichloroethane (10 mL) was cooled in an ice bath to 0°C

under a nitrogen atmosphere and treated with $TiCl_4$ (0.18 mL, 1.6 mmol) drop wise. After stirring for 5 minutes, pyridine (0.375 mL, 4.6 mmol) was added drop wise over 20 minutes. The ice bath was removed and the mixture was allowed to warm up to room temperature (22 °C). The purple solution was heated at reflux for 10 minutes during which time a precipitate formed and the colour changed to yellow-brown. After cooling back to room temperature (22 °C), the solvents were evaporated under reduced pressure. The solid green-brown residue was dissolved in 15% HCl (20 mL) with vigorous stirring, the aqueous layer was separated and extracted with chloroform (3 x 25 mL) and the combined organic layers were dried over Na_2SO_4, filtered and evaporated *in vacuo*. Purification by column chromatography (SiO_2, 4:1 hexane/acetone) on a long silica column (2.5 cm x 80cm) yielded 58.1 mg of 2-2-((3,3,4,4,5,5-hexafluoro-2-(2-methyl-5-phenylthiophen-3-yl)cyclopent-1-enyl)(4-methoxyphenyl)methylene)malononitrile (57%) as an orange oil. ^{1}H NMR ($CDCl_3$, 500 MHz): δ (ppm) = 2.45 (s, 3H), 3.89 (s, 3H), 6.87 (s, 1H), 7.01 (d, 2H, J = 9 Hz), 7.29 (m, 1H), 7.36 (m, 4H), 7.68 (d, 2H, J = 9 Hz). ^{13}CNMR ($CDCl_3$, 125 MHz): δ = 15.3, 56.1, 84.5, 112.6, 113.0, 114.8, 115.3, 122.7, 123.2, 124.0, 125.9, 128.4, 129.3, 129.9, 132.2, 133.0, 143.2, 159.5, 164.9 (19 of 23 carbons found); LRMS (CI-methanol): m/z = 531 $[M+H]^+$

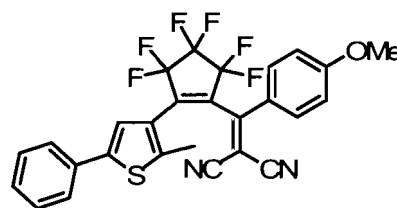**Photochemical ring-closing of 2-((3,3,4,4,5,5-hexafluoro-2-(2-methyl-5-phenylthiophen-3-yl)cyclopent-1-enyl)(4-methoxyphenyl)methylene)malononitrile.** A standard glass NMR tube was charged with a 1 mL $CDCL_3$ solution containing 1 mg of **6o**. The entire tube was irradiated with 365 nm light from a handheld TLC visualization lamp for 5 minute intervals and the photo-conversion was periodically monitored by ^1H NMR spectroscopy. The progress of the photocyclization was assessed by monitoring the methyl peak of the thiophene ring. At this concentration and wavelength, approximately 15 minutes was required to reach the photostationary state, which consisted of 56% of **6c**. The majority of the remaining material was assigned as the ring-open isomer. ^1H NMR ($CDCl_3$, 500 MHz): δ (ppm) = 1.83 (s, 3H), 3.89 (s, 3H), 6.92 (d, 1H), 7.05 (s, 1H), 7.49 (m, 6H), 7.66 (d, 2H J = 8 H).
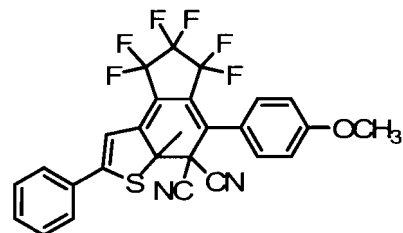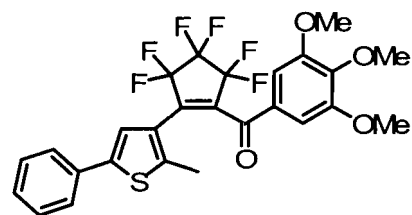
Synthesis of (3,3,4,4,5,5-hexafluoro-2-(2-methyl-5-phenylthiophen-3-yl)cyclopent-1-enyl)(3,4,5-trimethoxyphenyl)methanone . In a 25 mL three-necked flask, 3-(3,3,4,4,5,5-hexafluoro-2-iodocyclopent-1-enyl)-2-methyl-5-phenylthiophene (250mg, 0.53 mmol) was dissolved in anhydrous Et_2O (10 mL). The solution was cooled in an acetone/dry-ice bath to -78 °C under a nitrogen atmosphere and treated with *n*-butyllithium (240 µL, 2.5 M in hexane, 0.59 mmol) in one portion via a syringe. The resulting pale yellow solution was stirred for an additional15 minutes at -78 °C, upon which a solution of anhydrous zinc chloride (80 mg, 0.58 mmol) in anhydrous THF (1.0 mL) was added drop wise via cannulation. The acetone/dry-ice bath was exchanged with an ice bath and after stirring for a further 30 minutes, and all solvents were removed under reduced pressure. The resulting residue was dissolved in anhydrous THF (0.5 mL), cooled in an ice bath to 0 °C, treated with 3,4,5-trimethoxy benzoyl chloride (0.5 mmol), followed by a catalyst solution (1.0 mL) prepared from [Pd(PPh₃)₂]Cl₂ (21 mg) and *i*-Bu₂AlH (36 µL, 1.5 M in toluene) dissolved in anhydrous benzene (1 mL). Stirring was continued for 30 minutes at which time the ice bath was removed and the solution was stirred overnight at room temperature (22 °C). After quenching with 1 N aqueous HCl, the aqueous layer was separated and extracted with hexanes (3 x 20 mL). The combined organic extracts were then washed with saturated $NaHCO_3$, then brine, dried over Na_2SO_4, filtered and evaporated to dryness *in vacuo*. Purification by column chromatography (SiO₂, 5:1 hexane/ethyl acetate), followed by recrystalization in hexanes, yielded 200

mg of (3,3,4,4,5,5-hexafluoro-2-(2-methyl-5-phenylthiophen-3-yl)cyclopent-1-

enyl)(3,4,5-trimethoxyphenyl)methanone (70%) as a yellow solid. Mp = 111-112

°C; ^{1}HNMR (CDCl$_3$, 500 MHz): δ (ppm) = 2.33 (s, 3H), 3.82 (s, 6H), 3.88 (s, 3H),

7.02 (s, 2H), 7.14 (s, 1H), 7.30 (m, 1H), 7.36 (t, 2H, J = 8 Hz), 7.43 (m, 2H);

^{13}CNMR (CDCl$_3$, 125 MHz): δ = 14.8, 56.4, 61.2, 107.1, 122.4, 124.2,

125.7,128.4, 129.2, 129.8, 133.0, 143.1, 143.2, 144.7, 153.3, 187.2 (16 of 21

carbons found). FT-IR: 3065, 1662, 1581, 1272, 1145, 1074, 1024, 816, 750 cm$^-$
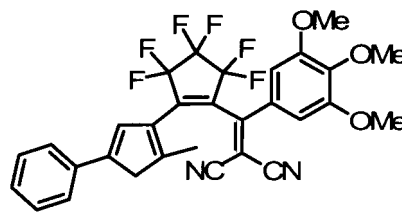
^{1}. LRMS (CI - methanol): m/z =543 [M+H]$^+$.

Synthesis of 2-((3,3,4,4,5,5-hexafluoro-2-(2-methyl-5-phenylthiophen-3-

yl)cyclopent-1-enyl)(3,4,5-trimethoxyphenyl)methylene)malononitrile. A

solution of (3,3,4,4,5,5-hexafluoro-2-(2-methyl-5-phenylthiophen-3-yl)cyclopent-

1-enyl)(3,4,5-trimethoxyphenyl)methanone (90 mg, 0.19 mmol) and malanonitrile

(30 mg, 0.45 mmol) in anhydrous dichloroethane (10 mL) was cooled in an ice

bath to 0°C under a nitrogen atmosphere and treated with TiCl$_4$ (0.17 mL, 1.6

mmol) drop wise. After stirring for 5 minutes, pyridine (0.33 mL, 4.1 mmol) was

added drop wise over 20 minutes. The ice bath was removed and the mixture

was allowed to warm up to room temperature (22 °C). The purple solution was

heated to reflux for 10 minutes during which time a precipitate formed and the

colour changed to yellow-brown. After cooling back to room temperature (22 °C), the solvents were evaporated under reduced pressure. The solid green-brown residue was dissolved in 15% HCl (20 mL) with vigorous stirring, the aqueous layer was separated and extracted with chloroform (3 x 25 mL) and the combined organic layers were dried over Na_2SO_4, filtered and evaporated *in vacuo* . Purification by column chromatography (SiO_2, 4:1 hexane/acetone) on a long silica column (2.5 cm x 80cm) yielded 66.7 mg of 2-((3,3,4,4,5,5-hexafluoro-2-(2-methyl-5-phenylthiophen-3-yl)cyclopent-1-enyl)(3,4,5-trimethoxyphenyl)methylene)malononitrile (67%) as an orange oil. ^{1}H NMR ($CDCl_3$, 500 MHz): δ (ppm) = 2.46 (s, 3H), 3.85 (s, 6H), 3.96 (s, 3H), 6.84 (s, 1H), 6.92 (s, 2H), 7.32 (m, 1H), 7.37 (m, 4H). ^{13}CNMR ($CDCl_3$, 125 MHz): δ = 15.2, 29.9, 32.9, 56.6, 61.5, 86.1, 107.3, 112.2, 112.8, 122.7, 123.1, 125.8, 126.4, 128.5, 129.3, 132.2, 143.1, 143.3, 143.8, 153.5, 159.8 (21 of 24 carbons found) (15 of 22 carbons found).FT-IR: 2937, 2884, 2227, 1545,1504, 1335, 1276, 1140, 995, 968, 766, 555 cm^{-1}. LRMS (CI - methanol): *m/z* =591 [M+H]$^+$.
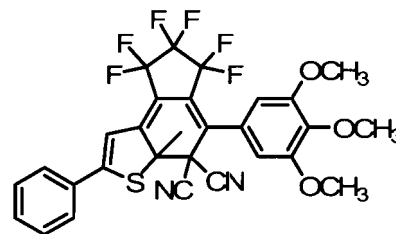
Photochemical ring-closing of 2-((3,3,4,4,5,5-hexafluoro-2-(2-methyl-5-phenylthiophen-3-yl)cyclopent-1-enyl)(3,4,5-trimethoxyphenyl)methylene)malononitrile. A standard glass NMR tube was charged with a 1 mL CD_2Cl_2 solution containing 1 mg of **7o**. The entire tube was irradiated with 365 nm light from a handheld TLC visualization lamp for 5 minute intervals and the photo-conversion was periodically monitored by ^1H NMR spectroscopy. The progress of the photocyclization was assessed by monitoring the methyl peak of the thiophene ring. At this concentration and wavelength, approximately 15 minutes was required to reach the photostationary state, which consisted of 41% of **7c**. The majority of the remaining material was assigned as the ring-open isomer. ^1H NMR (CD_2C_2, 500 MHz): δ (ppm) = 1.85 (s, 3H), 3.86 (s, 3H), 3.89 (s, 6H), 6.69 (s, 2H), 7.09 (s, 1H), 7.52 (m, 2H), 7.57 (m, 1H), 7.71 (d, 2H, J = 8 Hz).

112

Synthesis of (3,3,4,4,5,5-hexafluoro-2-(2-methyl-5-phenylthiophen-3-yl)cyclopent-1-enyl)(4-nitrophenyl)methanone. In a 25 mL three-necked flask, 3-(3,3,4,4,5,5-hexafluoro-2-iodocyclopent-1-enyl)-2-methyl-5-phenylthiophene (245 mg, 0.52 mmol) was dissolved in anhydrous Et$_2$O (15 mL). The solution was cooled in an acetone/dry-ice bath to -78 °C under a nitrogen atmosphere and treated with n-butyllithium (230 µL, 2.5 M in hexane, 0.67 mmol) in one portion via a syringe. The resulting pale yellow solution was stirred for an additional 15 minutes at -78 °C, upon which 4 - (dimethylamino) benzoyl chloride (114 mg, 0.62 mmol) was added in one portion. The ice bath was removed and the mixture was allowed to warm up to room temperature (22 °C) and stir for 30 minutes. After quenching with 1 N HCl, the aqueous layer was separated and extracted with hexanes (3 x 20 mL). The combined organic extracts were washed with saturated NaHCO$_3$, then brine, dried over Na$_2$SO$_4$, filtered and evaporated to dryness *in vacuo*. Purification by column chromatography (SiO$_2$, 5:1 hexane/ethyl acetate), followed by recrystalization in hexanes, yielded 124.8 mg of (4-(dimethylamino)phenyl)(3,3,4,4,5,5-hexafluoro-2-(2-methyl-5-phenylthiophen-3-yl)cyclopent-1-enyl)methanone (46.3%) as a yellow solid. Mp = 95-97 °C; ^{1}HNMR (CDCl$_3$, 500 MHz): δ (ppm) = 2.27 (s, 3H), 7.11 (s, 1H), 7.29 (m, 1H, J = 7 Hz), 7.36 (t, 2H, J = 7 Hz),7.40 (d, 2H,), 7.86 (d, 2H J = 9 Hz), 8.19 (d, 2H, J =

9 Hz) ; ^{13}CNMR (CDCl$_3$, 125 MHz): δ = 14.8, 22.7, 122.0, 124.1, 125.9, 128.6, 129.3, 130.0, 132.6, 139.2, 143.7, 144.0, 151.1, 187.6. (14 of 19 carbons found); LRMS (CI-methanol): m/z = 498 [M+H]$^+$.

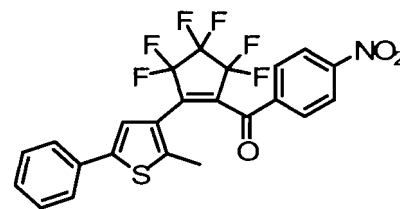**Synthesis of 2-((3,3,4,4,5,5-hexafluoro-2-(2-methyl-5-phenylthiophen-3-yl)cyclopent-1-enyl)(4-nitrophenyl)methylene)malononitrile.** A solution of (3,3,4,4,5,5-hexafluoro-2-(2-methyl-5-phenylthiophen-3-yl)cyclopent-1-enyl)(4-nitrophenyl)methanone (115 mg, 0.23 mmol) and malanonitrile (40 mg, 0.23 mmol) in anhydrous dichloroethane (10 mL) was cooled in an ice bath to 0 °C under a nitrogen atmosphere and treated with TiCl$_4$ (0.25 mL, 2.3 mmol) drop wise. After stirring for 5 minutes, pyridine (0.46 mL, 5.7 mmol) was added drop wise over 20 minutes. The ice bath was removed and the mixture was allowed to warm up to room temperature (22 °C). The purple solution was heated at reflux for 10 minutes during which time a precipitate formed and the colour changed to yellow-brown. After cooling back to room temperature (22 °C), the solvents were evaporated under reduced pressure. The solid green-brown residue was dissolved in 15% HCl (20 mL) with vigorous stirring, the aqueous layer was separated and extracted with chloroform (3 x 25 mL) and the combined organic layers were dried over Na$_2$SO$_4$, filtered and evaporated *in vacuo* . Purification by column chromatography (SiO$_2$, 4:1 hexane/acetone) on a long silica column (2.5
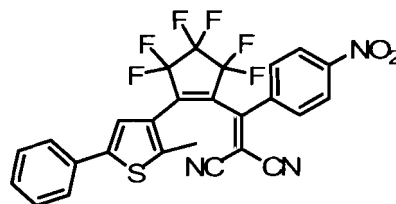
cm x 80cm) yielded 45 mg of 2-((3,3,4,4,5,5-hexafluoro-2-(2-methyl-5-phenylthiophen-3-yl)cyclopent-1-enyl)(4-nitrophenyl)methylene)malononitrile

(35%) as an orange oil. ^{1}H NMR (CDCl$_3$, 500 MHz): δ (ppm) = 2.46 (s, 3H), 6.77

(s, 1H), 7.34 (m, 5H), 7.67 (d, 2H, J = 9 Hz), 8.33 (d, 2H, J = 9 Hz); ^{13}CNMR

(CDCl$_3$, 125 MHz): δ = 15.2, 66.0, 92.4, 110.9, 111.1, 121.9, 124.7, 125.9, 128.9,

129.4, 130.2, 132.2, 137.8, 143.8, 144.2, 150.3, 159.0 (17.of 22 carbons found);

LRMS (CI-methanol): m/z = 546 [M+H]$^+$.
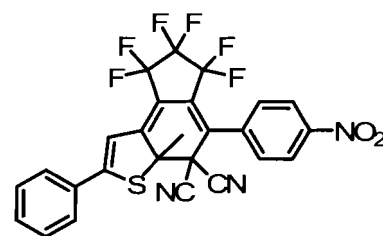
Photochemical ring-closing of 2-((3,3,4,4,5,5-hexafluoro-2-(2-methyl-5-phenylthiophen-3-yl)cyclopent-1-enyl)(4-nitrophenyl)methylene)malononitrile. A standard glass NMR tube was

charged with a 1 mL CD$_2$Cl$_3$ solution containing 1 mg of **8o**. The entire tube was

irradiated with 365 nm light from a handheld TLC visualization lamp for 5 minute

intervals and the photo-conversion was periodically monitored by ^{1}H NMR

spectroscopy. The progress of the photocyclization was assessed by monitoring

the methyl peak of the thiophene ring. At this concentration and wavelength,

approximately 25 minutes was required to reach the photostationary state, which

consisted of 40% of **8c**. The majority of the remaining material was assigned as

115

the ring-open isomer. ^{1}H NMR (CD$_2$C$_2$, 500 MHz): δ (ppm) = 1.85 (s, 3H), 7.15 (s, 1H), 7.54 (m, 2H), 7.29 (m, 1H), 7.73 (m, 4H), 8.39 (d, 2H, J = 8 Hz).
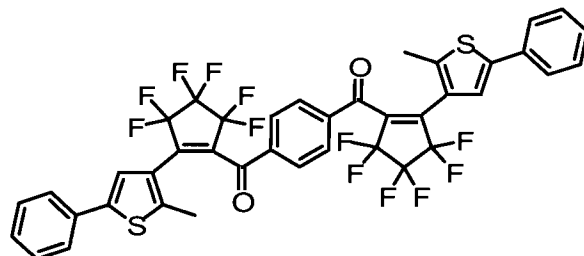

Synthesis of 1,2-bis(((3,3,4,4,5,5-hexafluoro-2-(2-methyl-5-phenylthiophen-3-yl)cyclopent-1-enyl)methanone) benzene. In a 25 mL three-necked flask, 3-(3,3,4,4,5,5-hexafluoro-2-iodocyclopent-1-enyl)-2-methyl-5-phenylthiophene (290 mg, 0.61 mmol) was dissolved in anhydrous Et$_2$O (15 mL). The solution was cooled in an acetone/dry-ice bath to -78 °C under a nitrogen atmosphere and treated with n-butyllithium (250 µL, 2.5 M in hexane, 0.62 mmol) in one portion via a syringe. The resulting pale yellow solution was stirred for an additional 15 minutes at -78 °C, upon which a solution of anhydrous zinc chloride (110 mg, 0.75 mmol) in anhydrous THF (1.0 mL) was added drop wise via cannulation. The acetone/dry-ice bath was exchanged with an ice bath and after stirring for a further 30 minutes, and all solvents were removed under reduced pressure. The resulting residue was dissolved in anhydrous THF (0.5 mL), cooled in an ice bath to 0 °C, treated with excess terephthaloyl chloride(500 mg, 2.5 mmol) in one portion, followed by a catalyst solution (1.0 mL) prepared from [Pd(PPh$_3$)$_2$]Cl$_2$ (21 mg) and i-Bu$_2$AlH (36µL, 1.5 M in toluene) dissolved in anhydrous benzene (1

mL). Stirring was continued for 30 minutes at which time the ice bath was removed and the solution was stirred overnight at room temperature (22 °C). After quenching with 1 N HCl, the aqueous layer was separated and extracted with hexanes (3 x 20 mL). The combined organic extracts were washed with saturated $NaHCO_3$, then brine, dried over Na_2SO_4, filtered and evaporated to dryness *in vacuo*. Purification by column chromatography (SiO_2, 10:1 hexane/ethyl acetate), followed by recrystalization in hexanes, yielded 75 mg of 1,2-bis(((3,3,4,4,5,5-hexafluoro-2-(2-methyl-5-phenylthiophen-3-yl)cyclopent-1-enyl)methanone) benzene (30%) as a yellow solid. Mp = 171-172 °C; ^{1}HNMR (CDCl$_3$, 500 MHz): δ (ppm) = 2.11 (s, 6H), 7.05 (s, 2H), 7.30 (m, 2H), 7.36 (m, 8H), 7.67 (s, 4H,); ^{13}CNMR (CDCl$_3$, 125 MHz): δ =14.6, 59.5, 122.2, 124.1, 125.9, 128.6, 129.2,132.7, 138.9, 143.4, 143.7, 188.0 (12 of 17 carbons found) . FT-IR: 3069, 1670, 1277, 1219, 1148, 1075, 1035, 756. LRMS (CI-methanol): m/z = 827 [M+H]$^+$.
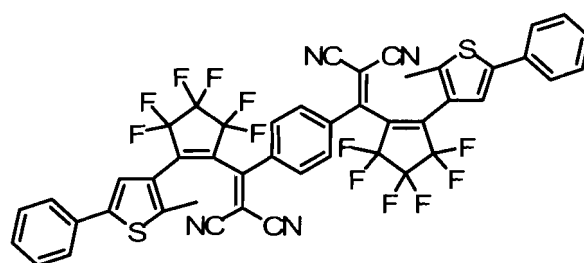
Synthesis of 1,4-bis(2-((3,3,4,4,5,5-hexafluoro-2-(4,5-dihydro-2-methyl-5-phenylthiophen-3-yl)cyclopent-1-enyl)methyl-1-enyl)malononitrile)benzene.

A solution of 1,2-bis(((3,3,4,4,5,5-hexafluoro-2-(2-methyl-5-phenylthiophen-3-

yl)cyclopent-1-enyl)methanone) benzene (50 mg, 0.060 mmol) and malanonitrile

(20 mg, 0.30 mmol) in anhydrous dichloroethane (10 mL) was cooled in an ice

bath to 0°C under a nitrogen atmosphere and treated with $TiCl_4$ (0.1 mL, 0.9

mmol) drop wise. After stirring for 5 minutes, pyridine (0.33 mL, 2.5 mmol) was

added drop wise over 20 minutes. The ice bath was removed and the mixture

was allowed to warm up to room temperature (22 °C). The purple solution was

heated at reflux for 10 minutes during which time a precipitate formed and the

colour changed to yellow-brown. After cooling back to room temperature (22 °C),

the solvents were evaporated under reduced pressure. The solid green-brown

residue was dissolved in 15% HCl (20 mL) with vigorous stirring, the aqueous

layer was separated and extracted with chloroform (3 x 25 mL) and the combined

organic layers were dried over Na_2SO_4, filtered and evaporated *in vacuo*.

Purification by column chromatography (SiO_2, 10:1 hexane/ethyl acetate),

followed by recrystalization in hexanes, yielded 27 mg of 1,4-bis(2-((3,3,4,4,5,5-

hexafluoro-2-(4,5-dihydro-2-methyl-5-phenylthiophen-3-yl)cyclopent-1-

enyl)methyl-1-enyl)malononitrile)benzene (48%) as an orange solid. Mp = 162-

164 °C; ^{1}HNMR (CDCl$_3$, 500 MHz): δ (ppm) = 2.35 (s, 6H), 7.33 (m, 10H), 7.61

(s, 4H) ^{13}CNMR (CDCl$_3$, 125 MHz): δ = 15.1, 31.8, 34.9, 91.6, 111.0, 111.2,

121.8, 123.3, 125.9, 128.8, 129.3, 129.4, 129.8, 132.4, 136.5, 143.5, 144.2,

158.7 (17 of 20 carbons found). FT-IR: 3065, 1662, 1581, 1271, 1145, 1073,

1024, 971, 816, 750, 523.
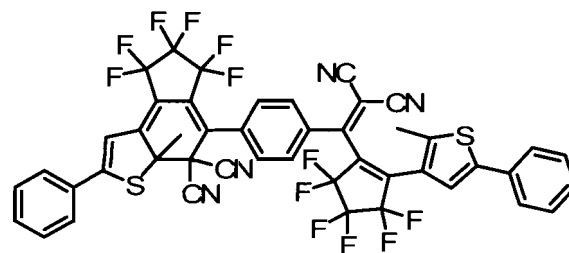
Photochemical ring-closing of 1,4-bis(2-((3,3,4,4,5,5-hexafluoro-2-(4,5-dihydro-2-methyl-5-phenylthiophen-3-yl)cyclopent-1-enyl)methyl-1-enyl)malononitrile)benzene. A standard glass NMR tube was charged with a 1 mL CDCl₃ solution containing 1 mg of **9o**. The entire tube was irradiated with 365 nm light from a handheld TLC visualization lamp for 5 minute intervals and the photo-conversion was periodically monitored by ^{1}H NMR spectroscopy. The progress of the photocyclization was assessed by monitoring the methyl peak of the thiophene ring. At this concentration and wavelength, approximately 30 minutes was required to reach the photostationary state, which consisted of 15% of **9c**. The majority of the remaining material was assigned as the ring-open isomer. ^{1}H NMR (CDCl₃, 500 MHz): δ (ppm) = 1.79 (s, 3H), 2.39 (s, 3H), 6.87 (s, 1H), 7.05 (s, 1H), 7.08 (s, 1H), 7.47 (s,1H), 7.53 (m, 2H), 7.59 (m, 1H), 7.63 (m, 2H), 7.69 (m, 2H), 7.73 (m, 2H).
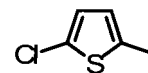
Synthesis of 2-chloro-5-methylthiophene . A solution of 2-methylthiophene (18.0 mL, 180 mmol) and 1-chloro-2,5-pyrrolidinedione (25.0 g, 187 mmol) in benzene (200 mL) and acetic acid (85 mL) was heated at reflux for 18 hours. With the heat source removed, the reaction was allowed to cool to room temperature (22 °C). The reaction mixture was then neutralized with saturated Na_2CO_3, after which the aqueous layer was separated and extracted with Et_2O (3x50 mL) and the combined organic layers were washed with water, then brine, dried over Na_2SO_4, and filtered. The solution was evaporated *in vacuo* until approximately 100 mL remained, and then distilled under reduced pressure (20 mmHg) using a fractional column. Collection at 42 – 45 °C yielded 20.5 g of 2-chloro-5-methylthiophene (83%) as a colourless liquid. ^1H NMR ($CDCl_3$, 500 MHz): δ (ppm) = 2.41 (s, 3H), 6.62 (m, 1H), 6.68 (d, 1H).
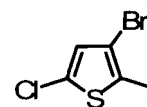
Synthesis of 3-bromo-5-chloro-2-methylthiophene . A solution of 2-chloro-5-methylthiophene (20.0 g, 150 mmol) in chloroform (150 mL) was stirred an cooled in an ice bath to 0 °C. A mixture of bromine (44.0 g, 150 mmol) dissolved in chloroform (50 mL) was added via a dropping funnel over 1 hr. The reaction was warmed to 22 °C and stirred for 90 additional minutes. The mixture was

quenched with water (300 mL) and the layers were separated and extracted with CHCl₃ (2x200 mL) and the combined organic layers were washed with water (2x100 mL), then brine, dried over Na₂SO₄, and evaporated *in vacuo* to a crude black oil. The crude product was distilled under reduced pressure (20 mmHG) using a fractional column. Collection at 35 °C yielded 23.1 g of 3,5-dibromo-2-methylthiphene (86%) as a colourless liquid. ^{1}H NMR (CDCl₃, 500 MHz): δ (ppm) = 2.32 (s, 3H), 6.72 (s, 1H).
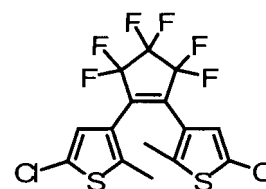
Synthesis of 1,2-bis-(3-(5-chloro-2-methylthienyl))perfluorocyclopentene. A solution of 3-bromo-5-chloro-2-methylthiophene (1.00 g, 4.73 mmol) in anhydrous Et₂O (40 mL) was cooled in an acetone/dry-ice bath to -78 °C under a nitrogen atmosphere and treated with *n*-butyllithium (1.9 mL, 2.5M in hexane, 4.7 mmol) drop wise via syringe until TLC provided no evidence of the starting material. The resulting suspension was stirred at this temperature for 15 minutes upon which octafluorocyclopentene (0.32 mL, 2.4 mmol) was added in one portion using a syringe previously cooled on dry ice. The solution continued to stir at -78 °C for another hour. The cooling bath was removed and the reaction was allowed to warm to room temperature (22 °C) where it stirred for an additional 30 minutes. After quenching with saturated aqueous NH₄Cl (50 mL)

the aqueous layer was separated and extracted with Et_2O (3x50 mL). The combined organic layers were washed with water, then brine, dried over Na_2SO_4, filtered and evaporated to dryness *in vacuo*. Purification by column chromatography (SiO_2, hexanes) yielded 1.15 g of 1,2-bis-(3-(5-chloro-2-methylthienyl))perfluorocyclopentene (55%) as a white solid Mp = 149-150 °C. ^1H NMR ($CDCl_3$, 500 MHz): δ (ppm) = 1.88 (s, 6H), 6.88 (s, 2H); LRMS (EI): 437 (M^+).
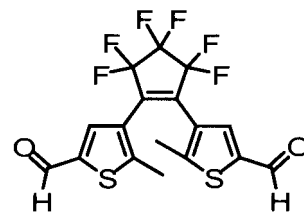
Synthesis of 1,2-bis-(2-methyl-5-formyl-3-thienyl)perfluorocyclopentene. A solution of 1,2-bis-(3-(5-chloro-2-methylthienyl))perfluorocyclopentene (500 mg, 1.14 mmol) in anhydrous Et_2O (50 mL) was cooled in an acetone/dry-ice bath to -78 °C under a nitrogen atmosphere and treated with *t*-butyllithium (1.5 mL, 2.4 M in hexane, 2.4 mmol) drop wise via syringe until TLC provided no evidence of the starting material. Anhydrous DMF (0.21 mL, 2.8 mmol) was added in one portion using a syringe and the resulting suspension was stirred at this temperature for 15 minutes. The cooling bath was removed and the reaction was allowed to warm to room temperature (22 °C) where it stirred for an additional 60 minutes. After quenching with saturated aqueous NH_4Cl (50mL) the aqueous layer was separated and extracted with Et_2O (3x50 mL). The combined organic layers were

washed with water, then brine, dried over Na$_2$SO$_4$, filtered and evaporated to dryness *in vacuo*. Purification by column chromatography (SiO$_2$, hexanes/ethyl acetate 5:1) yielded 361 mg of 1,2-bis-(2-methyl-5-formyl-3-thienyl)perfluorocyclopentene (69%) as a white solid Mp = 182-183 °C. ^{1}H NMR (CDCl$_3$, 500MHz): δ (ppm) = 2.03 (s, 6H), 7.73 (s, 2H), 9.85 (s, 2H); LRMS (CI-methanol): *m/z* = 425 [M+H]$^+$.
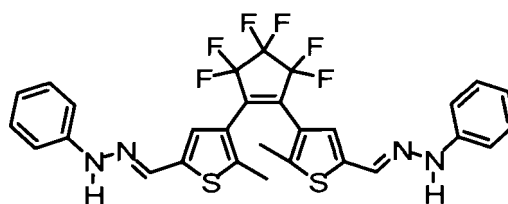
Synthesis of 1,2-bis(2-methyl-5-formyl-3-thienyl)perfluorocyclopentene Phenyl Hydrazone. A solution of 1,2-bis-(2-methyl-5-formyl-3-thienyl)perfluorocyclopentene (284 mg, 0.66 mmol), 2.5 mL of ethanol, phenylhayrazine (0.80 mL, 14 mmol), and acetic acid (0.2 mL) were heated at reflux for 4 hours. The mixture was cooled to room temperature (22 °C), then down to -20 °C for 24 hours, obtaining a precipitate. Filtration followed by washing with cool methanol yielded 238 mg of 1,2-bis(2-methyl-5-formyl-3-thienyl)perfluorocyclopentene Phenyl Hydrazone (59%) as a yellow solid Mp = 187-189 °C. ^{1}H NMR (CD$_2$Cl$_2$, 500 MHz): δ (ppm) = 1.95 (s, 6H), 6.86 (t, 2H, *J* = 7 Hz), 7.03 (s, 2H), 7.05 (s, 4H), 7.25 (t, 4H, *J* = 8 Hz), 7.59 (br.s, 2H), 7.79 (s, 2H); LRMS (CI-methanol): *m/z* = 549 [M+H]$^+$

5 Appendix

5.1 ¹H NMR Spectra for 3c - 9c
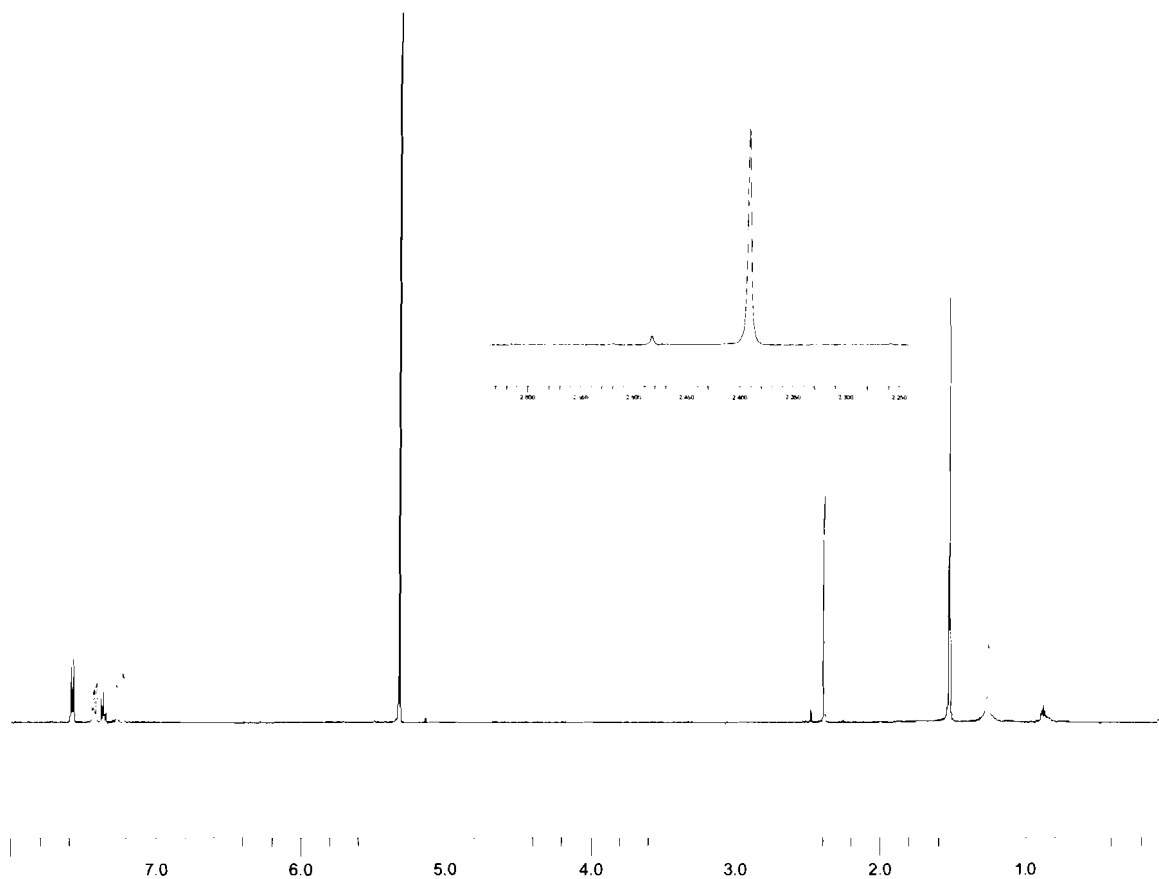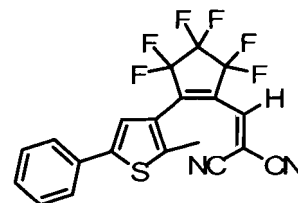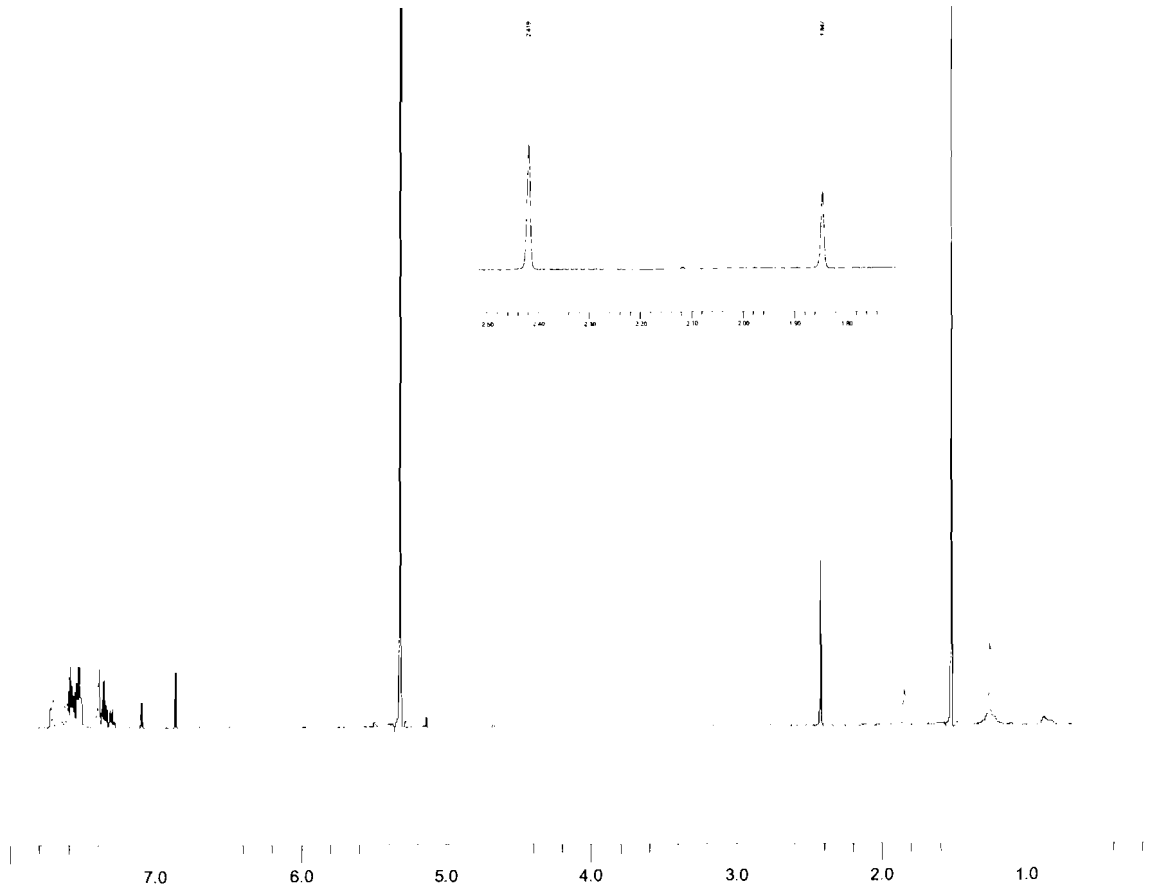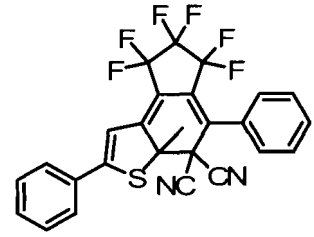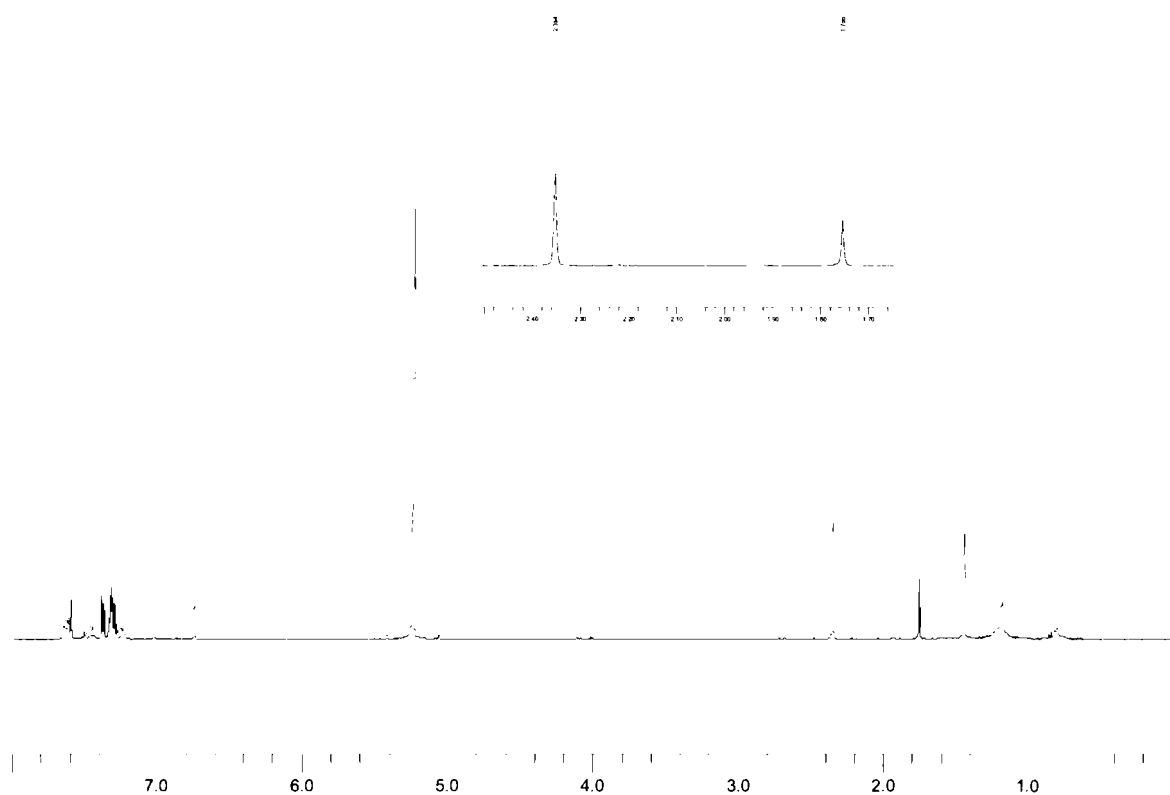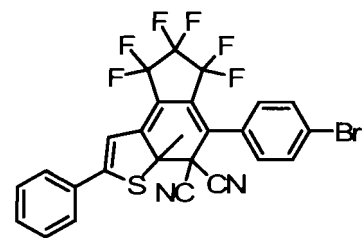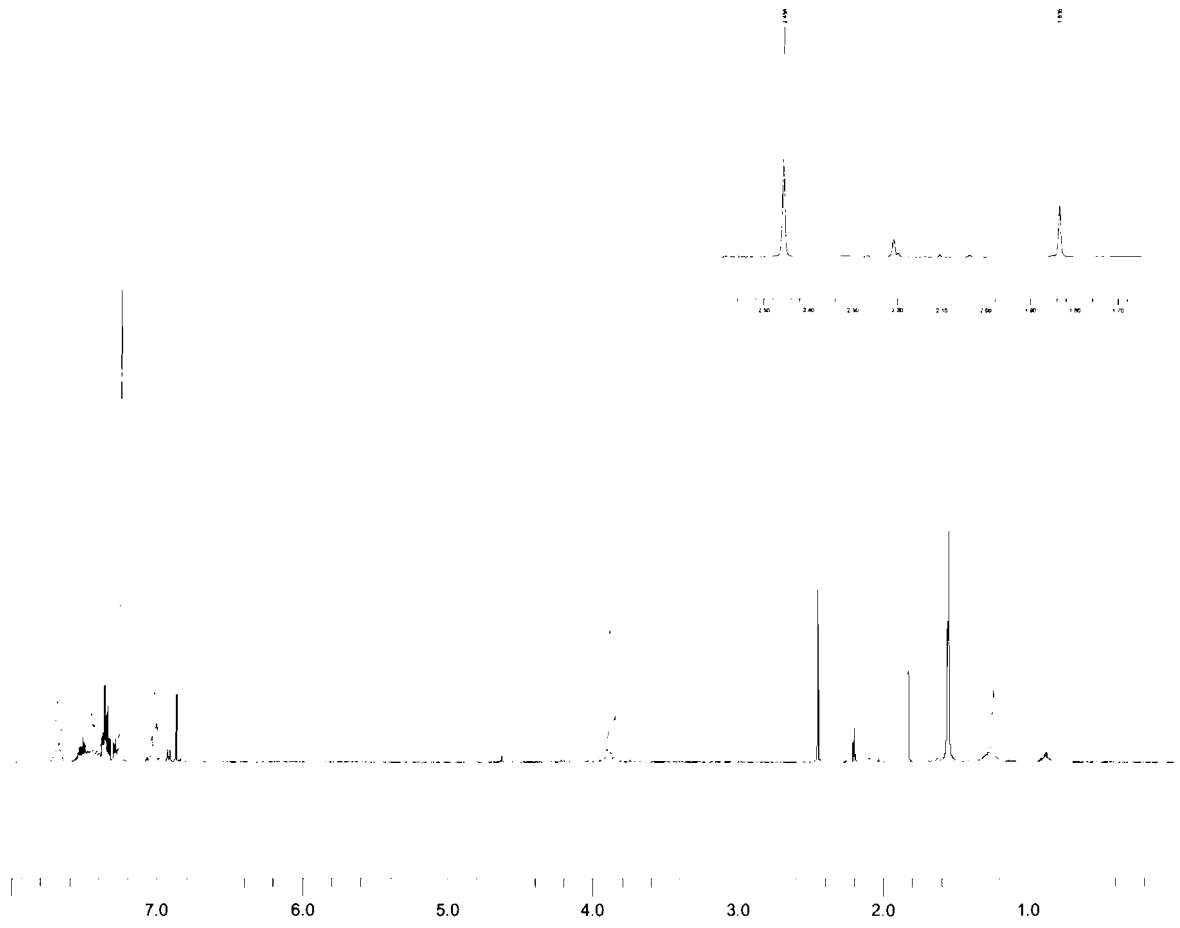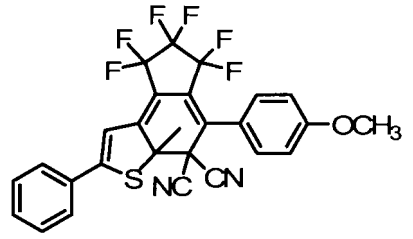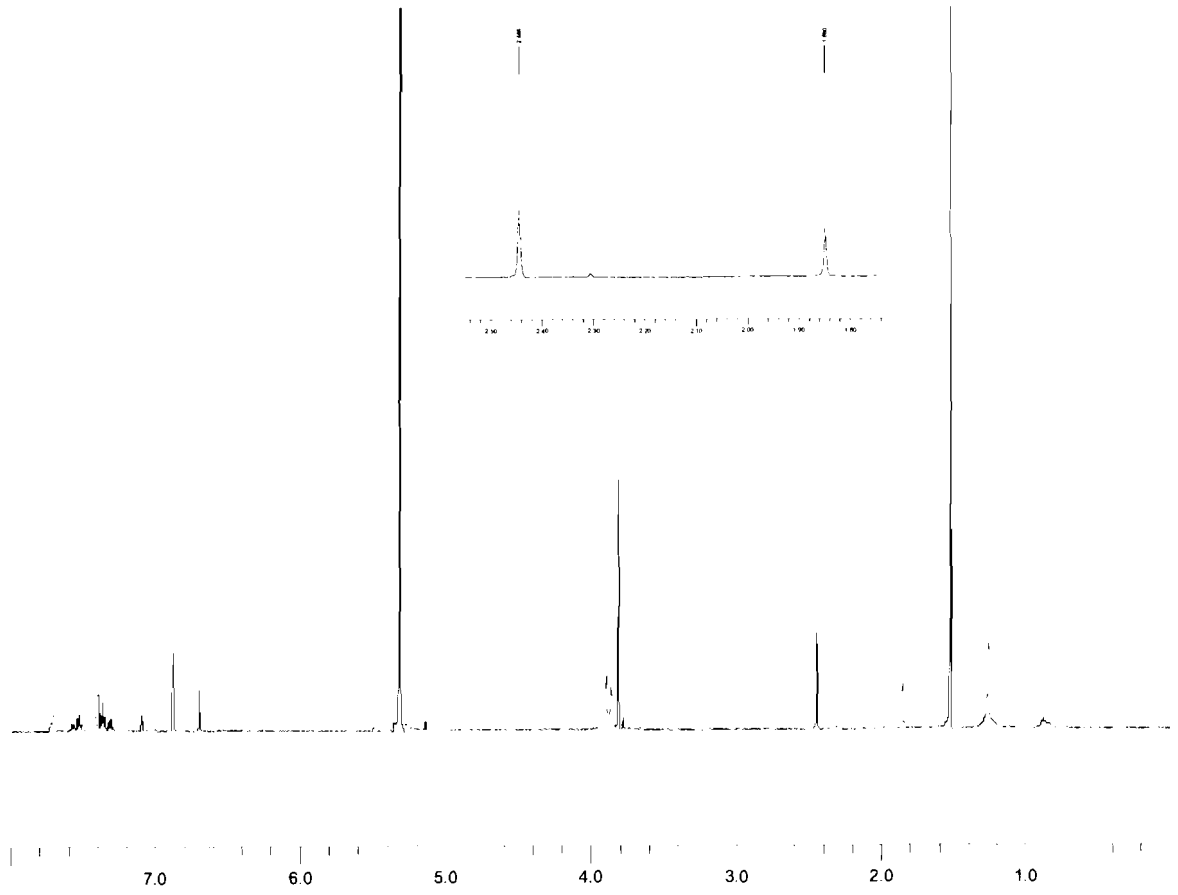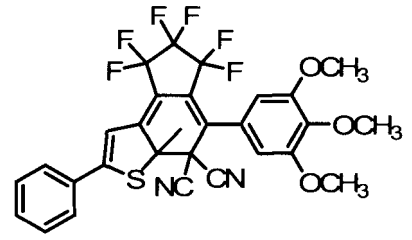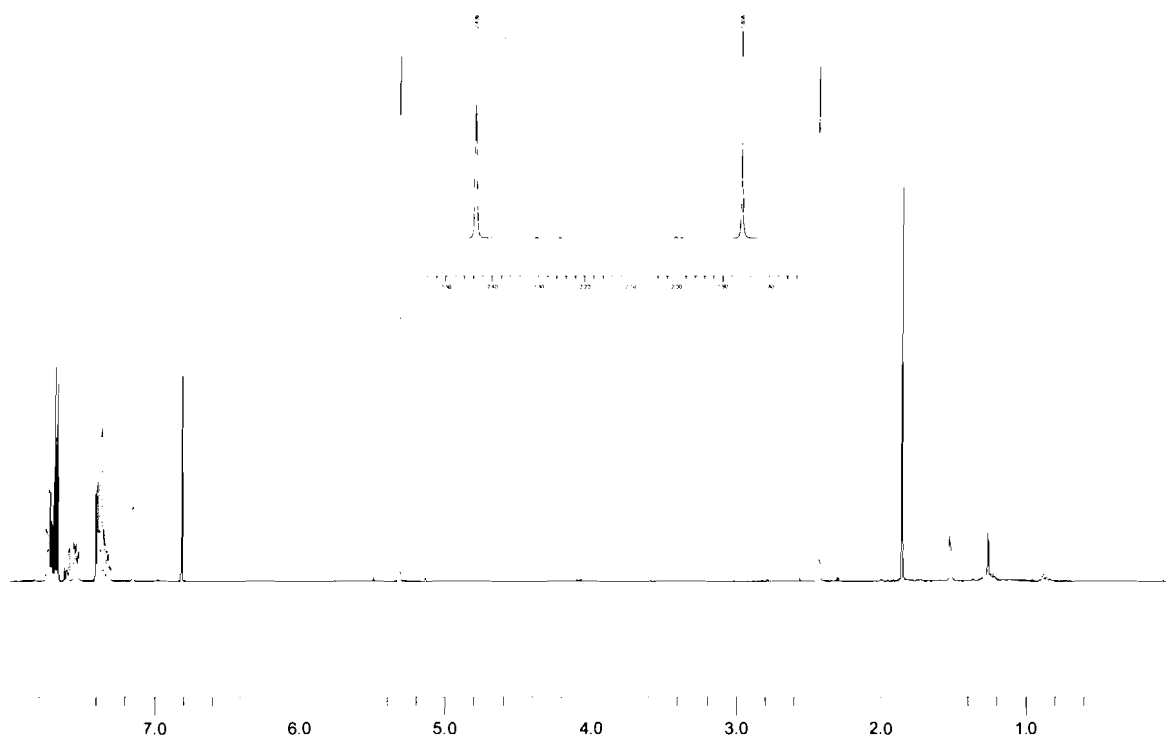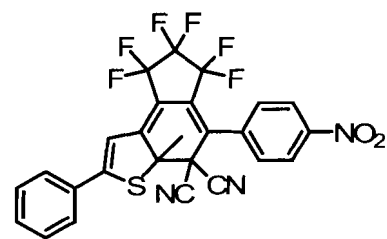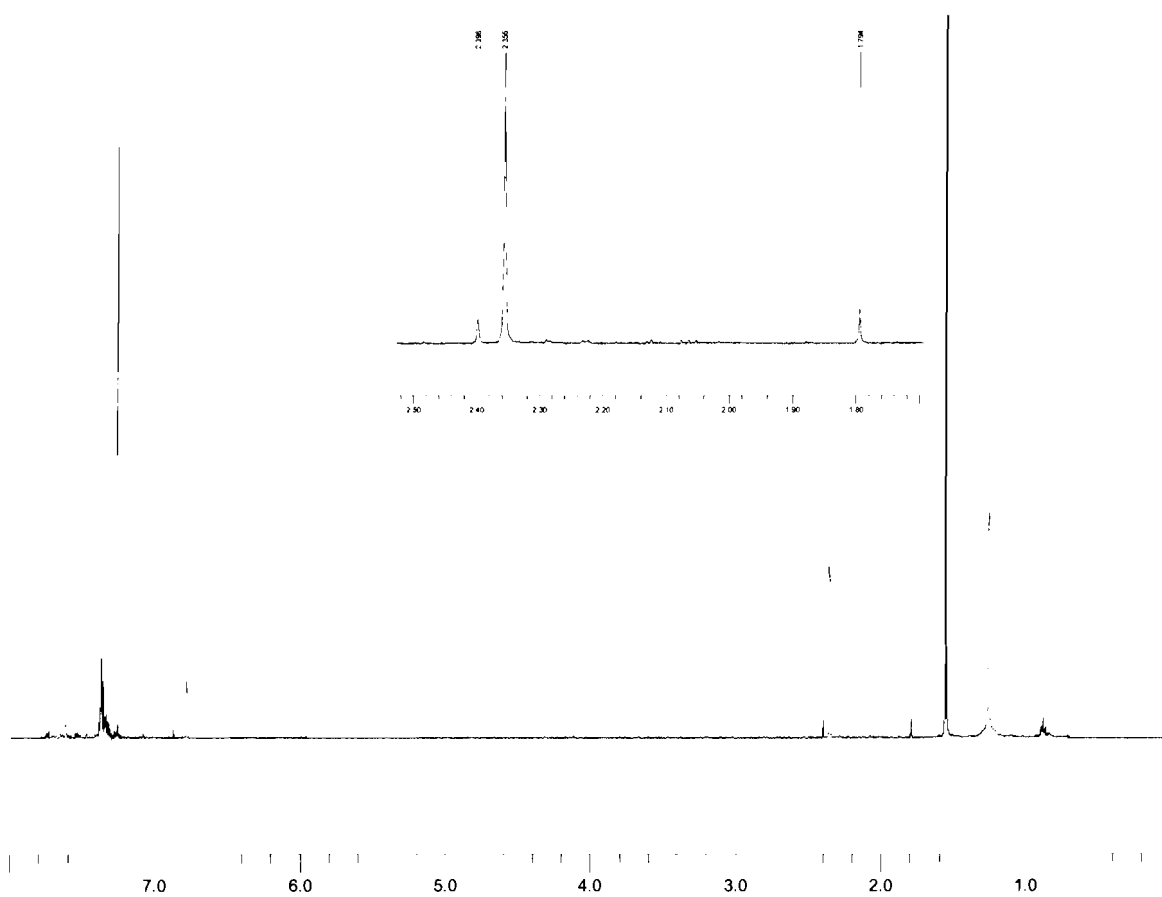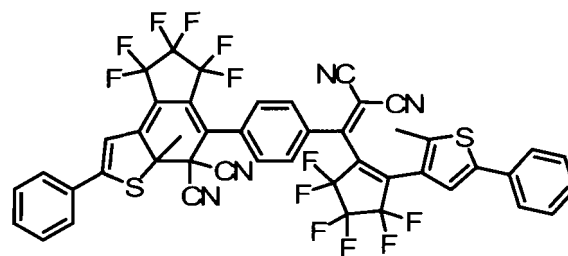
5.2 Supplementary Ellipsometry Data For Chapter 3

Table 5.2.1. Ellipsometry fits for duplicate locations on **3o-10o**.and **3c-10c**.

Film[a]/ χ^2	Thickness (Å)	ε_∞[b]	A	B	C	ε_g (eV)
3o	835.8	2.33924	0.12220	8.07388	25.77773	3.54562
0.052	±1.6	±0.017	±0.0210	±0.373	±1.47	±0.124
3o	833.8	2.23133	0.04626	7.31564	20.59603	2.56460
0.144	±2.8	±0.0336	±0.0182	±0.551	±1.44	±0.230
3c	836.6	2.25832	0.03865	3.55372	9.0302	1.92999
0.095	±2.4	±0.01859	±0.00818	±0.259	±0.642	±0.146
3c	835.5	2.28093	0.03891	3.49384	11.53047	1.55235
0.215	±3.8	±0.0243	±0.0138	±0.357	±1.71	±0.192
4o	309.3	2.42571	-0.024152	7.19736	18.89009	2.90480
0.023	±0.7	±0.0150	±.0.00720	±0.271	±1.02	±0.146
4o	311.2	2.448341	0.10105	8.03466	16.52467	3.77869
0.024	±0.8	±0.0387	±0.0372	±0.0992	±0.454	±0.0701
4c	309.4	2.36276	-0.03264	4.40392	7.04295	2.50862
0.023	±1.0	±0.0368	±0.0140	±0.216	±0.307	±0.115

4c	310.4	2.36950	-0.03074	4.74459	7.20703	2.41644
0.054	±1.5	±0.0185	±0.0237	0.313±	0.501±	±0.169
5o	432.5	2.21750	0.04699	8.22649	17.2749	5.44716
0.036	±1.0	±0.0340	±0.0253	±0.114	±0.431	±0.272
5o	43208	2.22050	0.05971	8.31171	17.56403	5.27017
0.023	±0.8	±0.0247	±0.0273	±0.0903	±0.344	±0.225
5c	429.5	2.17051	-0.05787	4.60030	7.08846	2.80328
0.028	±1.1	±0.0452	±0.0138	±0.193	±0.264	±0.126
5c	431.8	2.20897	-0.05115	4.83715	6.88926	2.63770
0.033	±1.3	±0.0344	±0.0179	±0.212	±0.248	±0.125
6o[1]	564.0	2.19165	0.04215	9.00639	17.23627	2.78159
0.052	±1.2	±0.0279	±0.00843	±0.212	±0.0548	±0.138
6o[1]	563.8	2.19212	0.04338	8.95136	17.19389	2.86213
0.012	±1.1	±0.0127	±0.00911	±0.344	±2.14	±0.159
6c[1]	563.5	2.21617	0.02120	4.99472	6.31902	3.24075
0.051	±1.6	±0.0245	±0.0169	±0.104	±.0250	±0.230
6c[1]	597.6	2.21326	0.01260	5.04123	6.44529	3.39651

	0.060	1.7	±0.0267	±0.0102	±0.115	±0.285	±0.231
6o^2	576.6	2.16222	0.05039	9.55818	18.97506	2.87043
	0.030	±0.9	±0.0228	±0.00714	±0.244	±0.481	±0.122
6o^2	576.7	2.17136	0.04329	9.00522	16.37732	2.53054
	0.059	±1.3	±0.0328	±0.0113	±0.428	±0.650	±0.149
6c^2	570.6	2.16790	-0.03461	4.27972	6.4185	2.92692
	0.65	±1.7	±0.0417	±0.0122	±0.227	±0.334	±0.0175
6c^2	570.5	2.14102	-0.04891	4.46047	6.92974	2.87661
	0.33	±1.2	±0.0314	±0.0107	±0.182	±0.247	±0.124
6o^3	577.6	2.19747	0.05257	8.89095	18.73796	3.52449
	0.044	±1.1	±0.0266	±0.0139	±0.430	±0.771	±0.155
6o^3	578.2	2.17208	0.06111	9.30570	20.16551	3.54681
	0.031	±0.9	±0.0209	±0.0106	±0.358	±0.755	±0.137
6c^3	577.9	2.19384	0.01228	5.00716	6.37710	3.56677
	0.041	±1.4	±0.0226	±0.00742	±0.100	±0.246	±0.209
6c^3	578.7	2.18601	0.01604	5.02785	6.42156	3.45875
	0.043	±1.5	±0.021	±0.0102	±0.100	±0.243	±0.216

7o	304.7	2.37755	0.01094	8.26654	15.2440	1.92554
0.049	±1.2	±0.0543	±0.0228	±0.170	±0.626	±0.329
7o	303.8	2.33244	0.02148	8.16189	17.07709	5.62019
0.35	±0.9	±0.0312	±0.00897	±0.277	±0.732	±.0154
7c	304.7	2.28011	-0.04898	4.76200	6.86172	2.65057
0.039	±1.5	±0.0543	±0.0334	±0.256	±0.287	±0.112
7c	304.5	2.241967	-0.05045	4.15623	5.89089	2.67494
0.073	±2.0	±0.0731	±0.0235	±0.290	±0.354	±0.205
8o	662.0	2.20188	0.03171	8.78964	19.36590	3.75052
0.041	±1.1	±0.0200	±0.0376	±0.148	±0.648	±0.190
8o	660.9	2.15552	0.04769	8.87588	16.68715	2.68324
0.049	±1.2	±0.0249	±0.00842	±0.142	±0.422	±0.0336
8c	660.5	2.02027	0.017843	4.99306	6.30059	3.16343
0.031	±1.2	±0.0171	±0.0113	±0.0794	±0.191	±0.157
8c	660.9	2.20232	0.03403	5.00023	6.29304	2.93565
0.016	±1.5	±0.0198	±0.0292	±0.0765	±0.184	±0.173
9o	352.2	2.36726	0.01192	8.30668	16.56956	3.41212

0.029	±0.8	±0.0236	±0.00959	±0.443	±0.942	±0.143
9o	354.1	2.28780	-0.01585	6.53335	17.27094	5.34042
0.011	±1.1	±0.0381	±0.00767	±0.330	±1.01	±0.312
9c	355.7	2.26138	-0.03729	4.94370	7.99882	2.95409
0.045	±1.5	±0.0285	±.0220	±0.270	±0.425	±0.181
9c	355.1	2.26079	-0.03710	4.16405	5.56818	2.56443
0.061	±1.8	±0.0525	±0.0168	±0.264	±0.273	±0.191
10o	331.7	1.27124	-3.36334	7.64435	15.70042	3.38823
0.125	±1.2	±.202	±.403	±.241	±1.09	±0.0962
10o	330.	1.01152	0.96545	7.85173	16.32096	6.01175
0.153	±1.5	±0.193	±0.190	±0.192	±0.875	±0.371
10c	348.4	2.39901	0.01149	3.48154	3.07034	1.26259
0.027	±1.5	±0.0269	±0.00147	±0.0227	±0.0389	±0.0355
10c	349.2	2.19233	0.01021	3.60281	3.32562	0.99781
0.060	±4.7	±0.0646	±0.00341	±0.0648	±0.125	±0.115

[a] Films were sampled twice on the same location for the ring-open (o) and ring-closed (c) isomer, which was generated by irradiation with 365 nm light for 10 minutes. Film thicknesses were determined by fitting the ellipsometry data to the model for amorphous material. [b] Amorphous fit parameters where A, B, and C are constants, ε_g is the optical energy gap and ε_∞ is a constant greater than unity.

6 References

(1) *Macmillan Contemporary Dictionary*; Halsey, W. D., Ed.; Macmillan Publishing Co.: London, **1979**.

(2) Tour, J. M. *Molecular Electonics*; World Scientific: USA, **2003**; pp 1-24.

(3) *The Coming of Material Science*; Cahn, R. W., Ed.; Elsevier Science Ltd.: Oxford, UK, **2001**; Vol. 5; pp 253-265.

(4) *Chemistry of Nanomolecular Systems: Towards the Realization of Nanomolecular Devices*; Nakamura, T., Matsumoto, T., Tada, H., Sugiura, K., Eds.; Springer: New York, USA, **2003**.

(5) Ball, P. *Made to Measure : New Materials for the 21st Century*; Princeton University Press: Princeton, NJ, **1997**; pp 15-62.

(6) Gasman, L. *Nanotechnology applications and markets*; Artech House: Boston, USA, **2006**; pp 71-100.

(7) Verbiest, T.; Houbrechts, S.; Kauranen, M.; Clays, K.; Persoons, A. *J. Mater. Chem.* **1997**, *7*, 2175-2189.

(8) Liao, R. B.; Liu, C. P.; Sa, R. J.; Wu, K. C. *Journal of Molecular Structure-Theochem* **2007**, *823*, 28-33.

(9) Gainsford, G. J.; Bhuiyan, M. D. H.; Kay, A. J. *Acta Crystallographica Section C-Crystal Structure Communications* **2007**, *63*, O633-O637.

(10) Sigmundova, I.; Zahradnik, P.; Loos, D. *Collection of Czechoslovak Chemical Communications* **2007**, *72*, 1069-1093.

(11) Bures, F.; Schweizer, W. B.; May, J. C.; Boudon, C.; Gisselbrecht, J. P.; Gross, M.; Biaggio, I.; Diederich, F. *Chem.-Eur. J.* **2007**, *13*, 5378-5387.

(12) *Infrared Holography for Optical Communications : techniques, materials, and devices*; Boffi, P., Piccinin, D., Ubaldi, M. C. Eds.; Springer-Verlag: Berlin, Germany, **2003**.

(13) Young, M. *Optics and Lasers*; Springer: Berlin, Germany, **2000**; Vol. 5; pp 319-335.

(14) Ong, B. H.; Yuan, X. C.; Tjin, S. C. *Appl. Optics* **2006**, *45*, 8036-8039.

(15) Carey, F. A., Sundberg, R.J. *Advanced Organic Chemistry*; 3rd ed.; Plenum Press: New York, USA, **1999**; pp 232-234.

(16) Asselberghs, I.; Clays, K.; Persoons, A.; Ward, M. D.; McCleverty, J. *J. Mater. Chem.* **2004**, *14*, 2831-2839.

(17) Wustenberg, B.; Branda, N. R. *Adv. Mater.* **2005**, *17*, 21342138.

(18) Di Bella, S. *Chem. Soc. Rev.* **2001**, *30*, 355-366.

(19) Prasad, P. N.; Reinhardt, B. A. *Chem. Mat.* **1990**, *2*, 660-669.

(20) Puccetti, G.; Blancharddesce, M.; Ledoux, I.; Lehn, J. M.; Zyss, J. *J. Phys. Chem.* **1993**, *97*, 9385-9391.

(21) *Molecular Switches*; Feringa, B. L., Ed.; Wiley-VCH: Weinheim, Germany, **2001**.

(22) *Organic Photochromic and Thermochromic Compounds*; Crano, J. C., Guglielmetti, R. J., Eds.; Plenum Press: New York, USA, **1999**; Vol. 1 and 2.

(23) Katsonis, N.; Kudernac, T.; Walko, M.; van der Molen, S. J.; van Wees, B. J.; Feringa, B. L. *Adv. Mater.* **2006**, *18*, 1397-+.

(24) Dulic, D.; van der Molen, S. J.; Kudernac, T.; Jonkman, H. T.; de Jong, J. J. D.; Bowden, T. N.; van Esch, J.; Feringa, B. L.; van Wees, B. J. *Phys. Rev. Lett.* **2003**, *91*.

(25) Kawai, T.; Nakashima, Y.; Irie, M. *Adv. Mater.* **2005**, *17*, 309-314.

(26) Jiang, G. Y.; Wang, S.; Yuan, W. F.; Jiang, L.; Song, Y. L.; Tian, H.; Zhu, D. B. *Chem. Mat.* **2006**, *18*, 235-237.

(27) Matsuda, K.; Irie, M. *J. Photochem. Photobiol. C-Photochem. Rev.* **2004**, *5*, 169-182.

(28) Norsten, T. B.; Branda, N. R. *Adv. Mater.* **2001**, *13*, 347-349.

(29) Murguly, E.; Norsten, T. B.; Branda, N. R. *Angewandte Chemie-International Edition* **2001**, *40*, 1752-1755.

(30) Wigglesworth, T. J.; Sud, D.; Norsten, T. B.; Lekhi, V. S.; Branda, N. R. *Journal of the American Chemical Society* **2005**, *127*, 7272-7273.

(31) de Jong, J. J. D.; Lucas, L. N.; Kellogg, R. M.; van Esch, J. H.; Feringa, B. L. *Science* **2004**, *304*, 278-281.

(32) Pu, S. Z.; Yang, T. S.; Yao, B. L.; Wang, Y. L.; Lei, M.; Xu, J. K. *Mater. Lett.* **2007**, *61*, 855-859.

(33) In *Optomechanicl Technologies for Astronomy*; Eli Atad-Ettedgui, Ed.; Proc. of SPIE: Milano, Italy, **2006**; Vol. 6273.

(34) Bertarelli, C.; Gallazzi, M. C.; Zerbi, G.; Molinari, E.; Bianco, A.; Giro, E. *Mol. Cryst. Liquid Cryst.* **2005**, *430*, 187-192.

(35) Kim, M. S.; Maruyama, H.; Kawai, T.; Irie, M. *Chem. Mat.* **2003**, *15*, 4539-4543.

(36) Irie, M. *Chem. Rev.* **2000**, *100*, 1685-1716.

(37) Ebisawa, F.; Hoshino, M.; Sukegawa, K. *Appl. Phys. Lett.* **1994**, *65*, 2919-2921.

(38) Irie, M.; Mohri, M. *J. Org. Chem.* **1988**, *53*, 803-808.

(39) Tian, H.; Yang, S. *J. Chem. Soc. Rev.* **2004**, *33*, 85-97.

(40) Kawai, S. H.; Gilat, S. L.; Ponsinet, R.; Lehn, J. M. *Chem.-Eur. J.* **1995**, *1*, 285-293.

(41) Tian, H.; Wang, S. *Chem. Commun.* **2007**, 781-792.

(42) Raymo, F. M.; Tomasulo, M. *Chem. Soc. Rev.* **2005**, *34*, 327-336.

(43) Raymo, F. M.; Tomasulo, M. *Chem.-Eur. J.* **2006**, *12*, 3186-3193.

(44) Bertarelli, C.; Gallazzi, M. C.; Stellacci, F.; Zerbi, G.; Stagira, S.; Nisoli, M.; De Silvestri, S. *Chem. Phys. Lett.* **2002**, *359*, 278-282.

(45) Stellacci, F.; Bertarelli, C.; Toscano, F.; Gallazzi, M. C.; Zotti, G.; Zerbi, G. *Adv. Mater.* **1999**, *11*, 292-295.

(46) Irie, M.; Uchida, K. *Bull. Chem. Soc. Jpn.* **1998**, *71*, 985-996.

(47) Irie, M.; Sakemura, K.; Okinaka, M.; Uchida, K. *J. Org. Chem.* **1995**, *60*, 8305-8309.

(48) Matsuda, K.; Irie, M. *Chem. Lett.* **2000**, 16-17.

(49) Kawai, S. H.; Gilat, S. L.; Lehn, J. M. *J. Chem. Soc.-Chem. Commun.* **1994**, 1011-1013.

(50) Hanazawa, M.; Sumiya, R.; Horikawa, Y.; Irie, M. *J. Chem. Soc.-Chem. Commun.* **1992**, 206-207.

(51) Nakamura, S.; Irie, M. *J. Org. Chem.* **1988**, *53*, 6136-6138.

(52) McMurry, J. *Organic Chemistry*; 7th ed.; Thompson Learning: USA, **2008**; pp 1178-1196.

(53) Breslow, R. *Organic Reaction Mechanisms*; 2nd ed.; W. A. Benjamin, Inc.: New York, USA, **1969**; pp 256-267.

(54) Tanio, N.; Irie, M. *Jpn. J. Appl. Phys. Part 1 - Regul. Pap. Short Notes Rev. Pap.* **1994**, *33*, 3942-3946.

(55) Biteau, J.; Chaput, F.; Lahlil, K.; Boilot, J. P.; Tsivgoulis, G. M.; Lehn, J. M.; Darracq, B.; Marois, C.; Levy, Y. *Chem. Mat.* **1998**, *10*, 1945-1950.

(56) Hoshino, M.; Ebisawa, F.; Yoshida, T.; Sukegawa, K. *J. Photochem. Photobiol. A-Chem.* **1997**, *105*, 75-81.

(57) Kawai, T.; Koshido, T.; Yoshino, K. *Appl. Phys. Lett.* **1995**, *67*, 795-797.

(58) Bens, A. T.; Frewert, D.; Kodatis, K.; Kryschi, C.; Martin, H. D.; Trommsdorff, H. P. *Eur. J. Org. Chem.* **1998**, 2333-2338.

(59) Irie, M. In *Molecular Switches*; Feringa, B. L., Ed.; Wiley-VHC: Weinheim, Germany, **2001**, pp 33-60.

(60) Gilat, S. L.; Kawai, S. H.; Lehn, J. M. *Chemistry-a European Journal* **1995**, *1*, 275-284.

(61) Kobatake, S.; Uchida, K.; Tsuchida, E.; Irie, M. *Chem. Lett.* **2000**, 1340-1341.

(62)   Morimitsu, K.; Shibata, K.; Kobatake, S.; Irie, M. *J. Org. Chem.* **2002**, *67*, 4574-4578.

(63)   Irie, M.; Eriguchi, T.; Takada, T.; Uchida, K. *Tetrahedron* **1997**, *53*, 12263-12271.

(64)   Peters, A.; Vitols, C.; McDonald, R.; Branda, N. R. *Org. Lett.* **2003**, *5*, 1183-1186.

(65)   Shrestha, S. M.; Nagashima, H.; Yokoyama, Y. *Bull. Chem. Soc. Jpn.* **2003**, *76*, 363-367.

(66)   Peters, A. "*Novel Photochromic Dithienylalkenes for the Development of Molecular Scale Device*," Simon Fraser, **2003**. pp 43-64.

(67)   Bertarelli, C.; Bianco, A.; D'Amore, F.; Gallazzi, M. C.; Zerbi, G. *Adv. Funct. Mater.* **2004**, *14*, 357-363.

(68)   *CRC HandbookofChemistry and Physics 72nd Ed.*; Lide, D. R., Ed.; CRC Press: Boca-Raton, USA, **1991**; Vol. 10-194.

(69)   Wigglesworth, T. J. "*Photoresponsive Materials Based on Dithienylethenes*," Simon Fraser University, **2006**. pp 93-94.

(70)   Jisha, C. P., Kuriakose, V.C., Porsezian, K. *Optics Communications* **2008**, *281*, 1093-1098.

(71)   Shirota, Y.; Utsumi, H.; Ujike, T.; Yoshikawa, S.; Moriwaki, K.; Nagahama, D.; Nakano, H. *Opt. Mater.* **2003**, *21*, 249-254.

(72)   Asaro, M.; Sheldon, M.; Chen, Z. G.; Ostroverkhova, O.; Moerner, W. E. *Opt. Lett.* **2005**, *30*, 519-521.

(73)   Burns, W. K. M., A. F. *Guided-Wave Optoelectronics*; Tamir, T.; Springer-Velag: Berlin, Germany, **1988**; pp 89-144.

(74)   *Organic Thin Films for Waveguiding Nonlinear Optics*; Kajzar, F., Swalen, J. D., Eds.; Gordon and Breach: Amsterdam, Netherlands, **1996**; Vol. 3.

(75)   Chaput, F.; Biteau, J.; Lahlil, K.; Boilot, J. P.; Darracq, B.; Levy, Y.; Peretti, J.; Safarov, V. I.; Parent, G.; Fernandez-Acebes, A.; Lehn, J. M. *Mol. Cryst. Liquid Cryst.* **2000**, *344*, 77-82.

(76)   Takami, S.; Irie, M. *Journal of Photochemistry and Photobiology a-Chemistry* **2007**, *187*, 202-208.

(77)   Wigglesworth, T. J.; Myles, A. J.; Branda, N. R. *European Journal of Organic Chemistry* **2005**, 1233-1238.

(78)   Tompkins, H. G. M., William A.; *Spectroscopic Ellipsometry and Reflectometry, A Users Guide*; John Wiley & Sons, Inc.: USA, **1999**.

(79)   Isaacs, N. *Physical Organic Chemistry*; 2nd ed.; Longman: New York, USA, **1995**; pp 30-45.

(80)   Tanio, N.; Irie, M. *Jpn. J. Appl. Phys. Part 1 - Regul. Pap. Short Notes Rev. Pap.* **1994**, *33*, 1550-1553.

(81)   Yoshida, T. A., K.; Ebisawa, F.; Hoshino, M.; Sukegawa, K.; Ishikawa, A.; Kobayashi, T.; Hanazawa, M.; Horikawa, Y *Polym. Mater. Sci. Eng.* **1996**, *75*, 368.

(82)   Yoshida, T.; Arishima, K.; Ebisawa, F.; Hoshino, M.; Sukegawa, K.; Ishikawa, A.; Kobayashi, T.; Hanazawa, M.; Horikawa, Y. *J. Photochem. Photobiol. A-Chem.* **1996**, *95*, 265-270.

(83)   Kang, J. W.; Kim, J. J.; Kim, E. *Appl. Phys. Lett.* **2002**, *80*, 1710-1712.

(84)   Kim, E.; Choi, Y. K.; Lee, M. H. *Macromolecules* **1999**, *32*, 4855-4860.

(85)   Forouhi, A. R.; Bloomer, I. *Physical Review B* **1986**, *34*, 7018-7026.

(86)   Pickering, W. F. *Pollution Evaluation*; Morris, J. C.; Marcel Dekker: New York USA, **1977**; Vol. 2; pp 17-18.

(87)   *Surface and Thin Flim Analysis*; Bubert, H., Jenett, H., Eds.; Wiley-VHC: Weinheim, Germany, **2002**; pp 265-283.

(88)   *The handbook of Surface Imaging and Visualization*; Hubbard, A. T., Ed.; CRC Press: Boca-Raton FL., **1995**; pp 23-32.

(89)   Uchida, K.; Takata, A.; Saito, M.; Murakami, A.; Nakamura, S.; Irie, M. *Adv. Funct. Mater.* **2003**, *13*, 755-762.

(90)   Kobatake, S.; Irie, M. *Tetrahedron* **2003**, *59*, 8359-8364.

(91)   Wigglesworth, T. J.; Branda, N. R. *Adv. Mater.* **2004**, *16*, 123-+.

(92)   Hori, H.; Nagasawa, H.; Ishibashi, M.; Uto, Y.; Hirata, A.; Saijo, K.; Ohkura, K.; Kirk, K. L.; Uehara, Y. *Bioorganic & Medicinal Chemistry* **2002**, *10*, 3257-3265.